

ONE

This is to certify that the

dissertation entitled

Synthesis, Characterization and Properties
of Clay -Reinforced Thermoset Nanocomposites

presented by

Peter C. LeBaron

has been accepted towards fulfillment
of the requirements for

Ph. D. degree in 2001

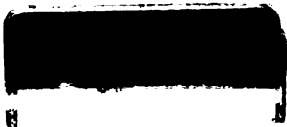
Thomas J. Pinnavaia
Major professor *T. M.*

Date 12/13/01

MSU is an Affirmative Action/Equal Opportunity Institution

O-12771

LIBRARY
Michigan State
University



**SYNTHESIS, CHARACTERIZATION AND PROPERTIES OF
CLAY – REINFORCED THERMOSET NANOCOMPOSITES**

By

Peter C. LeBaron

A DISSERTATION

Submitted to Michigan State University in partial fulfillment of the requirements

for the degree of

DOCTOR OF PHILOSOPHY

Department of Chemistry

2001

ABSTRACT

SYNTHESIS, CHARACTERIZATION AND PROPERTIES OF CLAY – REINFORCED THERMOSET NANOCOMPOSITES

By

Peter C. LeBaron

Nanocomposites are formed upon the uniform mixture of two or more distinct phases over a nanometer length scale. Typically the components consist of a stiff reinforcement phase dispersed in a polymeric matrix. Due to the improved surface contact and interfacial properties of nanocomposites, these materials commonly exhibit superior mechanical behavior relative to conventionally filled systems. The first example of layered silicate materials employed as a reinforcement phase was shown by Toyota researchers in exfoliating organoclay in a nylon-6 matrix. The hybrid material exhibited a dramatic improvement in thermal and mechanical properties, and ultimately found practical use in under-the-hood applications in the automobile industry.

The present work focuses on nanocomposite syntheses of two distinctly different polymeric systems, elastomeric polydimethylsiloxanes and rigid epoxies. Each polymeric medium requires unique layered silicate organo-modification, reaction conditions and sample treatment. These concepts are addressed along with the mechanism of clay exfoliation and an investigation on the final properties.

Silicone rubbers gained remarkable toughness, as the stiffness, elongation and tensile strength were notably improved upon the exfoliation of clay particles. Permeability of the silicone samples was not substantially influenced by the presence of silicate layers, however, and this lead to further investigations on the post – cure reactivity of the silicone nanocomposites.

The nanocomposites formed in a glassy epoxy network also showed substantial mechanical improvement compared to the unfilled epoxy. In the case with epoxies, the amount and type of organic modification used on the clay was scrutinized. Nanocomposites were synthesized from reduced organic – content clays and were noted to retain epoxy intercalation and exfoliation properties.

ACKNOWLEDGEMENTS

First and foremost, I am especially thankful to have had the opportunity to complete my Ph.D. under the best advisor in the business, Professor Thomas J. Pinnavaia. He has served as a close friend, providing helpful advice on some of the more important aspects in life (relationships, health and fishing), along with his excellent tutelage and guidance in research. I wish every graduate student would have the chance to work for such an intelligent, creative, kind preceptor.

I am also extremely appreciative for the support and patience my terrific wife has shown me throughout my graduate career. Higher education is an investment many do not understand, however she never complained (to me at least) about the partial delay graduate school placed on our lives. For this reason I would like to dedicate my thesis to her, even though she really doesn't care for chemistry and certainly won't read any of this book.

Many former and current Pinnavaia group members have had an impact on my life, but I would especially like to thank my original mentor, Zhen Wang, and my current lab mate Costas Triantafillidis for their help and collaborations. My close friends Liu and Kimbo have been wonderful sources of knowledge and incite through the years, and I know someday they will be highly successful industrial scientists. Other group members barely worth mentioning are In Park, Mark Sislo, Abhi Karkamkar and Randy Hicks, whom I thank for eating pizza with me. I would also like to acknowledge Jainisha Shah and Emily McKimmy as they were indispensable in helping me format my thesis, a job I am not cut out for.

TABLE OF CONTENTS

LIST OF TABLES

LIST OF FIGURES

CHAPTER 1 INTRODUCTION

1.1	Nanocomposite Materials	1
1.1.1	Nanocomposite Concept	1
1.1.2	Nanocomposite Significance	1
1.1.3	Sol-Gel Synthesized Nanocomposites	2
1.1.4	Layered Silicate Nanocomposites	5
1.1.5	Smectite Clay Structure	6
1.1.6	Organoclay Structures and Properties	8
1.1.7	Organoclay – Polymer Interactions	11
1.1.8	Properties of Thermoset – Clay Nanocomposites	14
1.1.9	Exfoliated Nylon-6 – Clay Nanocomposites	17
1.2	Recent Developments in Polymer – Clay Nanocomposites	20
1.3	Research Objectives	22
1.3.1	Current Issues and New Directions	22
1.3.2	Research Goals	23
1.3.3	References	25

**CHAPTER 2 CLAY NANOLAYER REINFORCEMENT OF A SILICONE
ELASTOMER: EXFOLIATION OF FLUOROHECTORITE IN
POLYDIMETHYLSILOXANE**

2.1	Introduction	30
2.2	Experimental	33
2.3	Physical Measurements	38
2.4	Results	41
2.5	Discussion	49
2.6	Conclusions	75
2.7	References	76

**CHAPTER 3 POST-CURE ION EXCHANGE OF EXFOLIATED
FLUOROHECTORITE CLAY IN
POLYDIMETHYLSILOXANE NANOCOMPOSITES**

3.1	Introduction	79
3.2	Experimental	95
3.3	Results and Discussion	99
3.4	Conclusions	108
3.5	References	109

**CHAPTER 4 EXFOLIATION OF DIAMINE – MODIFIED CLAYS IN A
GLASSY EPOXY MATRIX**

4.1	Introduction	111
------------	---------------------	------------

4.2	Experimental	115
4.3	Results and Discussion	119
4.4	Conclusions	151
4.5	References	152

**CHAPTER 5 REDUCING THE ORGANIC MODIFIER CONTENT IN
EPOXY NANOCOMPOSITES: MIXED-ION
INORGANIC/ORGANIC MONTMORILLONITE AND
FLUOROHECTORITE HOMOSTRUCTURES**

5.1	Introduction	155
5.2	Experimental	159
5.3	Results and Discussion	164
5.4	Conclusions	188
5.5	References	189

LIST OF TABLES

Table 1.1	Mechanical and Thermal Properties of Nylon-6	20
Table 2.1	Silanol Terminated PDMS Monomers	34
Table 2.2	Mechanical Properties of Silicone Elastomer - C ₁₆ FH	47

Organoclay Nanocomposites

Table 2.3	Permeability and Solvent Uptake Properties of Silicone Elastomer ^a - C ₁₆ FH Organoclay Nanocomposites	48
Table 3.1	Silanol Terminated PDMS Monomers	96
Table 3.2	Copper Content Present After Post – Cure Ion Exchange	103
Table 4.1	Composition and Basal Spacings of the Inorganic and Organic Clays used for the Preparation of the Nanocomposites	125
Table 4.2	Dynamic Mechanical Analysis and Thermal Analysis data of the pristine epoxy polymer and the clay-polymer nanocomposite samples	141
Table 5.1	Composition and Basal Spacings of the Homoionic and Mixed-ion Inorganic/Organic clays	167
Table 5.2	Dynamic Mechanical Analysis and Thermal Analysis Data of the Pristine Epoxy Polymer and the Clay-Polymer Nanocomposite Samples	183

LIST OF FIGURES

- Figure 1.1** Depiction of the sol-gel approach to synthesizing nanocomposites indicating the metal oxide filler phase and the polymeric silicone precursor. 4
- Figure 1.2** Illustration of the layered oxide framework of smectite clays. Clay layers consist of two tetrahedral sheets sandwiching a central octahedral layer. $M^{n+} \cdot yH_2O$ represents the interlayer exchangeable cation with its coordination sphere of water molecules. 7
- Figure 1.3** Illustration of four possible organoclay structures based on surfactant packing density. Given the same surfactant, increasing the charge density of the clay will move from a monolayer arrangement towards the paraffin structure. 9
- Figure 1.4** Schematic of the different composite morphologies possible when attempting to synthesize polymer - clay nanocomposites. Representative XRD patterns are displayed for each type. 13
- Figure 1.5** Schematic representation of the tortuous path invoked on permeants by having dispersed clay layers in a polymer 16

matrix.

Figure 1.6 General synthetic route for synthesizing nylon – 6 19
nanocomposite materials. The caprolactam precursors
were first melted, then added to the organoclay to permit
intercalation (causing a 15 Å basal spacing increase), and
finally polymerized at 250°C.

Figure 2.1 Schematic illustrating the organic ion exchange of 35
fluorohectorite clay using cetyltrimethylammonium
bromide.

Figure 2.2 General silicone nanocomposite synthesis scheme. After 37
polymerization silicone samples were carefully removed
from the steel molds for final property assessment.

Figure 2.3 X-ray diffraction patterns of synthetic 42
hexadecyltrimethylammonium fluorohectorite, abbreviated
C₁₆FH, intercalated by PDMS polymers with molecular
weights of 400, 1500-2000, and 4200. The pattern for the
initial organo clay is included for comparison.

Figure 2.4 X-ray diffraction patterns for mixtures of 44
hexadecyltrimethylammonium fluorohectorite and PDMS
– 4200 at different stages of cure. The curing agent was

tetraethylorthosilicate and the catalyst was tin(II) octoate. The inset indicates the presence of an in-plane 060 clay peak in the exfoliated composite

Figure 2.5 Comparison of the stress – strain curves for pristine PDMS and PDMS - C₁₆FH nanocomposites containing 5.0 and 10 wt % C₁₆FH organoclay. 46

Figure 2.6 Schematic depicting potential intragallery surfactant arrangements typically found in organomontmorillonites. 50

Figure 2.7 Inclined paraffin surfactant orientation found in higher charge density clays, including fluorohectorite. 52
Cetyltrimethylammonium fluorohectorite has a paraffin arrangement with an approximate angle of inclination with the clay surface of 50°.

Figure 2.8 Schematic representation of the swelling of an alkylammonium ion exchanged fluorohectorite by a long chain PDMS polymer (MW = 4200) containing terminal OH groups. Shorter PDMS chains with molecular weight fractions of 400 and 1750 may have only one end of the chain associated with the gallery surfaces. 55

- Figure 2.9** Photograph of PDMS polymer - C₁₆FH suspensions 58
containing 5.0 wt % organoclay. The tubes are filled in
left to right order with methyl terminated PDMS - 400 and
silanol terminated PDMS - 400, - 1750, and - 4200,
respectively.
- Figure 2.10** Tin octoate – catalyzed PDMS crosslinking. Although 60
there is some debate as to the exact mechanism, the
active species is widely thought to be the hydrolysis
product of the tin bis(2-ethylhexanoate) catalyst.
- Figure 2.11** Photographs of a pristine silicone elastomer formed from 64
PDMS - 4200 (upper specimen) and the corresponding
nanocomposite containing 5.0 wt % C₁₆FH organoclay
(lower specimen) after equilibration in a cyclohexane bath
and subsequent removal from the bath to allow for
solvent evaporation: (a) immediately after removal from
the bath, (b) after 15 seconds, and (c) after 20 minutes.
No structural damage was noted for the nanocomposite
after complete evaporation of the solvent.
- Figure 2.12** Depiction of permeant flow through nanocomposite films. 66
A more tortuous path is found perpendicular to the film
when clay particles are oriented parallel to the film
surface. Low surface tension fluids and thick films limit
the percentage of parallel – to – surface oriented

nanolayers.

- Figure 2.13** TEM image of silicone nanocomposite showing parallel orientation of nanolayers stemming from the same tactoids. Prior to intercalation and exfoliation in silicone, the organofluorohectorite galleries were separated by 2.7 Å, and after completion of crosslinking layers are 70-150 nm apart. 68
- Figure 2.14** TEM image of silicone nanocomposite showing neighboring tactoids with near orthogonal orientations. Such an image is rare in clay nanocomposites where adjacent clay tactoids are usually oriented parallel to one another. 70
- Figure 2.15** Schematic of tin catalyst existing in different forms during crosslinking of the silicone rubber. The moisture sensitive tin carboxylate will hydrolyze more readily when in close contact with the fluorohectorite clay due to the small amount (2-6% by wt.) of water present at the silicate surface. 74
- Figure 3.1** Schematics representing known reactive membrane and selective gas separation 82

procedures using functionalized aluminosilicates.

- Figure 3.2 Schematic showing the reduced swelling observed in 85
nanocomposites due to the constrained polymer at the
interface of the reinforcer.
- Figure 3.3 XRD patterns of silicone nanocomposites cured under 88
different conditions. Accelerating the cure with premature
heating (top pattern) leads to a lower degree of exfoliated
clay layers.
- Figure 3.4 Schematic of the procedure involved in synthesizing and 91
post-cure ion exchanging silicone nanocomposites.
- Figure 3.5 Representation of the crosslinked silicone nanocomposite 94
before and after immersion in THF.
- Figure 3.6 Copper content following post-cure ion exchanges for 100
silicone nanocomposites examined after successive THF
washes. Unleachable copper accounted for roughly 70%
of the fluorohectorite ion exchange capacity in the filled
systems, while pristine silicone retained almost no copper
after washing.
- Figure 3.7 Schematic representation of the post-cure ion exchanges 102

using a CuCl_2/THF exchange bath and pure THF as the wash. Uptake of copper into both nanocomposite and pristine samples was observed, however upon purging with THF only the nanocomposites retained copper.

- Figure 3.8 Schematic illustrating copper ion exchanges carried out in THF for different parent clay systems. Excess copper successfully substitutes for both the inorganic cations in lithium fluorohectorite as well as the majority of surfactant ions on organofluorohectorite exfoliated in a silicone matrix. However, despite increasing the copper concentration to 20 times the CEC of the clay, organic cations could not be appreciably displaced by Cu^{+2} in THF. 107
- Figure 4.1 Acid catalyzed intragallery ring – opening of an epoxy resin. 114
- Figure 4.2 X-ray diffraction patterns of the Li^+ -Fluorohectorite (Li-FH) and organically modified FH-clays (with diprotonated diamines D230, D400, D2000). 122
- Figure 4.3 X-ray diffraction patterns of mixtures of the organic clays D2000-FH, the epoxy monomer EPON 826 and the curing agent D230: (A) after intercalation of EPON 826 in 128

D2000-FH at 50°C for 6 hrs, (B) after intercalation of EPON 826 for 24 hrs, (C) after addition of D230 in the mixture of step C, outgassing and heating at 75°C for 0.5 hrs, (D) after curing at 75°C, 3 hrs and 125°C, 3hrs (the clay loading was 6 wt. % silicate basis). The inset shows the presence of an in-plane 060 clay reflection in the cured nanocomposite.

Figure 4.4 TEM images of thin sections of the glassy epoxy 131 nanocomposites prepared from D2000-FH. The clay loading of the nanocomposite samples was 6 wt. % silicate.

Figure 4.5 TEM images of thin sections of the glassy epoxy 133 nanocomposites prepared from D2000-PGW. The clay loading of the nanocomposite samples was 6 wt. % silicate.

Indeed, the nanolayers of the lower aspect ratio D2000-PGW clay were more randomly dispersed in the polymer matrix and existed in a more exfoliated arrangement.

Figure 4.6 X-ray diffraction patterns of EPON 826 – montmorillonite 135 PGW clay composites and nanocomposites using: (A) H-PGW, (B) D230-PGW, (C) D400-PGW and (D) D2000-PGW clays. No intercalation occurred for the inorganic, nor the D230 and D400-PGW clays. The inset shows the presence of an in-plane 060 clay reflection in the cured D2000-PGW nanocomposite.

- Figure 4.7** Schematic portraying the three point bending device 139
used in obtaining DMA data and the plot of DMA testing parameters. The amount of energy the material returns is related to its storage modulus, the energy dissipated in the internal motions of the polymer chains is related to its loss modulus and the actual measured material lag in experiencing the oscillatory force is the phase angle.
- Figure 4.8** Dynamic Mechanical Analysis measurements indicating 143
storage modulus vs. temperature curves for (A) Pristine-A epoxy polymer and for the nanocomposite samples prepared from (B) H-PGW, (C) D2000-PGW, (D) D2000-FH, (E) D230-PGW, (F) D230-FH. The clay loading of the nanocomposite samples was 6 wt. % silicate basis
- Figure 4.9** Dynamic Mechanical Analysis measurements indicating 145
 $\tan\delta$ vs. temperature, for (A) Pristine-A epoxy polymer and for the nanocomposite samples prepared from (B) H-PGW, (C) D2000-PGW, (D) D2000-FH, (E) D230-PGW, (F) D230-FH. The clay loading of the nanocomposite samples was 6 wt. % silicate basis
- Figure 4.10** TGA curves of the organic clays (A) D2000-PGW and (B) 149
D2000-FH, of the nanocomposites prepared from (C) D2000-PGW and (D) D2000-FH clays, and of the Pristine-

A epoxy polymer (E). The clay loading of the nanocomposite samples was 6 wt. % silicate basis.

Figure 4.11 TGA curves of the organic clays (A) D230-PGW and (B) 150
D400-PGW, of the nanocomposites prepared from (C)
D230-PGW and (D) D400-PGW clays, and of the Pristine-
A epoxy polymer (E). The clay loading of the
nanocomposite samples was 6 wt. % silicate basis.

Figure 5.1 X-ray diffraction patterns of the homoionic and mixed-ion 169
inorganic/organic montmorillonite (PGW) and
fluorohectorite (FH) clays prepared by ion exchange of
the inorganic cations Na^+ , Li^+ or H^+ with onium ions of
diprotonated D2000.

Figure 5.2 X-ray diffraction patterns of mixtures of the mixed-ion clay 173
 $\text{Li}/\text{D}2000_{0.65}\text{-FH}$, the epoxy monomer EPON 826 and the
curing agent D230: (A) after intercalation of EPON 826 in
 $\text{Li}/\text{D}2000_{0.65}\text{-FH}$ at 50°C for 12 hrs, (B) after addition of
D230 to the mixture of step A and outgassing at 25°C ,
and (C) after curing at 75°C , 3 hrs and 125°C , 3hrs (the
clay loading was 6 wt. % silicate basis). The inset shows
the presence of an in-plane 060 clay reflection in the
cured nanocomposite

Figure 5.3 TEM images of thin sections of the glassy epoxy 177

nanocomposites prepared from the mixed-ion clays (a,b) Li/D2000_{0.65}-FH. The clay loading of the nanocomposite samples was 6 wt. % silicate basis.

Figure 5.4 TEM images of thin sections of the glassy epoxy 178 nanocomposites prepared from the mixed-ion clays (a,b) H/D2000_{0.5}-PGW. The clay loading of the nanocomposite samples was 6 wt. % silicate basis.

Figure 5.5 Dynamic Mechanical Analysis measurements: (a) Storage 181 Modulus vs. temperature and (b) $\tan\delta$ vs. temperature, for (A) Pristine-A epoxy polymer and for the nanocomposite samples prepared from (B) H-PGW, (C) H/D2000_{0.25}-PGW, (D) Li/D2000_{0.65}-FH, (E) D2000-PGW. The clay loading of the nanocomposite samples was 6 wt. % silicate basis .

Figure 5.6 TGA curves of the mixed-ion clays (A) H/D2000_{0.35}-PGW 187 and (B) Li/D2000_{0.35}-PGW, the nanocomposites prepared from (C) H/D2000_{0.25}-PGW and (D) D2000-PGW clays, and of the Pristine-A epoxy polymer (E). The clay loading of the nanocomposite samples was 6 wt. % silicate basis.

Chapter 1

INTRODUCTION

1.1 Nanocomposite Materials

1.1.1 Nanocomposite Concept

Multi-matrix materials consisting of a stiff reinforcement phase embedded in a polymeric phase fall into the general class of composite materials. Due primarily to the improvement in mechanical properties not obtainable by either parent end member independently, such materials have found widespread applications in nearly every facet of the modern world. For this reason, accompanied with the drive to produce more environmentally sensitive materials in place of energy consuming metal -based components, composites have been intently studied recently and a variety of new classes have been explored. One such relatively young category of composite materials exhibits a change in composition and structure over a nanometer length scale.¹⁻⁷ These nano-scaled hybrid materials, termed nanocomposites, have been shown in the last decade to afford remarkable property enhancements relative to conventionally scaled composites.

1.1.2 Nanocomposite Significance

The macroscopic effect of downsizing the filler size of composite materials is remarkably manifested on the performance properties of the final material.

Through decreasing the size of the reinforcement phase by three orders of magnitude, which is typical in going from conventionally scaled composites to nanocomposites, the surface area to volume ratio, and thus the interfacial contact between the dissimilar components is monumentally greater for the nano-scaled material. This results in a more efficient transfer of potentially damaging forces to the stronger filler phase, rendering the strained polymer matrix more unaffected in nanocomposites compared to conventional composites. Also important to note is the ability of a smaller reinforcement phase to influence more of the polymer at much reduced loadings, giving rise to significantly lighter materials. This is a primary driving force for the expansion of nanocomposite use, as the notion of lower weight structural parts is of principal concern in modern development of the automobile and aeronautical industries. The need for large volume fractions of conventional fillers to achieve the desired characteristics in the final material also adds to the overall cost, as typical conventional reinforcers, such as fiber glass and graphite, are relatively expensive materials, especially if they need to be modified prior to addition to the polymer. The layered silicates, on the other hand, are found ubiquitously in nature and can be made polymer – ready through relatively inexpensive purification means.⁸⁻¹⁰

1.1.3 Sol-Gel Synthesized Nanocomposites

The use of naturally occurring layered silicates is not the only nano-scaled reinforcement phase used in strengthening polymer media. Another approach to inorganic – organic hybrid materials involves the hydrolysis and condensation of

metal oxide precursors from metal alkoxides in the presence of similarly functionalized polymer precursors.^{3, 11} The most common polymer reinforced in this way is polydimethylsiloxane, and a general depiction of this synthetic scheme is illustrated in figure 1.1.

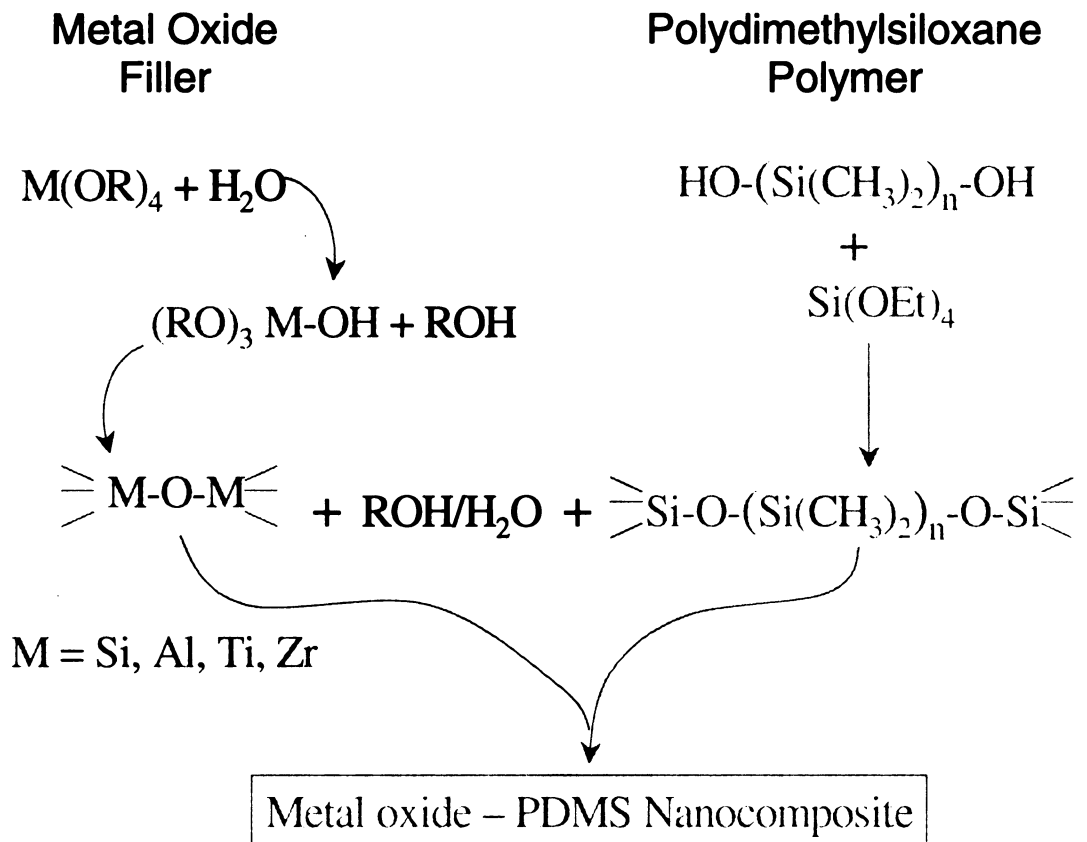


Figure 1.1 Depiction of the sol-gel approach to synthesizing nanocomposites indicating the metal oxide filler phase and the polymeric silicone precursor.

1.1.4 Layered Silicate Nanocomposites

The morphology of layered silicates, which will be described more in depth shortly, makes them particularly suitable for use as a reinforcement phase in engineering nanocomposites. Their platy, high aspect ratio structure lends such silicates towards better interfacial interactions at the polymeric boundary relative to larger scaled, more spherical reinforcement phases. The chemical makeup of these clay materials consists of a dimensionally stable silicon – oxygen network with four parallel oxide layers making up each individual silicate sheet.¹² The robust, stiff nature of the clay layers is not easily exploited in polymeric matrices, however, due to the strong tendency of the layers to form face – to – face stackings, or tactoids, that are difficult to separate into individual layers. This dilemma can be thwarted by the use of a particular class of layered silicates employed as the reinforcer, the smectite clays. As will be discussed in section 1.1.5, there are a variety of layered silicates that occur naturally, and these can be distinguished from one another and separated into classes based on the charge carried in each layer. Smectite clays are in the middle of the charge density continuum, giving maximum swellability of the layers and thus providing a means of disseminating the sheets. This occurs due to the fact that layered silicates carrying too low a charge density, ie talcs, reduces or nullifies (in the case of a neutral layer) the driving force to uptake solvent into the ionic gallery regions, while too high a charge density, ie micas, causes an electrostatic interaction between adjacent layers that cannot be overcome and the layers are essentially locked together. The ability to disseminate smectite tactoids through

solvent swelling is what has extended the practical applications of these minerals to absorbants, lubricants, rheological fluids and, more recently, polymeric reinforcers.

1.1.5 Smectite Clay Structure

Clay minerals are largely two - dimensional layered silicates with individual particle sizes on the order of $\sim 2\mu\text{m}$, depending on the specific type of clay. The aforementioned oxide network (composed of four discrete 001 planes) gives rise to what is known as a 2:1 mica – type morphology with a layer thickness of 9.6 \AA . In the notation, “2” indicates the presence of two tetrahedral silica – based sheets that lie on either side and form a sandwich with “1” octahedral sheet. The central octahedral layer is composed of edge – shared octahedra with the coordination sites generally occupied by aluminum or magnesium, while the tetrahedral layers are made up of corner – shared SiO_4 units. Variations in the clay charge density stems from isomorphous substitution of lower valent metal ions in either of the layers (e.g. Al^{+3} for Si^{+4} in the tetrahedral sheet, or Li^+ for Mg^{+2} ; Mg^{+2} or Fe^{+2} for Al^{+3} in the octahedral sheet), or site vacancies giving rise to a net negatively charged layer. The gallery cations, ordinarily Na^+ , K^+ or Ca^{+2} , are located between the clay layers and electrostatically balance the charge. Figure 1.2 illustrates a typical smectic clay layer.¹²

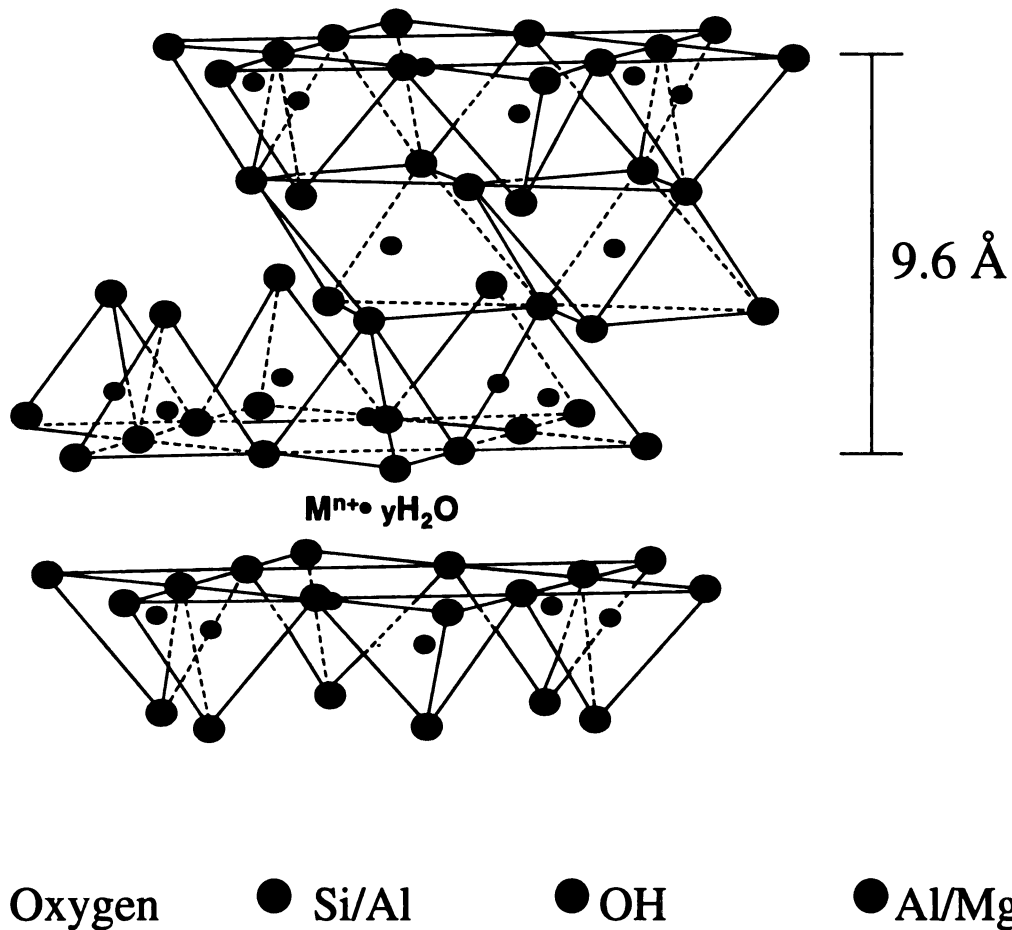
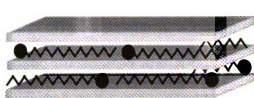


Figure 1.2 Illustration of the layered oxide framework of smectite clays. Clay layers consist of two tetrahedral sheets sandwiching a central octahedral layer. $M^{n+} \cdot yH_2O$ represents the interlayer exchangeable cation with its coordination sphere of water molecules.

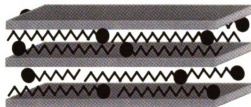
Clay does not exist naturally as discrete layers, but instead stacks face – to – face in turbostratic (only aligned in one direction) tactoids. While the presence of inorganic gallery cations makes the clay hydrophilic and, in the case of the smectites, easily swollen with water, the cations are readily exchangeable and upon the ion exchange with carbon - based surfactants the galleries become organophilic. The morphology and intercalation properties of these organic clays (organoclays) have been studied extensively and will be briefly covered here.

1.1.6 Organoclay Structures and Properties

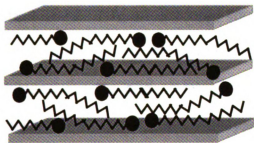
Unlike inorganic clays, the greater volume of the charge balancing surfactant molecules in organoclays yields multiple potential intragallery morphologies. Depending on the charge density of the clay and the alkyl chain length of the onium ion, a variety of well-documented surfactant packing orientations are possible. In general, the longer the surfactant chain length and the higher the charge density of the clay, the further apart the clay layers will be forced. This is expected since both these parameters contribute to increasing the volume occupied by the intragallery molecules. For low volume content organics, the onium ions may lie parallel to the clay surface as a monolayer, and as the amount of organic in the galleries is increased the adopted conformations exist as a lateral bilayer, a pseudo – trilayer or an inclined paraffin structure. At very high surfactant concentrations, a lipid bilayer may be necessary to account for such a large organic content between the clay sheets. Figure 1.3 indicates the different organoclay arrangements possible for smectite clays.¹³



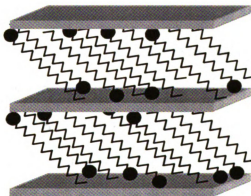
Monolayer organoclay arrangement



Bilayer organoclay arrangement



Tri-layer organoclay arrangement



Paraffin organoclay arrangement

Figure 1.3 Illustration of four possible organoclay structures based on surfactant packing density. Given the same surfactant, increasing the charge density of the clay will move from a monolayer arrangement towards the paraffin structure.

The orientations of onium ion chains in organoclay were initially deduced based on infrared and X-ray diffraction measurements. More recent modeling experiments have provided further insights into the packing arrangements of the alkyl chains in the confined environments of layered silicates.¹⁴ Molecular dynamics simulations were used to study molecular properties such as density profiles, normal forces, chain configurations and trans – gauche conformer ratios. For the mono-, bi- and psuedo – trilayers, with respective basal spacings of 13.2, 18.0 and 22.7 Å, a disordered liquid – like arrangement of chains was preferred in the gallery. In this disordered arrangement the chains do not remain flat, but instead overlap and co-mingle with onium ions in opposing layers within the galleries. However, for the trilayer orientation, the methylene groups are found primarily with a span of two atomic layers and only rarely do they continue into the layer opposite to the positive head group. As anticipated, the onium head group is also noted to reside nearer the silicate surface relative to the aliphatic portion of the surfactant. The highest preference conformer is trans over guache for the maximum surfactant chain length just before the system progresses to the next highest layering pattern. This is expected since the alkyl chains must be optimally packed under such dense surfactant concentrations.

The replacement of inorganic exchange cations by organic onium ions on the gallery surfaces of smectite clays not only expands the interclay distance, but also serves to match the clay surface polarity with the polarity of the polymer. Given a sufficient polarity match between the polymer and clay galleries, the organoclay galleries will swell further upon intercalation by the polymer.

Exemplary pre-polymers that have shown such behavior include caprolactam¹⁵, epoxides¹⁶⁻¹⁸, silicones^{19, 20} and polyols²¹. For long chain onium – exchanged organoclays, the galleries swollen by these precursors typically show a d-spacing indicative of a paraffin monolayer arrangement.

1.1.7 Organoclay – Polymer Interactions

Despite having an ideally matched system, where unreacted polymeric precursors intercalate readily into organoclay galleries, there is still a large possibility that these will not form a true nanocomposite. Only when the clay layers are forced apart and no longer interact through the onium chains is an ideal nanocomposite formed²². The complete dispersal, or exfoliation, of the clay nanolayers yields composites with the highest degree of property enhancement. Composite materials retaining a regular gallery height equal to less than two times the surfactant chain length, then the amount of polymer interacting with the clay surface is limited, and intercalated composites are formed. Such materials lack the desired degree of layer expansion and as a result will have distinct regions with either a very high or low to non-existent concentration of reinforcement fillers. This non-uniform dispersal of nanolayers limits stress transfer throughout the composite, giving comparatively less than optimal reinforcement. Still poorer, conventionally scaled composites are possible if the polymer and smectic clay exhibit only partial miscibility. Here the clay persists as tactoids of face – to – face stacked agglomerates throughout the polymer matrix. This incomplete dispersal of the reinforcing phase inhibits ideal surface contact between the polymer and clay²³, creating large voids of pure polymer in the

composite. Figure 1.4 represents the different possible composite morphologies and representative XRD patterns of each.

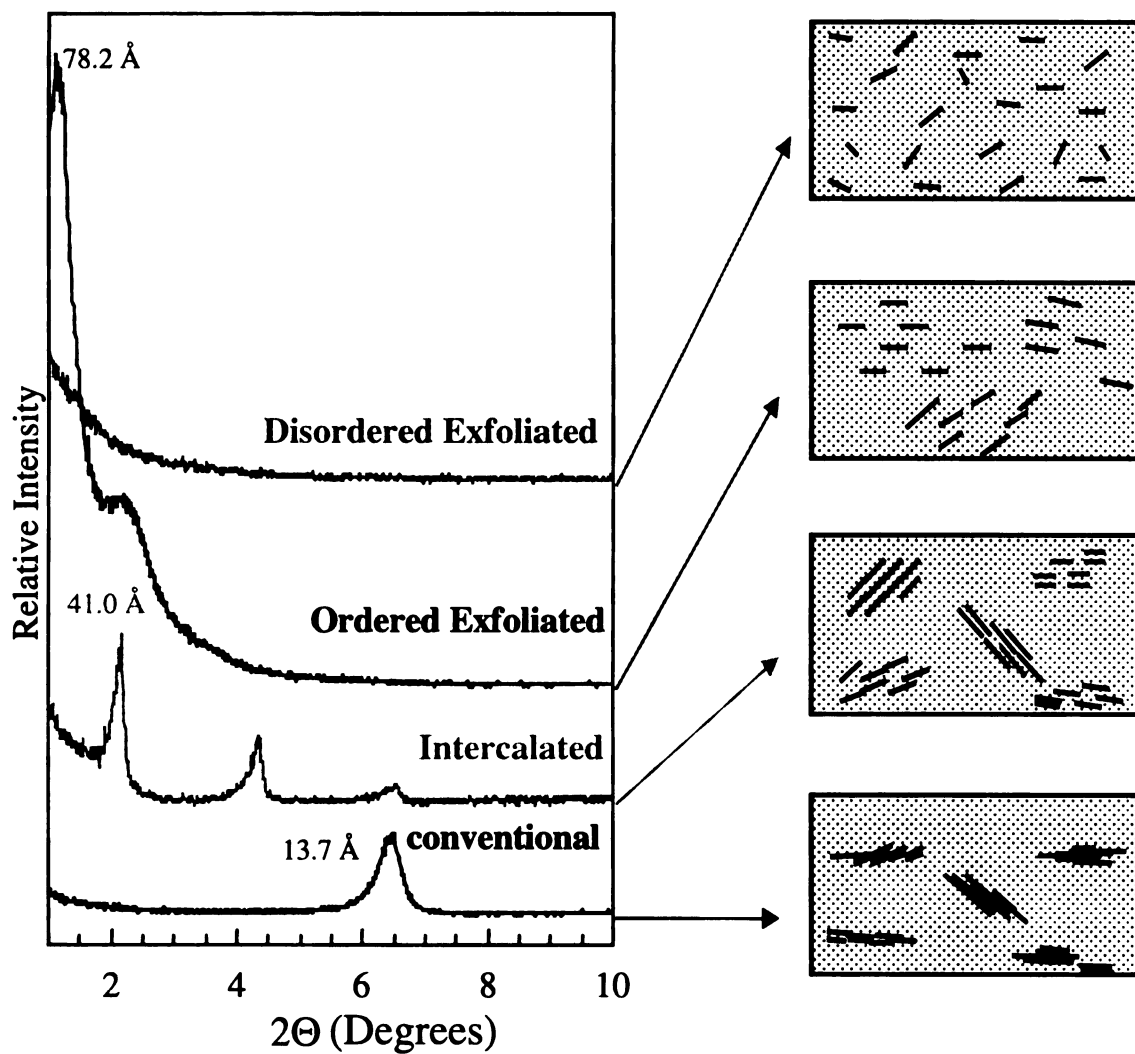


Figure 1.4 Schematic of the different composite morphologies possible when attempting to synthesize polymer - clay nanocomposites. Representative XRD patterns are displayed for each type.

Above and beyond intercalation of the polymer precursors, the ideal exfoliated case requires an increased reaction rate in the confined gallery spaces relative to the bulk crosslinking. This creates larger and faster forming crosslinked polymer domains between clay layers, thus providing a driving force for layer expansion. In the majority of successful exfoliated systems acidic sites present in the clay galleries provide the bias for intragallery polymerization.^{17, 24} These can catalyze the crosslinking process, as is the case in the ring opening polymerizations of epoxy and caprolactam.

1.1.8 Properties of Thermoset – Clay Nanocomposites

The presence of exfoliated clay layers in a polymer matrix has a dramatic affect on the physical properties of the filled system. Typically the most sought after final nanocomposite characteristics involve improved mechanical behavior. Increasing the tensile strength, the elongation at break and the modulus (stiffness) of polymer materials allows for a lighter weight alternatives to structural metals and conventionally filled plastics. The nanolayers, however, do not only provide a reinforcing affect to the polymer matrix. Other studies, for example, focusing strictly on the ablative performance of polymer – clay nanocomposites have also been explored.²⁵ Here the nanocomposites are subjected to extreme temperatures in the absence of oxygen, and their ability to form a protective ceramic char on the exterior are determined. Applications in the aerospace industry as protective shields serve as the driving force for such studies. The impermeable nature of the silicate layers have been shown to dramatically lower the diffusion of small molecule permeants in certain

nanocomposite materials.²⁶⁻²⁹ In this case the clay layers act as a barrier and mandate a more tortuous and longer effective diffusion pathway through the polymer matrix. A schematic representing this hypothesis for the reduction in permeability is shown in figure 1.5.

Another polymeric property that can be improved by the introduction of disseminated clay particles is thermal stability.³⁰⁻³⁴ This “inflammable” or self – extinguishing characteristic noted in certain nanocomposites likely stems from the tortuous diffusion path noted above. Both the influx of oxygen necessary for combustion to occur, and the outflux of small molecule degradation upon burning are slowed due to the presence of the clay layers. Other properties that can be influenced by the exfoliation of silicate layers include rheological behavior, minimizing solvent uptake and optical properties.^{29, 35, 36}

1.1.9 Exfoliated Nylon-6 – Clay Nanocomposites

The first example of successfully exfoliated layered silicates in a polymer matrix was accomplished by researches at Toyota^{15, 24, 37, 38}. By ion exchanging Na⁺ cations present on naturally occurring montmorillonite clay with organic amine surfactants, the intercalation of nylon – 6 precursors was possible. They used an amino acid – modified organo-montmorillonite to intercalate cyclical caprolactam, the precursor to thermoplastic nylon – 6. The seven membered ring caprolactam monomers can be liquefied at 70°C, at which point they were added to the organoclay, and a 15 Å basal increase upon intercalation was noted. Upon further heating, at a temperature of 250°C, the caprolactam begins to ring open and form nylon – 6. The organic modifier, a protonated C12 alpha, omega amino acid, was thought to aid in the intragallery ring opening polymerization by acid – catalysis. The clay layers were almost completely delaminated after completion of the polymerization, as noted by low angle X-ray

diffraction. The general synthetic procedure for forming nylon – 6 nanocomposites is illustrated in figure 1.6.

Synthetic Procedure for Nylon – 6 Nanocomposites

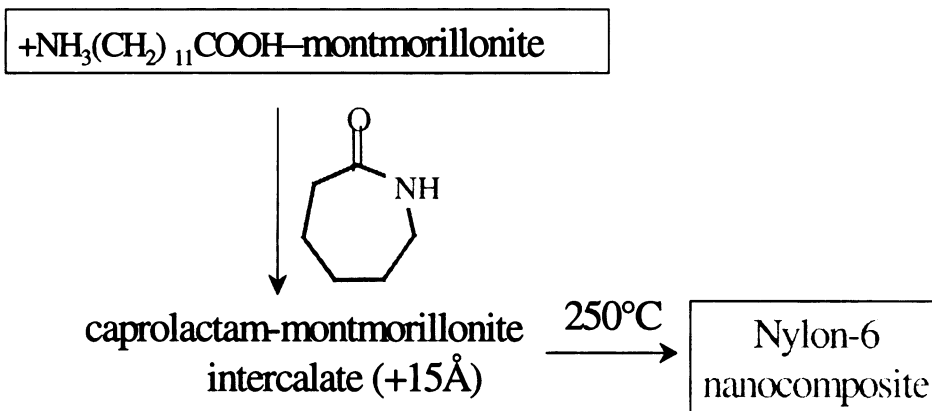


Figure 1.6 General synthetic route for synthesizing nylon – 6 nanocomposite materials. The caprolactam precursors were first melted, then added to the organoclay to permit intercalation (causing a 15 Å basal spacing increase), and finally polymerized at 250°C.

The nylon – 6 nanocomposites exhibited substantial increases in mechanical properties due to the reinforcing clay particles. These improvements ultimately lead to their use in under – the – hood applications in certain Toyota automobiles as a timing belt cover. The mechanical properties of the hybrid material compared to pristine nylon and unexfoliated clay in nylon is described in table 1.1.

Table 1.1 Mechanical and Thermal Properties of Nylon-6

Material type	Wt. % clay	Tensile strength (Mpa)	Tensile modulus (GPa)	Impact (kJ/m ²)	HDT (°C) at 18.5 kg/cm ²
Exfoliated Nanocomposite (clay layers)	4.2	107	2.1	2.8	145
Conventional Composite (clay tactoids)	5.0	61	1.0	2.2	89
Pristine nylon	0	69	1.1	2.3	65

1.2 Recent Developments in Polymer – Clay Nanocomposites

Many of the advances in nanocomposite technology over the past few years have involved the extension of the concept into different polymer systems. Each polymeric medium, whether it be polyimide, polyether, epoxy, or polysiloxane, demands its own reinforcement modification and synthetic

procedures to successfully exfoliate clay in the matrix. In general, the first requirement that must be met is to ensure that the interclay regions are compatible with the polymer precursors. This provides a driving force for intercalation and swelling of the clay galleries. While many systems have the potential for monomer intercalation, true nanocomposites are not formed due to the lack of clay expansion upon crosslinking. As aforementioned, the ability to chemically alter the environment inside the clay galleries so as to significantly bias the reaction rate over that of the bulk is paramount in achieving ideal nanocomposites.

Although statistically impressive to report, the rubbery polymer matrices that have been reinforced through the years are somewhat limited in their practical applications. A recent push to create nanocomposites from more rigid parent matrices has improved the possibilities of finding structural replacements for steel and other alloys^{39, 40}. Unlike the balance of epoxy nanocomposite work, the results expressed in this thesis are based on glassy systems.

One very practical and widely studied polymer nanocomposite system is polypropylene. Polypropylene is a thermoplastic that is widely used in low – stress situations, however, by stiffening the matrix through nanolayer reinforcement, researchers hope to extend its use to more demanding, load – bearing applications. The dispersal of clay nanolayers into polyolefin systems proved to be a challenge due to the extreme hydrophobicity of the polymer. Initial attempts to create polypropylene – clay hybrids were based on the introduction of a modified polypropylene with polar groups in attempt to mediate

the polarity between the clay surface and bulk polypropylene.^{41, 42} However, an organic solvent has to be used in order to facilitate the formation of a modified polypropylene intercalate. Only a limited degree of clay nanolayer dispersion was observed by this method. An alternative and more environmentally friendly approach was developed later by the Toyota research group⁴³⁻⁴⁵. A mixture of stearylammmonium - exchanged montmorillonite, maleic anhydride modified polypropylene oligomer and homopolypropylene was melt-processed to obtain a successful polypropylene - clay hybrid wherein a larger fraction of the clay nanolayers were found to be exfoliated. The hydrolyzed maleic anhydride polypropylene intercalated into the organoclay, expanding the galleries and facilitating the incorporation of unmodified polypropylene. Interestingly, the density of maleic anhydride groups has a significant effect on the final morphology and properties of the composite. A mixture of roughly 3:1 maleic anhydride polypropylene to organoclay was found to be the most effective in forming hybrid composites. The hybrids exhibit improved storage moduli compared to pristine polypropylene in the temperature range from T_g to 90°C. The significance of nanolayer reinforcement in polypropylene is not as great as in nylon 6, probably due to the lower degree of exfoliation and the introduction of a large amount of low molecular weight oligomer.

1.3 Research Objectives

1.3.1 Current Issues and New Directions

Although the nanocomposite concept has only been studied for roughly a decade, many significant developments pertaining to the importance of the clay –

polymer interactions, the use of different nanoscaled reinforcers, and the quantification of how much reinforcement is possible, or how much organic modification is necessary have been observed. The Pinnavaia group has been involved in several of these issues, including the recent drive to elucidate the type and extent of organic modification needed specifically in epoxy nanocomposites.

Other recent avenues in nanocomposite technology have revolved more on permeability reduction and packaging applications versus the mechanical improvement of engineering plastics. Although the physical fortification properties will always be the primary goal of nanocomposite materials, secondary improvements, such as inflammability and solvent resistance, will continue extend the applications of clay – modified polymers.

Thermoplastic melt intercalation of liquid polymer into clay galleries is another field that has become attractive for study. Here the polymer is heated in excess of its melting point and added to organo – functionalized clay. The mixture is then put through high shear in attempt to physically disperse the clay from aggregated tactoids to near individual layers. The high shear is provided by means of a twin – screw extruder, which forces the polymer melt and clay through a high pressure gap.

1.3.2 Research Goals

Two thermoset systems, silicones and epoxies, will be examined for their capability to form exfoliated nanocomposites. Instead of simply synthesizing the nanocomposites and comparing final properties with unfilled polymers, the

exfoliation mechanism is to be considered along with thorough investigations on the unreacted pre-polymer – clay interactions. Although in the past typical nanocomposite work has involved fully organo – exchanged layered silicates, the reliance on organic modification for successful nanocomposites will be examined, and composite materials lacking the customary surfactant molecules also will be explored.

Specifically, the pristine polydimethylsiloxane rubber is in dire need of mechanical improvement, and this is the area of primary concern. Silicones also are extremely permeable, and nanocomposites with improved barrier properties will also be addressed. Although silicone – clay hybrid materials have been previously studied, the reaction mechanism was unmentioned, and thus this work sets out to elucidate the nature of the clay layer expansion and the driving forces for exfoliation. Related somewhat to the high permeability of silicones is the susceptible nature to extensive swelling, and ultimately sample failure caused by large uptake of organic solvent into the matrix. Of primary concern in this work is to reduce this tendency in order to yield robust rubber materials that in the future may find applications as sealants and gaskets where current silicones would fail. While the high permeability of silicone rubber is often thought to be a detriment, this work will make use of this fact and investigate post – cure nanocomposite chemical modification previously unexplored.

As aforementioned, the main issue with epoxy nanocomposites is that previous work has focused primarily on subambient T_g networks that have limited practical implications. One goal in this work is to study glassy systems and

improve their already impressive mechanical properties. Instead of solely using purely organic modified clays to achieve this goal, various mixed ion inorganic – organic clay fillers will be explored.

Characterization of the pre-polymerized and post – cured nanocomposites will be performed primarily by X-ray diffraction, accompanied with Transmission Electron Microscopy in order to fully understand the nature of clay layers in the polymer matrix.

1.3.3 References

1. Novak, B.M., *Advanced Materials*, 1993. **5**(6): p. 422-433.
2. Schmidt, H., *J. Non-Cryst. Solids*, 1985. **73**: p. 681-691.
3. Mark, J.E., *Polym. Eng. Sci.*, 1996. **36**(6): p. 2905-2920.
4. Okada, A. and A. Usuki, *Materials Science & Engineering C- Biomimetic Materials Sensors and Systems*, 1995. **3**(2): p. 109-115.
5. Giannelis, E.P. and P.B. Messersmith, *PCT Int. Appl.* 1996, (Cornell Research Foundation, Inc., USA). Wo. p. 32 pp.
6. Ogawa, M. and K. Kuroda, *Bulletin of the Chemical Society of Japan*, 1997. **70**(11): p. 2593-2618.
7. Pinnavaia, T.J., Beall, G.W., eds., 2000: *Jonh Wiley & Sons Ltd*, New York.

8. Fukushima, H. and L.T. Drzal, Proc. Annu. Meet. Adhes. Soc., 2000. **23rd**: p. 189-191.
9. Kojima, Y., et al., Journal of Polymer Science Part a-Polymer Chemistry, 1993. **31(4)**: p. 983-986.
10. Gilman, J.W., et al., Proc. Int. Wire Cable Symp., 1997. **46th**: p. 761-774.
11. Giannelis, E.P. and J.L. Keddie, 1993, (Cornell Research Foundation, Inc., USA). Us. p. 9 pp.
12. Pinnavaia, T.J., Science, 1983. **220(4595)**: p. 365-371.
13. Lagaly, G., Solid State Ionics, 1986. **22(1)**: p. 43-51.
14. Hackett, E., E. Manias, and E.P. Giannelis, Journal of Chemical Physics, 1998. **108(17)**: p. 7410-7415.
15. Usuki, A., et al., Abstracts of Papers of the American Chemical Society, 1990. **200**: p. 218-POLY.
16. Wang, Z., T. Lan, and T.J. Pinnavaia, Abstracts of Papers of the American Chemical Society, 1996. **211**: p. 455-INOR.
17. Wang, Z. and T.J. Pinnavaia, Chemistry of Materials, 1998. **10(7)**: p. 1820-1826.
18. Massam, J., et al., Book of Abstracts, 215th ACS National Meeting, Dallas, March 29-April 2, 1998: p. PMSE-206.
19. LeBaron, P.C. and T.J. Pinnavaia, Chem. Mater., 2001: p. ACS ASAP.

20. Burnside, S.D. and E.P. Giannelis, *Chemistry of Materials*, 1995. **7(9)**: p. 1597-1600.
21. Wang, Z. and T.J. Pinnavaia, *Chemistry of Materials*, 1998. **10(12)**: p. 3769-+.
22. LeBaron, P.C., Z. Wang, and T.J. Pinnavaia, *Applied Clay Science*, 1999. **15(1-2)**: p. 11-29.
23. Shi, H.Z., T. Lan, and T.J. Pinnavaia, *Chemistry of Materials*, 1996. **8(8)**: p. 1584-&.
24. Okada, A., et al., *Mater. Res. Soc. Symp. Proc.*, 1990. **171**(Polym. Based Mol. Compos.): p. 45-50.
25. Vaia, R.A., et al., *Applied Clay Science*, 1999. **15(1-2)**: p. 67-92.
26. Kojima, Y., et al., *Journal of Applied Polymer Science*, 1993. **49(7)**: p. 1259-1264.
27. Kojima, Y., et al., *Journal of Materials Science Letters*, 1993. **12(12)**: p. 889-890.
28. Yano, K., A. Usuki, and A. Okada, *Journal of Polymer Science Part a-Polymer Chemistry*, 1997. **35(11)**: p. 2289-2294.
29. LeBaron, P.C. and T.J. Pinnavaia. *Abstracts of Papers*, 222nd ACS National Meeting, Chicago, IL, United States, August 26-30, 2001, 2001: p. IEC-041.
30. Gilman, J.W., T. Kashiwagi, and J.D. Lichtenhan, *Sampe Journal*, 1997. **33(4)**: p. 40-46.

31. Gilman, J.W. and A. Morgan, Recent Adv. Flame Retard. Polym. Mater., 1999. **10**: p. 56-67.
32. Gilman, J.W., et al., Chem. Technol. Polym. Addit., 1999: p. 249-265.
33. Gilman, J.W., et al., Polym. Mater. Sci. Eng., 2000. **83**: p. 59-60.
34. Giannelis, E.P., Annu. Tech. Conf. - Soc. Plast. Eng., 1996. **54th**(Vol. 3): p. 2998-3003.
35. Burnside, S.D. and E.P. Giannelis, Journal of Polymer Science Part B-Polymer Physics, 2000. **38**(12): p. 1595-1604.
36. Wang, Z., P.C. LeBaron, and T.J. Pinnavaia, Addit. '99, Int. Conf., 8th, 1999: p. Paper10/1-Paper10/9.
37. Usuki, A., et al., Journal of Materials Research, 1993. **8**(5): p. 1174-1178.
38. Usuki, A., et al., Polym. Prepr. (Am. Chem. Soc., Div. Polym. Chem.), 1990. **31**(2): p. 651-2.
39. Massam, J. and T.J. Pinnavaia, Material Research Society Symposium Proceedings, 1998. **520**: p. 223-232.
40. Triantafillidis, C.S., et al., Abstracts of Papers, 222nd ACS National Meeting, Chicago, IL, United States, August 26-30, 2001, 2001: p. IEC-109.
41. Kurokawa, Y., H. Yasuda, and A. Oya, Journal of Materials Science Letters, 1996. **15**(17): p. 1481-1483.

42. Kurokawa, Y., et al., *Journal of Materials Science Letters*, 1997. **16**(20): p. 1670-1672.
43. Kawasumi, M., et al., *Macromolecules*, 1997. **30**(20): p. 6333-6338.
44. Kato, M., A. Usuki, and A. Okada, *Journal of Applied Polymer Science*, 1997. **66**(9): p. 1781-1785.
45. Hasegawa, N., et al., *Journal of Applied Polymer Science*, 1998. **67**(1): p. 87-92.

Chapter 2

CLAY NANOLAYER REINFORCEMENT OF A SILICONE ELASTOMER: EXFOLIATION OF FLUOROHECTORITE IN POLYDIMETHYLSILOXANE

2.1 Introduction

As has been demonstrated quite convincingly in a recent comprehensive review,¹ the insertion of organic molecules into layered or porous inorganic hosts often results in nanocomposite materials with properties dramatically different from the parent end members. Nanocomposites differ from conventional composites in that the mixing of phases occurs over a much smaller length scale in comparison to the micrometer length scale of conventional composites.²⁻⁴ Employing a filler phase that has such a dramatic size reduction results in heightened interfacial interactions between the polymeric matrix and the fortifying inorganic support, thus facilitating a more efficient transfer of an applied load. When applied to the reinforcement of engineering polymers the nanocomposite concept can lead to compositions with properties far superior to conventional composites at a much reduced filler loading. The weight savings is particularly important for the automobile and aeronautical industries where 25-40% weight addition of reinforcement is necessary to achieve the desired properties.

Layered-silicate clays are particularly good candidates for the nanoparticle strengthening of polymers due, in part, to their high surface area, platy morphology and exceptionally stable oxide network.⁵ In certain respects the

layered silicate clays share some of the same characteristics as the aerogel silicas and precipitated silicas used for the reinforcement of silicones and other polymer systems. However, in comparison to small particle silicas⁶, clays are less costly and free of health risks, adding to their attractiveness as a replacement filler for silicones. Furthermore, the rich intercalation chemistry associated with smectic clays can be used to facilitate the dispersion of the nanolayers in a polymer matrix, a feat unobtainable with conventional silica nanoparticles that tend to undergo phase-segregation in a silicone matrix.⁷ The generally spherical particle morphology inherent in aerogel silica is also a detriment to reinforcement when compared to the high aspect ratio nanoplates of individual clay particles.

Toyota researchers were the first to demonstrate that small quantities (<10 wt %) of organoclays exfoliated in a Nylon-6 polymer matrix greatly improves the thermal, mechanical, barrier and flame retardant properties of the polymer.⁸⁻¹¹ In recent years, several other polymer systems have been investigated including epoxies¹²⁻¹⁵, polyimides¹⁶⁻¹⁸, polyurethanes¹⁹, polysiloxanes^{7,20} as well as various thermoplastics²¹⁻³⁰. In earlier studies of polysiloxane - organoclay nanocomposites, - dimethylditallow and - hexadecyltrimethyl ammonium exchanged montmorillonites were dispersed in polydimethylsiloxane (PDMS) with a molecular weights of 18,000 and 68,000, respectively, and crosslinked to a rubber by reaction with tetraethylorthosilicate (TEOS). The former system afforded an exfoliated clay nanocomposite, whereas in the latter the clay was only partially exfoliated, as indicated by low angle X-ray reflection in the final

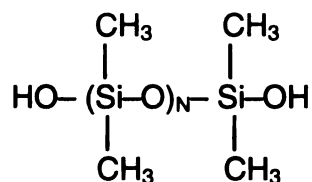
composite. Both clays, however, provided elastomer reinforcement, as well as improved thermal and solvent barrier properties^{7,20}. In order to influence the greatest portion of the polymer matrix at the same clay loading, the more exfoliated nanocomposite materials are generally the ultimate goal.

In an effort to elucidate the swelling of organoclay galleries by PDMS, we have examined the intercalation properties of a synthetic fluorohectorite in PDMS polymers with molecular weights in range 400 to 4200. These smaller PDMS polymers make it possible to follow the gallery expansion process quantitatively by wide angle X-ray diffraction methods. Also, the synthetic fluorohectorite used in this work has a substantially larger nanolayer aspect ratio (~2000) in comparison to naturally occurring montmorillonite (~ 200). The higher nanolayer aspect ratio should provide even better reinforcement and barrier properties, the two performance properties in need of greatest improvement for silicone rubbers. Having a larger individual particle size, the fluorohectorite also aids in monitoring the true nature of the hybrid materials during and after polymerization by X-ray diffraction, in agreement with the Scherrer Equation. Accordingly, we also have prepared a crosslinked silicone rubber - exfoliated fluorohectorite nanocomposite and investigated its tensile strength, dioxygen permeability and solvent uptake properties in comparison to the pristine elastomer. The results clearly demonstrate the substantial reinforcement that is possible at clay nanolayers loading of 5 to 10 wt%, though the permeability of the nanocomposites remains high despite the larger nanolayer aspect ratio.

2.2 Experimental

Materials. PDMS polymers with average molecular weight values of 400, 1750 and 4200 and tin(II) 2-ethylhexanoate were obtained from Gelest, Inc. Hexadecyltrimethylammonium bromide and all other chemicals were purchased from Aldrich Chemical Co. and used without further purification.

Polydimethylsiloxane (PDMS)



Tetraethylorthosilicate (TEOS)

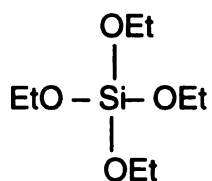


Table 2.1 Silanol Terminated PDMS Monomers

PDMS MW	N value (Si(CH₃)₂-O repeat)	Viscosity (cSt)
400	6	20
1500-2000	23	45-85
4200	57	90-120
18000	243	700-800

Organoclay Synthesis

Lithium fluorohectorite (Coming, Inc.) with an anhydrous unit cell formula of $\text{Li}_{1.12}[\text{Mg}_{4.88}\text{Li}_{1.12}](\text{Si}_{8.00})\text{F}_4$ was ion-exchanged with a two-fold stoichiometric excess of hexadecyltrimethylammonium bromide. A mixture of the surfactant cations and a 1.0 wt % aqueous suspension of the inorganic clay was stirred at room temperature for 12 hours. The flocculated organoclay was removed by vacuum filtration and the excess surfactant was washed from the clay by re-suspending the solid in water, filtering again, and then subjecting the solid to a final Soxhlet extraction in ethanol for 24 hours. The clay was then dried, crushed and sieved to a particle size $<106 \mu\text{m}$ prior to use in the intercalation and nanocomposite studies. The water and organic content of the air-dried organoclay, as determined by the weight loss at 150°C and 500°C , was 6 wt % and 24 wt %, respectively. A general depiction of the ion exchange is shown in figure 2.1.

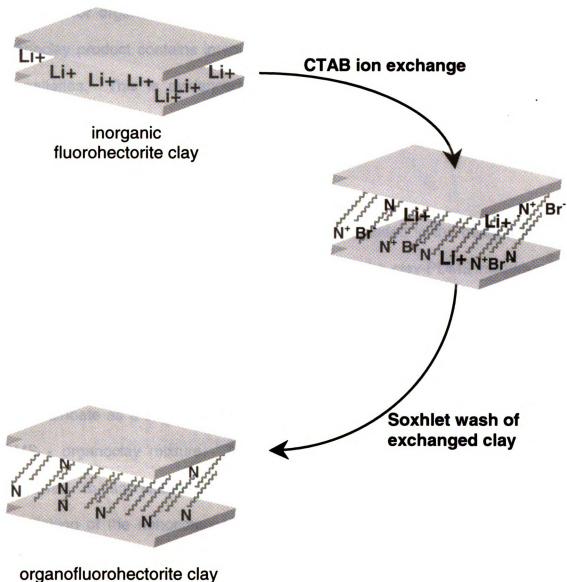


Figure 2.1 Schematic illustrating the organic ion exchange of fluorohectorite clay using cetyltrimethylammonium bromide.

The need for organoclay washing is shown in figure 2.1 as the intermediate organoclay product contains intersalated (intercalated salt) ion pairs trapped in the galleries. This is evidenced by powder diffraction as a secondary 001 shoulder at a slightly higher basal spacing than the pure (washed) organoclay.

Nanocomposite Synthesis

A predetermined amount of organoclay was added to the desired PDMS pre-polymer and mixed for 12 hours. Agitation of the clay-PDMS mixture was accomplished by first manual stirring with a spatula followed by vortexing the suspension for several minutes. A stoichiometric amount of tetraethylorthosilicate (TEOS) as a crosslinking agent and tin(II) 2-ethylhexanoate as a catalyst (TEOS : Sn = 4 : 1 by volume) were added to the PDMS - organoclay mixture. The resulting thixotropic intercalate was then transferred to an stainless steel mold and out gassed under vacuum. Crosslinking of the nanocomposite was carried out under vacuum at ambient temperature for 12 hours, followed by an additional 12 hours at 100 °C remaining under vacuum, as indicated in figure 2.2.

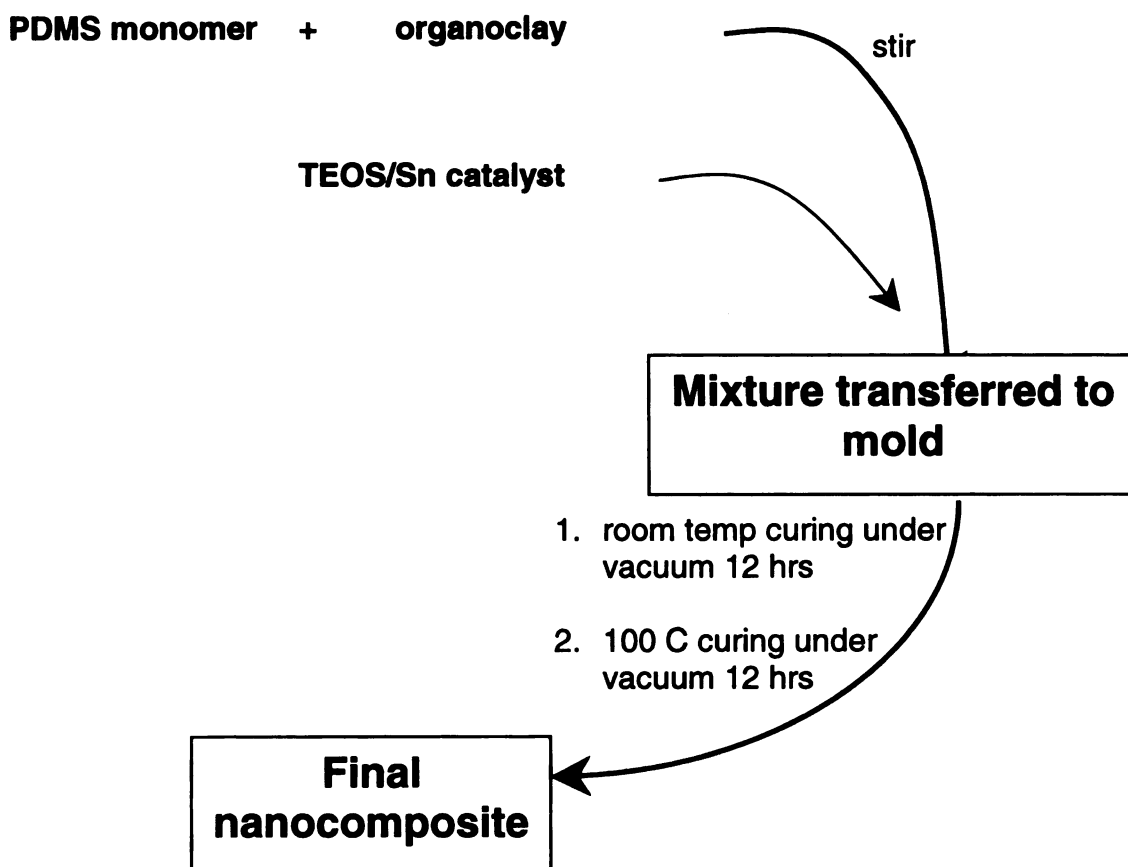


Figure 2.2 General silicone nanocomposite synthesis scheme. After polymerization silicone samples were carefully removed from the steel molds for final property assessment.

2.3 Physical measurements

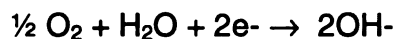
X-ray powder diffraction (XRD) patterns were recorded on a Rigaku rotaflex 200B diffractometer equipped with Cu K α X-ray radiation and a curved crystal graphite monochromator. X-ray analysis of liquid PDMS polymer – organoclay mixtures were accomplished by dropping the suspension onto filter paper mounted on a glass slide with two-sided tape, and blotting away the excess liquid. This technique was imperative in allowing for the low-angle XRD examination in a vertically oriented sample holder of the liquid clay-PDMS mixture. After the addition of TEOS and the Sn catalyst to the clay – PDMS mixture, the mixture was likewise dispersed onto a filter paper slide and the X-ray diffraction pattern was recorded during the polymerization process. While the polymerization is generally carried out under vacuum, this is only to facilitate the outflux of the condensation product ethanol, and the use of heat in non-vacuum systems likewise results in polymerization. Crosslinked nanocomposites were examined by mounting a rectangular flat specimen into an aluminum X-ray sample holder. After data collection, the sample was turned over to collect diffraction data from the opposite side of the casting in order to verify homogeneous distribution of the clay particles. This test of homogeneous particle distribution has proven to be important in studying nanocomposites, as poorly dispersed mixtures typically leads to settling of the clay particles during polymerization. In this latter case only the bottom surface of the casting will indicate the true nature of the clay component. We strongly feel that mistakes in this area by groups account for reported “exfoliated” systems which are more

likely a result of this settling nature of the more dense clay and clay-polymer intercalates.

Tensile measurements were made under ambient conditions according to ASTM procedure D3039 using an SFM-20 United Testing System. The dog bone - shaped samples used in the tensile measurements were 28 mm long in the narrow region, 3 mm thick and 3 mm wide along the center of the casting. The dog bone mold was a two piece stainless steel clamping – style mold which was separated by aluminum foil to aid in the removal of the rubbery bones. Prior to pre-polymer and crosslinker addition into the casting, the mold was treated with a non – stick release agent (Monocoat E-179) provided through Chem-Trend, Inc. and used without further modification.

Oxygen permeability data were acquired on a Mocon Ox-tran 2/60 oxygen permeability instrument with a test gas containing 5 vol % oxygen in nitrogen. Test gas for the Ox-tran 2/60 ordinarily contains 100% oxygen, or 21% oxygen, however the high permeability of silicone polymers mandates lower oxygen concentrations in order to achieve readable values (below the upper limit of oxygen detection for the permeability instrument). Film samples with a thickness between 0.7 - 1.0 mm, which were cast from an aluminum disk mold, were held in the testing cells with adhesive foil masks. Using the foil masks instead of encompassing the sample holder entirely with a polymer film reduces the exposed film area to the test gas, thus limiting the quantity of oxygen permeated through the film and ultimately reaching the detector. The Ox-tran 2/60 uses a Coulox fuel cell – type oxygen sensor where incoming oxygen molecules

undergo a redox reaction and ultimately give an electric current proportional to the amount of oxygen reacted. The half – cell cathodic and anodic reactions, respectively, are shown below:



Therefore, each oxygen molecule entering the Coulox sensor produces four free electrons, and so in accordance with Faraday's Law, one mole of oxygen at standard conditions would result in four Faradays of current. In more practical terms, one Faraday equals 96,500 Ampere-seconds, thus converting the oxygen amount into more reasonable terms a cubic centimeter of oxygen over a 24 hours period gives rise to 1.99E^{-4} amps of current.

Pristine and nanocomposite PDMS samples were soaked in cyclohexane until they reached a maximum uptake of solvent. The samples were then removed from the solvent and photographed after different stages of solvent evaporation to record the mechanical damage to the polymer. Any organic solvent can be used to demonstrate this concept, however cyclohexane has a vapor pressure that allows for the damage to occur on a relatively fast time scale, but not so rapid as to inhibit photographing the process.

TEM images were obtained on a JEOL JEM – 100CX II microscope using a CeB_6 filament and an accelerating voltage of 120 kV. Thin sectioned samples were prepared by embedding the PDMS nanocomposites in a glassy epoxy

matrix and sectioning on an ultramicrotome. The thin sections (~80 nm) were supported on 300 mesh nickel grids.

2.4 Results

The organoclay used in the synthesis of nanocomposites was a hexadecyltrimethylammonium ion exchanged fluorohectorite, abbreviated C₁₆FH. This organo clay, which was prepared by ion exchange reaction of Li⁺ - FH, exhibited a d₀₀₁ basal spacing of 27.4 Å. Solvating the organo clay in PDMS polymers with average molecular weights in the range 400 to 4200 caused the basal spacing of the clay to increase. As shown by the diffraction patterns in Figure 2.3 the basal spacing increased with increasing chain length of the PDMS polymer.

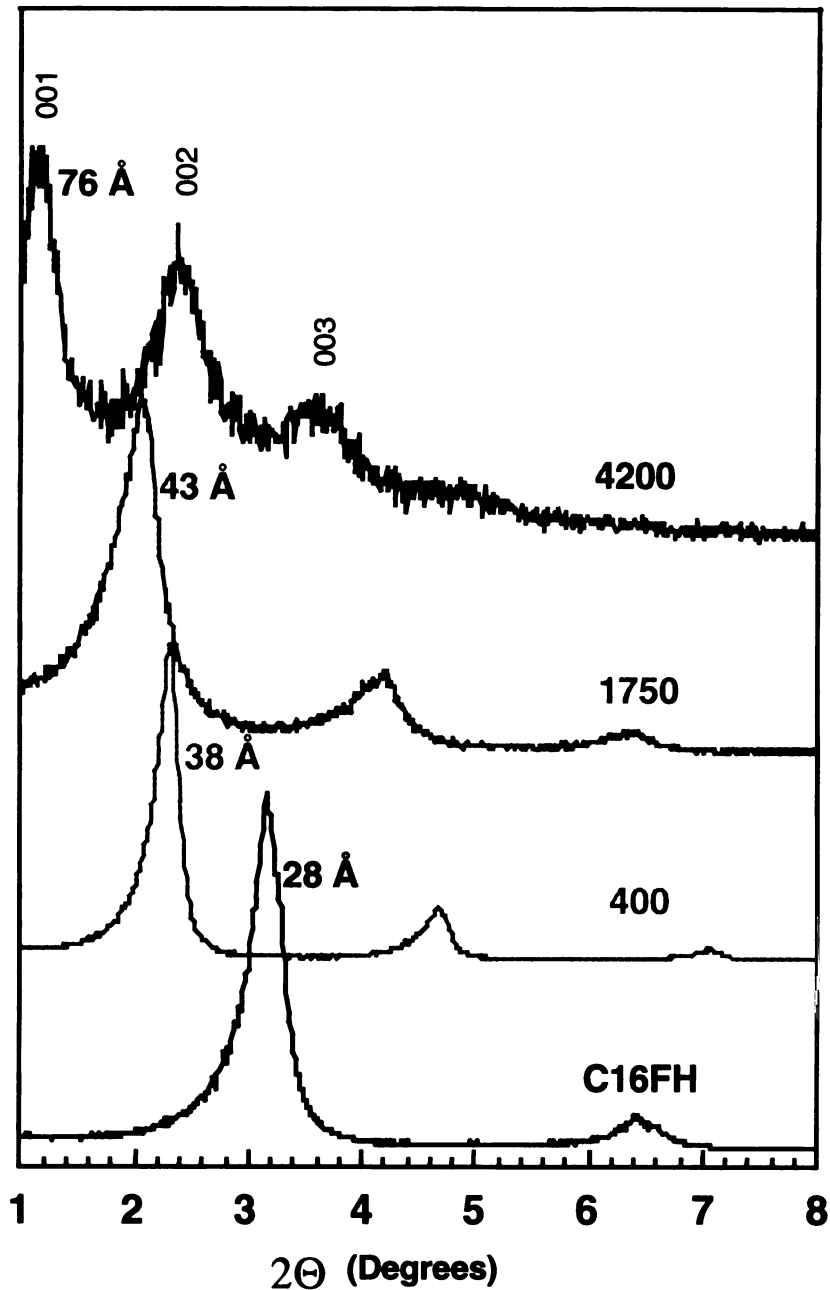


Figure 2.3 X-ray diffraction patterns of synthetic hexadecyltrimethylammonium fluorohectorite, abbreviated C₁₆FH, intercalated by PDMS polymers with molecular weights of 400, 1500-2000, and 4200. The pattern for the initial organo clay is included for comparison.

The PDMS with MW = 4200 gave the largest spacing (76 Å), corresponding to a gallery height of ~ 66 Å. Nanocomposites were synthesized using all of the available PDMS monomers, however since PDMS-4200 showed the greatest tendency to swell the galleries of the organoclay, this polymer was used to form silicone rubber - organoclay nanocomposites that were studied for mechanical properties as these nanocomposites will have more dispersed layers.

Silicone rubber nanocomposites containing up to 10 wt % organoclay were prepared by crosslinking mixtures of PDMS-4200 and C₁₆FH using tetraethylorthosilicate (TEOS) as the crosslinking agent and tin(II) 2-ethylhexanoate as the catalyst. XRD patterns of a representative reaction mixture at different stages of crosslinking are shown in Figure 2.4.

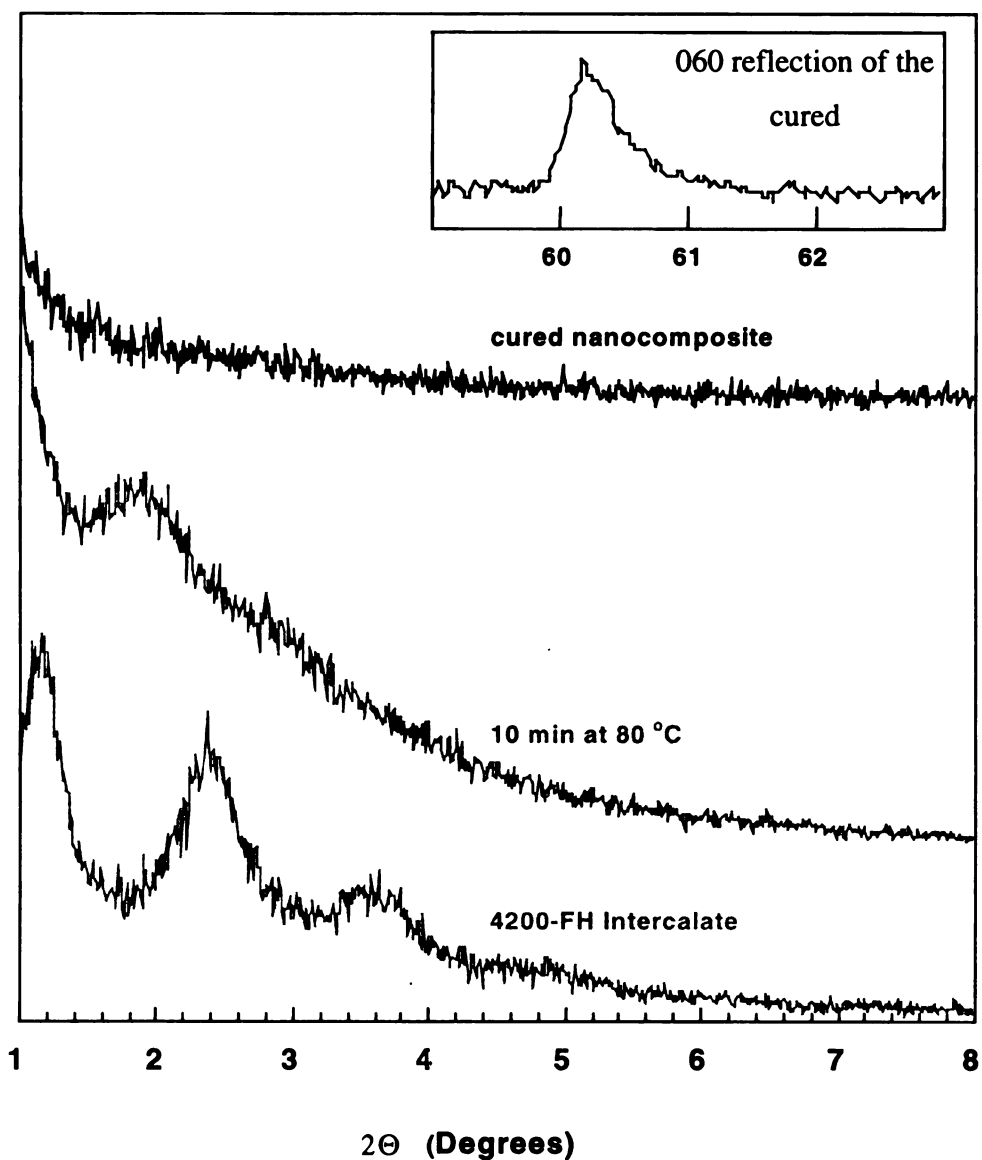


Figure 2.4 X-ray diffraction patterns for mixtures of hexadecyltrimethylammonium fluorohectorite and PDMS – 4200 at different stages of cure. The curing agent was tetraethylorthosilicate and the catalyst was tin(II) octoate. The inset indicates the presence of an in-plane 060 clay peak in the exfoliated composite.

Significantly, the 002 reflection increased from 38 Å in the initial intercalate to ~ 50 Å after only 10 minutes of partial curing at 80 °C. At this incomplete stage in the crosslinking process the nanolayers have been pushed apart by the by ~ 90 Å. The crosslinked nanocomposite (12 h, 100 °C) showed no evidence for a 00l clay reflection, indicating that the nanolayers were optimally exfoliated. Also, as shown by the inset in Figure 2.4, the clay in-plane 060 reflection near 60 degrees 2θ was observed in the cured composite, indicating the retention of nanolayer crystallinity, even though they are highly dispersed.

Tensile data were obtained for dog bone - shaped castings of the silicone elastomers containing 0.0, 5.0 and 10 wt % organoclay loadings. These organoclay loadings correspond to silicate loading of 0.0, 3.5 and 7.1 wt %, respectively, after accounting for the organic content in fluorohectorite. Figure 2.5 provides the stress-strain curves for each composition.

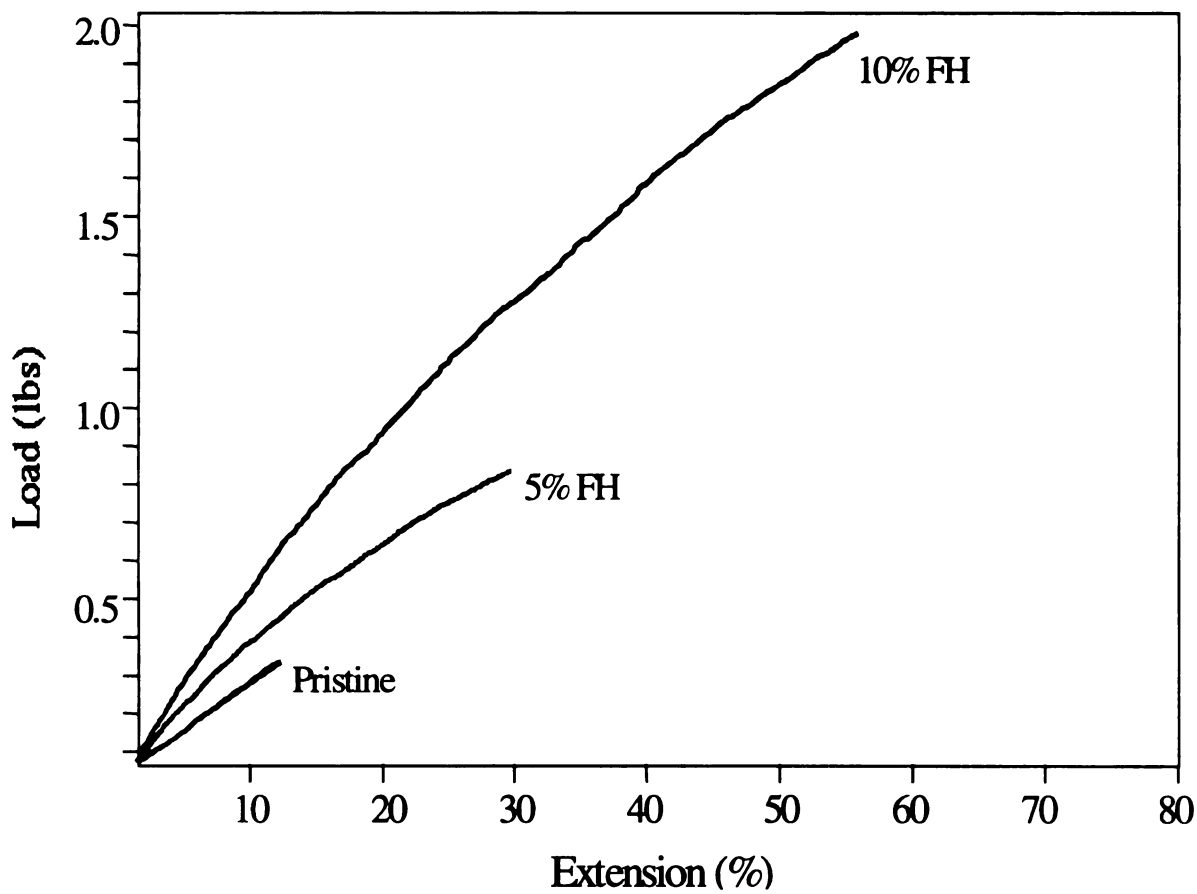


Figure 2.5 Comparison of the stress – strain curves for pristine PDMS and PDMS - C₁₆FH nanocomposites containing 5.0 and 10 wt % C₁₆FH organoclay.

While figure 2.5 represents stress – strain data for three different silicone samples, averaged tensile strength, modulus, and strain at break data for multiple dog bones is summarized Table 2.1.

Table 2.2 Mechanical Properties of Silicone Elastomer^a - C₁₆ FH Organoclay Nanocomposites

Organoclay Loading (wt%)^b	Strength (Kpa)	Modulus (Kpa)	Elongation (%)
0.0	152	1.8 x 10 ⁻³	11
5.0	361	2.3 x 10 ⁻³	31
10.0	880	3.5 x 10 ⁻³	52

Table 2.2 addresses a summary of non-mechanical nanocomposite properties including oxygen permeability results and cyclohexane uptake values for the pristine and clay - reinforced elastomers. The permeabilities represent the transmission rates of oxygen at a concentration of 5.0% in nitrogen as a carrier gas, and the cyclohexane uptake values are the loadings of liquid solvent contained in the elastomer at equilibrium at 25 °C.

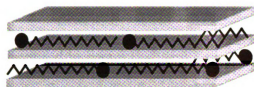
Table 2.3 Permeability and Solvent Uptake Properties of Silicone Elastomer^a - C₁₆ FH Organoclay Nanocomposites

Organoclay Loading (wt%)	Oxygen Permeability^c	Cyclohexane Uptake (g/g)^d
0.0	6.12 x 10 ⁴	2.55
5.0		1.07
1.5	5.75 x 10 ⁴	
8.0	4.56 x 10 ⁴	

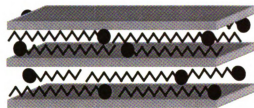
- a/ The elastomer was formed by crosslinking PDMS (MW = 4200) a with a stoichiometric amount of TEOS.
- b/ The organic and water content of the clay was 6% and 24%, respectively.
- c/ The units of permeability are cm³ mil m⁻² day⁻¹.
- d/ Grams cyclohexane/gram polymer

2.5 Discussion

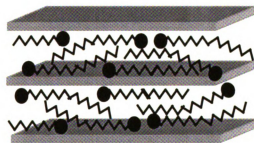
The replacement of Li^+ by hexadecyltrimethylammonium ions in the galleries of fluorohectorite resulted in a basal spacing of 27.4 Å. The difference between the observed basal spacing and the estimated clay layer thickness (9.6 Å) indicated of gallery height of 17.8 Å. This value is consistent with a paraffin – like orientation of the surfactant chains in the gallery region. If the carbon chains adopted an all anti conformation, the observed gallery height would correspond to an angle of inclination of $\sim 50^\circ$ between the chain axis and the clay surface. However, the chains are most likely kinked³¹ and oriented more vertically on the gallery surfaces. Ordinarily, long chain ammonium ion surfactants adopt lateral bilayer to pseudo trimolecular orientation in the gallery space of montmorillonite, resulting in gallery heights below 10 Å, as depicted in figure 2.6 along with a monolayer arrangement.³¹⁻³³



Monolayer organoclay
arrangement



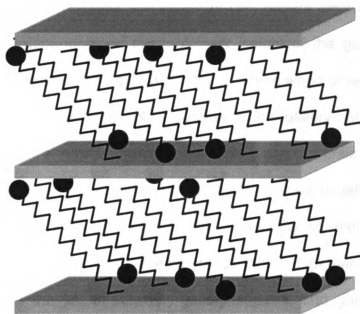
Bilayer organoclay
arrangement



Pseudotrilayer organoclay
arrangement

Figure 2.6 Schematic depicting potential intragallery surfactant arrangements typically found in organomontmorillonites.

However, synthetic fluorohectorite has a higher layer charge (1.12 e⁻ per O₂₀ per unit cell) in comparison to montmorillonite which usually has a layer charge density of ~ 0.75 e⁻ per O₂₀ per unit cell. Thus, the higher population of surfactant chains in fluorohectorite results in a paraffin - like packing of chains and a comparatively large gallery expansion, shown in figure 2.7.



Paraffin organoclay
arrangement

Figure 2.7 Inclined paraffin surfactant orientation found in higher charge density clays, including fluorohectorite. Cetyltrimethylammonium fluorohectorite has a paraffin arrangement with an approximate angle of inclination with the clay surface of 50° .

Somewhat surprisingly, the extent of clay gallery expansion upon PDMS intercalation is dependent on the molecular weight of the guest polymer (c.f., Figure 2.3). This is not the usual outcome observed when other linear molecules are intercalated into an organoclay. Ordinarily, the gallery height is determined by the orientation of organo cation in the gallery and the critical diameter of the intercalated polymer. The length of the guest species usually has no or little effect on the gallery height. That is, the organoclay normally permits a fixed volume of the pre-polymer to intercalate as dictated primarily by the polarity match between the linear polymer, gallery surface, and gallery cation. The gallery heights observed in the PDMS – fluorohectorite systems, however, are determined by the molecular weight or, equivalently, the ratio of $-\text{OSi}(\text{CH}_3)_2-$ repeat units to terminal $-\text{Si}(\text{CH}_3)_2\text{OH}$ groups. As this ratio increases, the gallery height increases.

The hydrophobicity of the organo cation surfactant undoubtedly plays an important role in allowing the initial penetration of PDMS into the galleries. However, the silanol end groups of the polymer interact at least in part with the gallery surfaces. These interactions most likely play a role in determining the space - filling configuration of the PDMS. The importance of specific interactions between the silanol end groups and the gallery surfaces is verified by the observation that PDMS polymers of the same molecular weight but terminated exclusively by methyl groups do not intercalate into C_{16}FH . As illustrated schematically in Figure 2.8, restricting the silanol end groups to specific contacts with the gallery surface will influence the packing of long chain PDMS molecule

(e.g., PDMS-4200) in the gallery. Shorter PDMS chains that are comparable in length to the organocation (e.g., PDMS-400, which contains ~ 6 $-\text{Si}(\text{CH}_3)_2\text{O}-$ units) cannot bridge opposite gallery surfaces and at the same time account for a 10-Å or more increase in gallery height in comparison to C_{16}FH (e.g., compare the diffraction patterns in Figure 2.3).

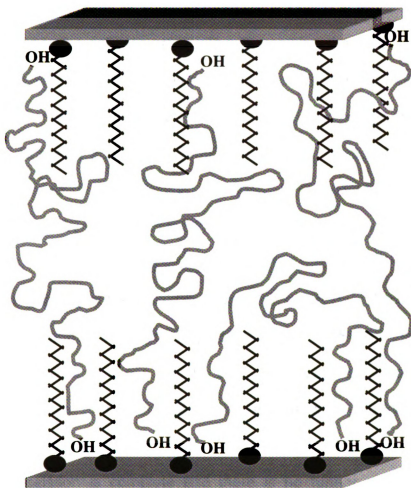
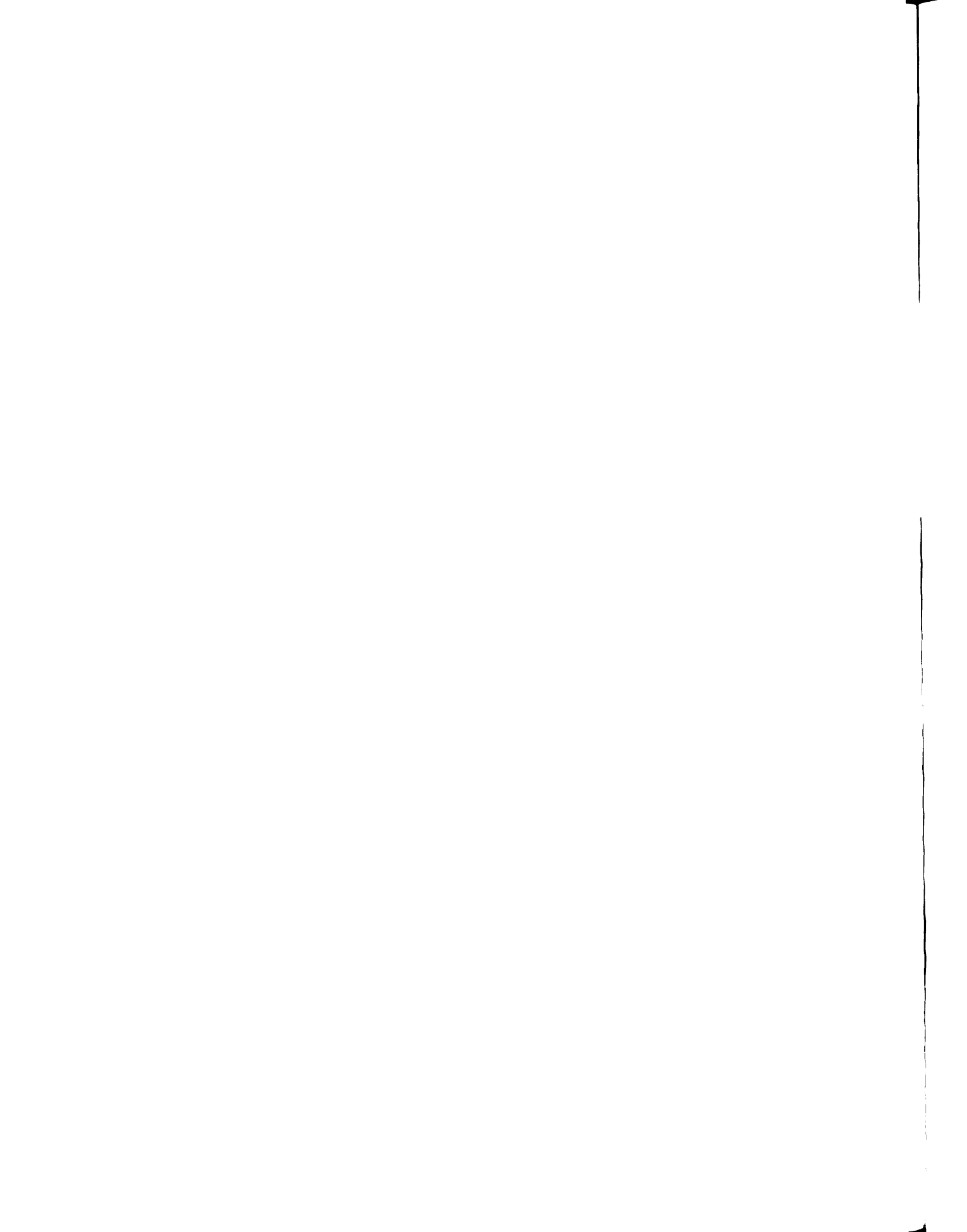


Figure 2.8 Schematic representation of the swelling of an alkyammonium ion exchanged fluorohectorite by a long chain PDMS polymer (MW = 4200) containing terminal OH groups. Shorter PDMS chains with molecular weight fractions of 400 and 1750 may have only one end of the chain associated with the gallery surfaces.



Thus, in the case of short PDMS chains only one terminal silanol group may be linked to the gallery surface. The charged head groups of the surfactant, the siloxane oxygens of the clay layer, and co-adsorbed water molecules may all contribute to the interactions of the terminal silanol groups with the gallery surfaces. Burnside and Giannelis have noted that a small amount of gallery water was needed to intercalate a PDMS-18,000 polymer into an organo montmorillonite. We have verified the need for gallery water to achieve PDMS intercalation. The air-dried organoclay used in the present work contained ~ 6 wt % water, as judged by the weight loss upon drying at 150 °C, but if the water is removed by drying at elevated temperatures, then no PDMS intercalation was observed. In view of these results, it is now clear that water is needed to facilitate interaction of the terminal silanols and the gallery surfaces, presumably through hydrogen bond formation. Once the H-bonding sites are saturated, PDMS intercalation is complete and there is no further swelling of the clay galleries.

Although the swelling of C₁₆FH is best monitored quantitatively by XRD, the dependence PDMS intercalation on molecular weight can be qualitatively judged by the physical behavior of the clay in PDMS suspensions. Figure 2.9 is a photograph of four different C₁₆FH - PDMS suspensions, each containing 5 wt % organoclay. The tubes are filled in left to right order with methyl terminated PDMS - 400 and silanol - terminated PDMS - 400, - 1750, and - 4200. The methyl - terminated PDMS does not intercalate into the galleries, and the unexpanded clay settles to the bottom of the tube. For the silanol - terminated

PDMS derivatives, however, the nanolayers are separated by PDMS molecules, allowing for the formation of a stable, scaffold - like suspension of swollen clay tactoids with an equilibrium height that increases with the PDMS polymer molecular weight.

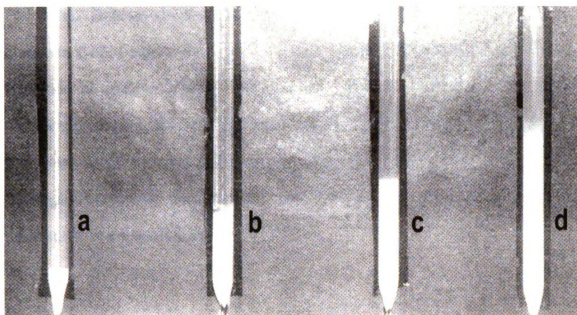


Figure 2.9 Photograph of PDMS polymer - $C_{16}FH$ suspensions containing 5.0 wt % organoclay. The tubes are filled in left to right order with methyl terminated PDMS - 400 and silanol terminated PDMS - 400, - 1750, and - 4200, respectively.

The Sn(II)-catalyzed crosslinking of PDMS - 4200 by TEOS in the presence C₁₆FH organoclay leads to further expansion of the galleries and the formation of silicone rubber - clay nanocomposite (c.f., Figure 2.2). While somewhat debated, the mechanism of condensative silicone polymerization in the presence of a tin octoate catalyst is generally thought to involve an initial hydrolysis of the tin carboxylate. The most widely accepted full catalytic mechanism is depicted in figure 2.10.

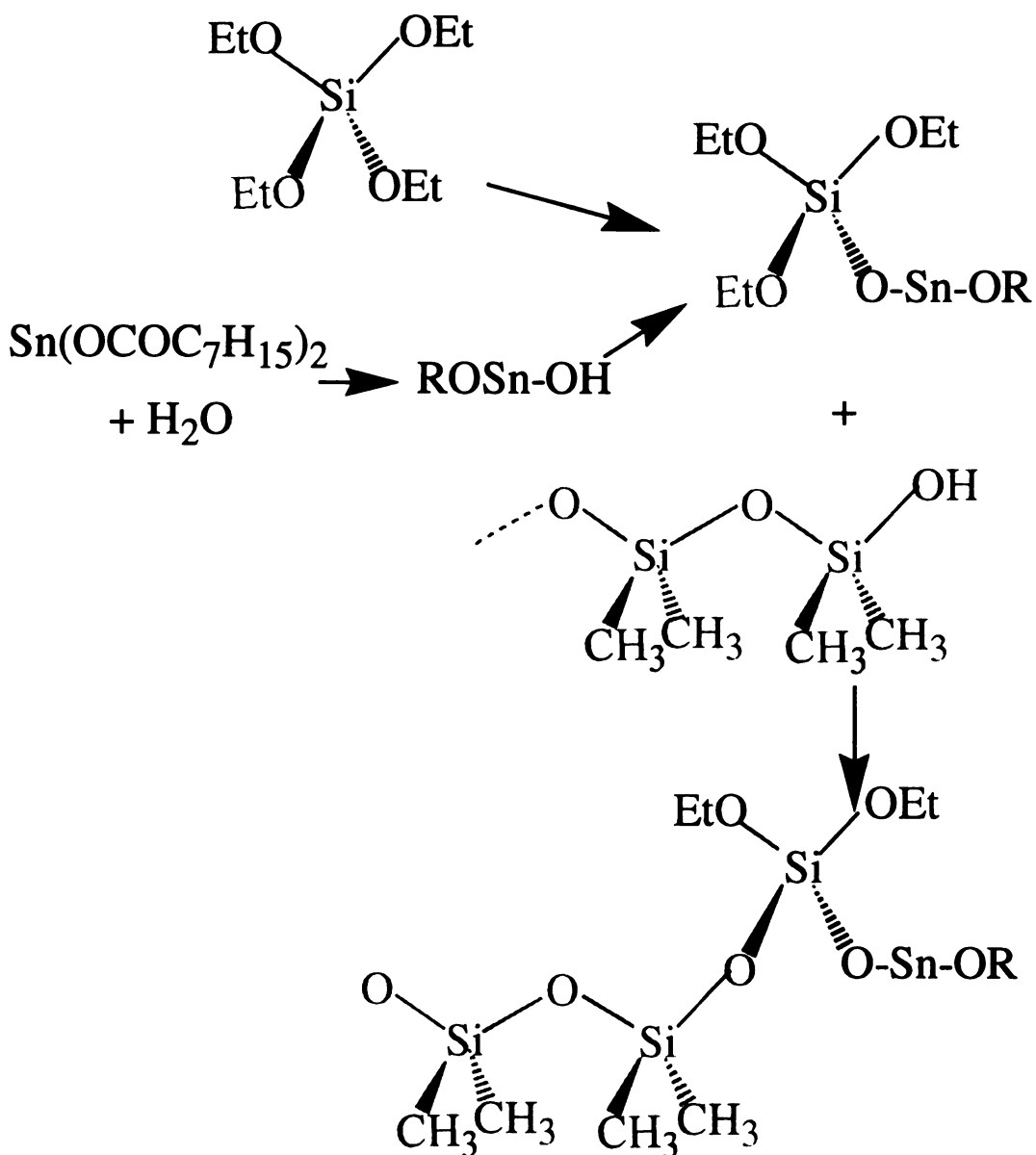


Figure 2.10 Tin octoate – catalyzed PDMS crosslinking. Although there is some debate as to the exact mechanism, the active species is widely thought to be the hydrolysis product of the tin bis(2-ethylhexanoate) catalyst.

The absence of an observable 001 diffraction peak in the cured elastomer implies that the clay nanolayers have been optimally separated (exfoliated) in the elastomer matrix. This means that the intragallery crosslinking rate was competitive with the extra gallery rate. For this to occur the catalyst and TEOS should be favorably partitioned between the PDMS solution and the organoclay galleries. Co-adsorbed water may also facilitate intragallery polymerization through TEOS hydrolysis, especially in the confined interclay regions where water associated with the quaternary amine head groups is more acidic. Verification that the individual clay nanolayers retained their structural integrity in the exfoliation process, and that the layers were still perceptible to the X-ray radiation was provided by the presence of a 060 in-plane reflection in the high 2θ region near 60° (see inset in Figure 2.3). The importance of probing for the 060 reflection can not be stressed enough, as an amorphous XRD pattern can result from a variety of circumstances. Low clay concentrations, or isolated clay tactoids in the nanocomposite both could give rise to minimal X-ray scattering. Also, a settling of the more dense clay and clay-polymer intercalate phases prior to polymer matrix gelation in certain systems, especially those which have limited polymer intercalation, could lead to an anisotropic clay dispersion and thus an amorphous top side (polymer only) even in intercalated nanocomposite. For this reason XRD patterns were taken of both top and bottom regions of the polymerized silicone nanocomposites. The high degree of pre-polymer intercalation and significant intragallery reaction bias support the notion observed in TEM imaging that the nanocomposites were indeed extensively exfoliated.

The uniform dispersion of clay nanolayers in the nanocomposite affords a marked improvement in the tensile strength, modulus and strain-at-break (see Figure 2.3 and Table 2.1). Similar improvements in tensile properties have been reported for silicone rubber - clay nanocomposites derived from PDMS polymers with molecular weights of 18,000 and 68,000^{7,20}. Through the absorption and dispersal of an applied load, the nanolayers layers delocalize stress, as well as toughen the matrix as indicated by the large increase in the strain-at-break. In contrast, conventional composites ordinarily compromise toughness for tensile strength as in general stiffer and stronger, but more brittle (less extendable) composites are formed from macro-scaled reinforcement. It has been previously noted^{14,20} that the clay nanolayer reinforcement of elastomers dramatically reduces the ability of the matrix to absorb solvents. An analogous reduction in cyclohexane uptake was observed for the clay nanolayer - reinforced silicone elastomers prepared in the present work (c.f., Table 2.2). However, the reinforcement effect goes far beyond simply limiting the uptake of solvent. The clay nanolayers can also dramatically reduce the structural damage that normally occurs when the solvent is allowed to evaporate from a solvent - saturated elastomer. As shown in Figure 2.11, the rapid evaporation of cyclohexane from the pristine silicone rubber causes internal strain that fractures the matrix, rendering the recovered elastomer useless. In contrast, the nanolayer - reinforced composite undergoes less solvent swelling and loses solvent more slowly, thus reducing internal strain and avoiding matrix fracture. The avoidance of structural damage caused upon exposure to solvents may represent one of the

most important benefits of nanolayer reinforcement in polymer technology. Polymers, and elastomers in particular, find uses in automotive and similar applications as sealants and gaskets where exposure to petroleum - based solvents is commonplace. Having the capability to influence large amounts of the polymer matrix at relatively low loadings, exfoliated clay - silicone nanocomposites could find applications where typical composites fail.

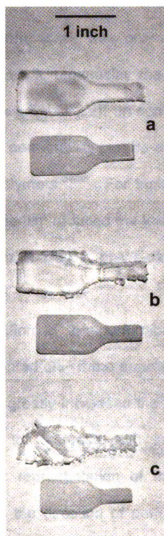
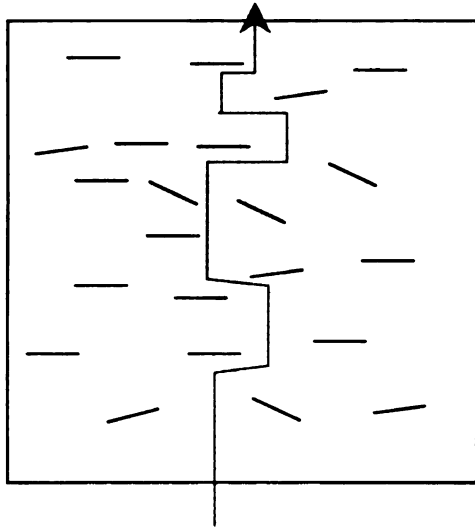


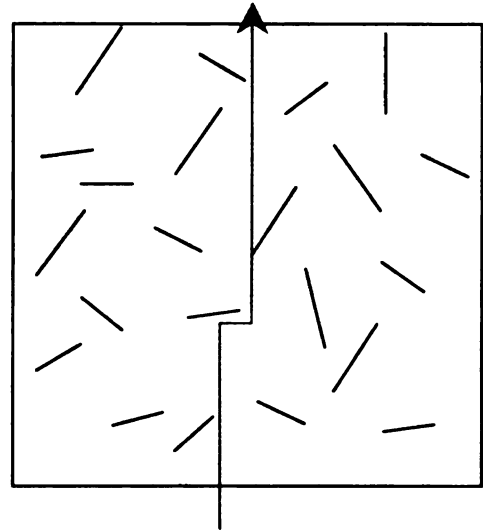
Figure 2.11 Photographs of a pristine silicone elastomer formed from PDMS - 4200 (upper specimen) and the corresponding nanocomposite containing 5.0 wt % $C_{16}FH$ organoclay (lower specimen) after equilibration in a cyclohexane bath and subsequent removal from the bath to allow for solvent evaporation: (a) immediately after removal from the bath, (b) after 15 seconds, and (c) after 20 minutes. No structural damage was noted for the nanocomposite after complete evaporation of the solvent.

Although the tensile and solvent resistance properties of a silicone rubber can be greatly enhanced through clay nanolayer reinforcement, the gas permeability of the nanocomposites was only slightly affected. Even at an organoclay loading of 8.0 wt % organoclay the oxygen permeability was only reduced only by ~ 25 % (see Table 2.2). In contrast, previous work has shown that dramatic reductions in permeability can be achieved for polyimide films and other thin film forms of polymers.³⁴⁻³⁸ For instance, the exfoliation of 2% wt synthetic mica in a polyimide film reduced the water vapor permeability 10 fold³⁷, and a 4.8 wt % dispersion of clay in poly(ϵ -caprolactone) reduced the water vapor permeability 5 fold.³⁵

In general, a reduction in the permeability of a nanolayer reinforced polymer film can be anticipated only if the nanolayers are highly aligned parallel to the film surfaces. This greatly increases the tortuosity of the diffusion path, causing the permeability to decrease with increasing aspect ratio of the nanolayers. A schematic representation of the importance of parallel clay alignment perpendicular to the direction of permeant flow is depicted in figure 2.12.



parallel – to – surface clay orientation



random clay orientation

Figure 2.12 Depiction of permeant flow through nanocomposite films. A more tortuous path is found perpendicular to the film when clay particles are oriented parallel to the film surface. Low surface tension fluids and thick films limit the percentage of parallel – to – surface oriented nanolayers.

Although synthetic fluorohectorite has one of highest nanolayer aspect ratios among smectite clays, it has not been effective in providing substantially reduced gas permeability in the case of silicone elastomers. Silicone rubbers are so permeable that it was necessary to use relatively thick 0.7 - 1.0 mm samples in obtaining permeability coefficients that were within the upper detection limit of the permeability instrument. Under the conditions needed to form these thick samples the surface tension forces are too weak to facilitate nanolayer ordering parallel to the sample surface. This affect is amplified with silicones as the weak intermolecular forces create an already low surface tension of the silicone fluid that limits the favored parallel-to-surface ordering of the clay layers. The relatively random orientation of the nanolayers was verified by transmission electron microscopy. As shown by the TEM image in Figure 2.13, the nanolayers generated by the exfoliation of a clay tactoid tend to orient parallel to one another.

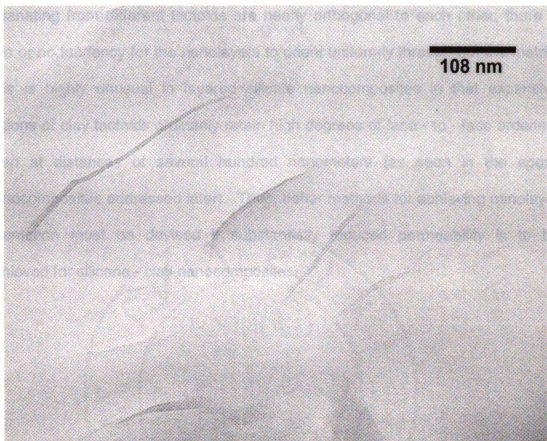


Figure 2.13 TEM image of silicone nanocomposite showing parallel orientation of nanolayers stemming from the same tactoids. Prior to intercalation and exfoliation in silicone, the organofluorohectorite galleries were separated by 2.7 nm, and after completion of crosslinking layers are 70-150 nm apart.

However, as shown by the image in Figure 2.14, wherein nanolayers emanating from different tactoids are nearly orthogonal to each other, there is little or no tendency for the nanolayers to orient uniformly through out the matrix. This is highly unusual in layered silicate nanocomposites in that expansive regions of clay tactoids ordinarily retain high degrees of face - to - face ordering, even at distances of several hundred nanometers (as seen in the epoxy nanocomposites addressed later). Thus, better methods for achieving nanolayer orientation must be devised if substantially reduced permeability is to be achieved for silicone - clay nanocomposites.

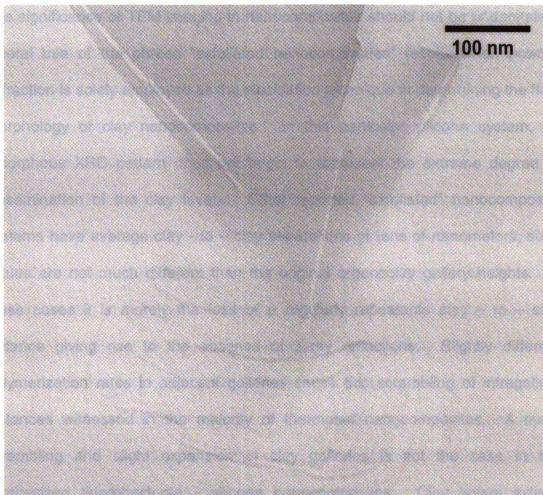


Figure 2.14 TEM image of silicone nanocomposite showing neighboring tactoids with near orthogonal orientations. Such an image is rare in clay nanocomposites where adjacent clay tactoids are usually oriented parallel to one another.

The significance of TEM imaging in nanocomposites should not be understated. Liberal use of the phrase “exfoliated nanocomposites” results when powder diffraction is solely employed as the elucidation technique in determining the final morphology of clay nanocomposites. In this particular silicone system, an amorphous XRD pattern does not begin to represent the extreme degree of dissemination of the clay layers. Other reported “exfoliated” nanocomposite systems have average clay - to - clay separations of tens of nanometers, such values are not much different than the original organoclay gallery heights. In these cases it is merely the loss of a regularly repeatable clay - to - clay distance giving rise to the absence of X-ray reflections. Slightly different polymerization rates in adjacent galleries cause this scrambling of intragallery distances witnessed in the majority of thermoset nanocomposites. A mere scrambling and slight expansion of clay galleries is not the case in the synthesized fluorohectorite - silicone nanocomposites. Clay layers initially separated by ~2.7 nm in the organoclay ultimately become forced apart through crosslinking to 70-150 nm in the final hybrid. The unprecedented degree of exfoliation in fluorohectorite in the silicone matrix in this system is manifested in the dramatic increase of tensile properties. Even at relatively low clay loadings (3-7% wt. silicate), tremendous affects are noted in the Young’s modulus, strain at break, tensile strength and overall toughness of the hybrids versus the pristine silicone. Such improvements are to be expected when dispersion of a nanoscaled reinforcement phase occurs to such a large extent. Efficient transfer

of the applied stress at the highly exposed polymer – clay interfacial regions readily permits the reinforcement phase to play its role as a load barer, and allows the matrix to remain intact under forces that would cause failure of the pristine silicone rubber.

Qualitatively, the successful exfoliation of clay layers could be noted early stages of crosslinking. While monitoring the partially cured silicone materials by powder diffraction, the loss of higher order reflections immediately occurred as the first samples were analyzed. This is somewhat surprising when compared to other thermoset systems where the registry of intercalated clay layers persist tens of minutes into the polymerization. The rapid dispersion of fluorohectorite particles, in particular, is especially noteworthy as the synthetic clay particles are much larger laterally than their naturally occurring counterparts, and thus expected to be more cumbersome in migrating through the silicone matrix. Reasons for the high degree of exfoliation in silicones likely revolve around the presence of water molecules at the clay surface previously mentioned. The need for small amounts of surface adsorbed water was previously noted for the initial intercalation of PDMS monomers, and its role as a catalyst for the condensation of TEOS was also alluded to, however yet another important function of the moisture found at the clay surface can be conceived. As aforementioned, the selective partitioning of tin catalyst into the galleries could account for an increase in the intragallery polymerization rate relative to the bulk rate, however, the high solubility of tin octoate in polydimethylsiloxane may restrict the selective uptake of catalyst into the gallery regions. Instead, the catalyst that does

partition into the interclay space, even if it is at the same concentration as in the bulk medium, is hydrolyzed to the active tin hydroxyl species more efficiently than in the water – deprived bulk silicone. An illustration depicting this mechanism is shown in figure 2.15.

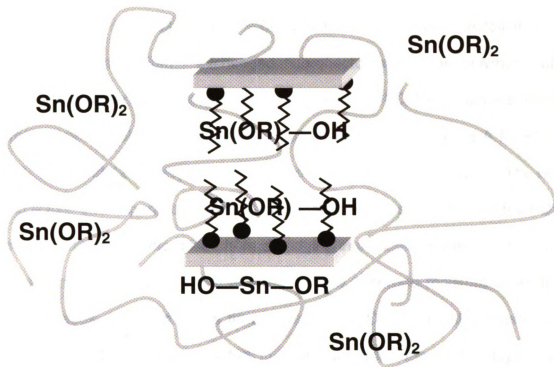


Figure 2.15 Schematic of tin catalyst existing in different forms during crosslinking of the silicone rubber. The moisture sensitive tin carboxylate will hydrolyze more readily when in close contact with the fluorohectorite clay due to the small amount (2-6% by wt.) of water present at the silicate surface.

2.6 Conclusions

Silicone rubber has been reinforced by exfoliating a cetyltrimethylammonium - exchanged fluorohectorite into the polymer matrix. Unique molecular weight dependant intercalation of PDMS monomers into the organoclay was observed by X-ray diffraction (38 Å, 43 Å and 76 Å for PDMS-400, 1750 and 4200, respectively) in the pre-polymerization analysis. The novel end – to – end separation intercalation dependence of silanol terminated PDMS in organofluorohectorite arises from a bridging interaction between both ends of the polydimethylsiloxane chain and the surface absorbed moisture at adjacent clay surfaces. Addition of the tin catalyst and TEOS crosslinking agent to the intercalated clay mixture resulted in rapid dissemination of the layers, and ultimately a 70-150 nm spacing between layers was observed by TEM imaging. The exfoliated layers improved tensile properties dramatically, as expected increasing the modulus and also the tensile strength at break dramatically with increasing clay content. Somewhat surprisingly, the nanocomposites also exhibited improved elongation at break with increased clay, a phenomenon not ordinarily attained with the introduction of a rigid filler. The exfoliated clay also reinforced the silicone polymer when exposed to an organic solvent as the matrix did not uptake as much solvent as pristine samples, and survived removal from the organic bath unlike the pristine samples. Although the presence of exfoliated nanolayers drastically improved the mechanical properties of silicones, the oxygen permeability was not significantly influenced.

2.7 References

- (1) Schollhorn, R. *Chem. Mater.* **1996**, *8*, 1747.
- (2) Messersmith, P.B.; Stupp, S. I. *J. Mater. Res.* **1992**, *7*, 2599.
- (3) Okada, A.; Usuki, A. *Mater. Sci. Eng.* **1995**, *C3*, 109.
- (4) Giannelis, E.P. *Adv. Mater.* **1996**, *8*, 29.
- (5) Pinnavaia, T.J. *Science* **1983**, *220*, 365.
- (6) Wang, Y.M. *Organosil. Mater. Appl. Chin.* **1992**, *5*, 11.
- (7) Wang, S.; Li, Q.; Qi, Z. *Key Eng. Mater.* **1998**, *137*, 87.
- (8) Usuki, A.; Kawasumi, M.; Kojima, Y.; Okada, A.; Kurauchi, T.; Kamigaito, O. *J. Mater. Res.* **1993**, *8*, 1174.
- (9) Usuki, A.; Kojima, Y.; Kawasumi, M.; Okada, A.; Fukushima, Y.; Kurauchi, T.; Kamigaito, O. *J. Mater. Res.* **1993**, *8*, 1179.
- (10) Kojima, Y.; Usuki, A.; Kawasumi, M.; Okada, A.; Fukushima, Y.; Kurauchi, T.; Kamigaito, O. *J. Mater. Res.* **1993**, *8*, 1185.
- (11) Kojima, Y.; Usuki, A.; Kawasumi, M.; Okada, A.; Kurauchi, T.; Kamigaito, O. *J. Appl. Polym. Sci.* **1993**, *49*, 1259.
- (12) Lan, T.; Pinnavaia, T.J. *Chem. Mater.* **1994**, *6*, 2216.
- (13) Messersmith, P.B.; Giannelis, E.P. *Chem. Mater.* **1994**, *6*, 1719.
- (14) Massam, J.; Pinnavaia, T.J. *Mater. Res. Soc. Symp. Proc.* **1998**, *520*, 223.
- (15) Wang, Z.; Pinnavaia, T.J. *Chem. Mater.* **1998**, *10*, 1820.
- (16) Yano, K.; Usuki, A.; Okada, A.; Kurauchi, T.; Kamigaito, O. *J. Polym. Sci., Part A: Polym. Chem.* **1993**, *31*, 2493.

- (17) Yano, K.; Usuki, A.; Okada, A. *J. Polym. Sci., Part A: Polym. Chem.* **1997**, *35*, 2289.
- (18) Lan, T.; Kaviratna, P.D.; Pinnavaia, T.J. *Chem. Mater.* **1994**, *6*, 573.
- (19) Wang, Z.; Pinnavaia, T.J. *Chem. Mater.* **1998**, *10*, 3769.
- (20) Burnside, S.D.; Giannelis, E.P. *Chem. Mater.* **1995**, *7*, 1597.
- (21) Kawasumi, M.; Hasegawa, N.; Kato, M.; Usuki, A.; Okada, A. *Macromolecules* **1997**, *30*, 6333.
- (22) Usuki, A.; Kato, M.; Okada, A.; Kurauchi, T. *J. Appl. Polym. Sci.* **1997**, *63*, 137.
- (23) Kurokawa, Y.; Yasuda, H.; Oya, A. *J. Mater. Sci. Lett.* **1996**, *15*, 1481.
- (24) Kato, M.; Usuki, A.; Okada, A. *J. Appl. Polym. Sci.* **1997**, *63*, 1781.
- (25) Hasegawa, N.; Kawasumi, M.; Kato, M.; Usuki, A.; Okada, A. *J. Appl. Polym. Sci.* **1998**, *67*, 87.
- (26) Porter, T.L.; Hagerman, M.E.; Reynolds, B.P.; Eastman, M.P.; Parnell, R.A. *J. Polym. Sci., Part B: Polym. Phys.* **1998**, *36*, 673.
- (27) Akelah, A.; Moet, A. *J. Mater. Sci.* **1996**, *31*, 3589.
- (28) Vaia, R.A.; Jandt, K.D.; Kramer, E.J.; Giannelis, E.P. *Macromolecules* **1995**, *28*, 8080.
- (29) Vaia, R.A.; Jandt, K.D.; Kramer, E.J.; Giannelis, E.P. *Chem. Mater.* **1996**, *8*, 2628.
- (30) Vaia, R.A.; Giannelis, E.P. *Macromolecules* **1997**, *30*, 8000.
- (31) Legaly, G. *Solid State Ionics* **1986**, *22*, 43.
- (32) Hackett, E., Manias, E., Gianellis, E.P. *J. Chem. Phys.* **1998**, *108*, 7410.

- (33) Teppen, B. J.; Rasmussen, K.; Bertsch, P.M.; Miller, D.M.; Schafer, L. J. *Phys. Chem. B* **1997**, *101*, 1579.
- (34) Messersmith, P.B.; Gianellis, E.P. *Chem. Mater.* **1993**, *5*, 1064.
- (35) Messersmith, P.B.; Gianellis, J. *Polym. Sci. Part A: Polym. Chem.* **1995**, *33*, 1047.
- (36) Yano, K.; Usuki, A.; Okada, A.; Kurauchi, T.; Kamigaito, O. *J. Polym. Sci. Part A: Polym. Chem.* **1993**, *31*, 2493.
- (37) Yano, K.; Usuki, A.; Okada, A. *J. Polym. Sci. Part A: Polym. Chem.* **1997**, *35*, 2289.
- (38) Kojima, Y.; Usuki, A.; Kawasumi, M.; Okada, A.; Kurauchi, T.; Kamigaito, O. *J. Appl. Polym. Sci.* **1993**, *49*, 125.

Chapter 3

POST-CURE ION EXCHANGE OF EXFOLIATED FLUOROHECTORITE CLAY IN POLYDIMETHYLSILOXANE NANOCOMPOSITES

3.1 Introduction

Formation of an ideal nanocomposite requires an intimate mixing of the inorganic reinforcement phase within a polymeric matrix such that the resultant composite undergoes a compositional change on a nanometer length scale¹⁻⁴. The use of organically modified smectite clays as the support for various thermoset polymers has proven an effective means for achieving this nanoscaled reinforcement. In particular, the uniform dispersal of various inorganic fillers in elastomeric silicones is one such system that has received notable attention recently⁵⁻⁷. Specifically, we have shown that the use of quaternary alkylamine-modified fluorohectorite is an effective layered silicate for achieving an exfoliated reinforcement phase in polydimethylsiloxane (PDMS)⁸. In this case insertion of the silanol-terminated PDMS monomers into organoclay galleries invokes a molecular weight - dependant swelling of the interclay regions, and, after tetraethylorthosilicate (TEOS) and Sn catalyst addition, the clay layers are forced apart further as gelation of the PDMS matrix occurs. In conjunction with the unique intercalation behavior PDMS monomers (001 spacings of 38 Å, 43 Å and 76 Å for monomers of average molecular weight 400, 1750 and 4200, respectively), the tensile, thermal, solvent uptake and permeability properties

were also explored. While the presence of highly exfoliated nanolayers (clay to clay separations averaging 70-150 nm noted by TEM imaging) in silicones yielded properties that were generally far superior relative to unfilled PDMS, the oxygen permeability was only slightly reduced with the introduction of exfoliated nanolayers.

The extreme permeability of silicones, and specifically the fluorohectorite - PDMS nanocomposites, coupled with the individually exposed clay layers in the synthesized hybrid materials offer a unique opportunity to explore subsequent chemistry on the cured system. Upon immersion in an organic solvent the crosslinked silicone polymer undergoes extensive swelling (comprehensive filled elastomer swelling has been examined by Giannelis⁷), thus providing a potential medium for accessing exchange sites of the exfoliated nanolayers. Once the matrix is highly distended, introduction of alternative cations become feasible and ultimately the formation of clay nanocomposites lacking the customary organic modifiers are possible. A secondary exchange of the quaternary alkylammonium ions present on the clay surfaces could prove to be significant in improving the mechanical properties of certain nanocomposites. It has been shown that the presence of these low molecular weight organic modifiers can plasticize the matrix through solvation of the polymer chains, and thus reduce the efficacy of the organoclay reinforcement phase in the nanocomposite⁹. Furthermore, location of the modifiers at the silicate surface interferes with the favorable and mechanically important interfacial contact between the polymer chains and the reinforcement phase^{10,11}. Containing 24% by weight organic content, the

modified clays in this particular system are likely compromising a portion of their fortification due to this plasticizing nature and a disruption of the desired interfacial interactions. Other clay - polymer systems require an even higher loading of organic modifier in order to successfully disperse nanolayers in the polymer matrix, and therefore could experience even more pronounced mechanical improvements by eliminating these alkyl surfactants. Another potential motivation for the post-cure ion exchange in nanocomposites is to create selectively reactive membranes for use in liquid and gas separations. Through discriminatory exchange for chemically active cations, the adsorption, coordination or selective reactivity of certain permeants and reactants could be biased by the reactive (catalytic or otherwise) membranes, and be employed in separations or flow-through reactor systems. Two representative examples of such chemistry involve the selective quadrupolar interaction of lithium and calcium cations with N_2 in O_2/N_2 mixtures (producing O_2 -rich gas mixtures on the post-diffusion side of the membrane)¹², and the use of catalytically active cation - containing zeolites in silicone membranes for the oxidative cleavage of certain alkanes (partitioning reactant and product concentrations on separate sides of the film.)¹³ Schematics summarizing the above described processes are shown below in figure 3.1.

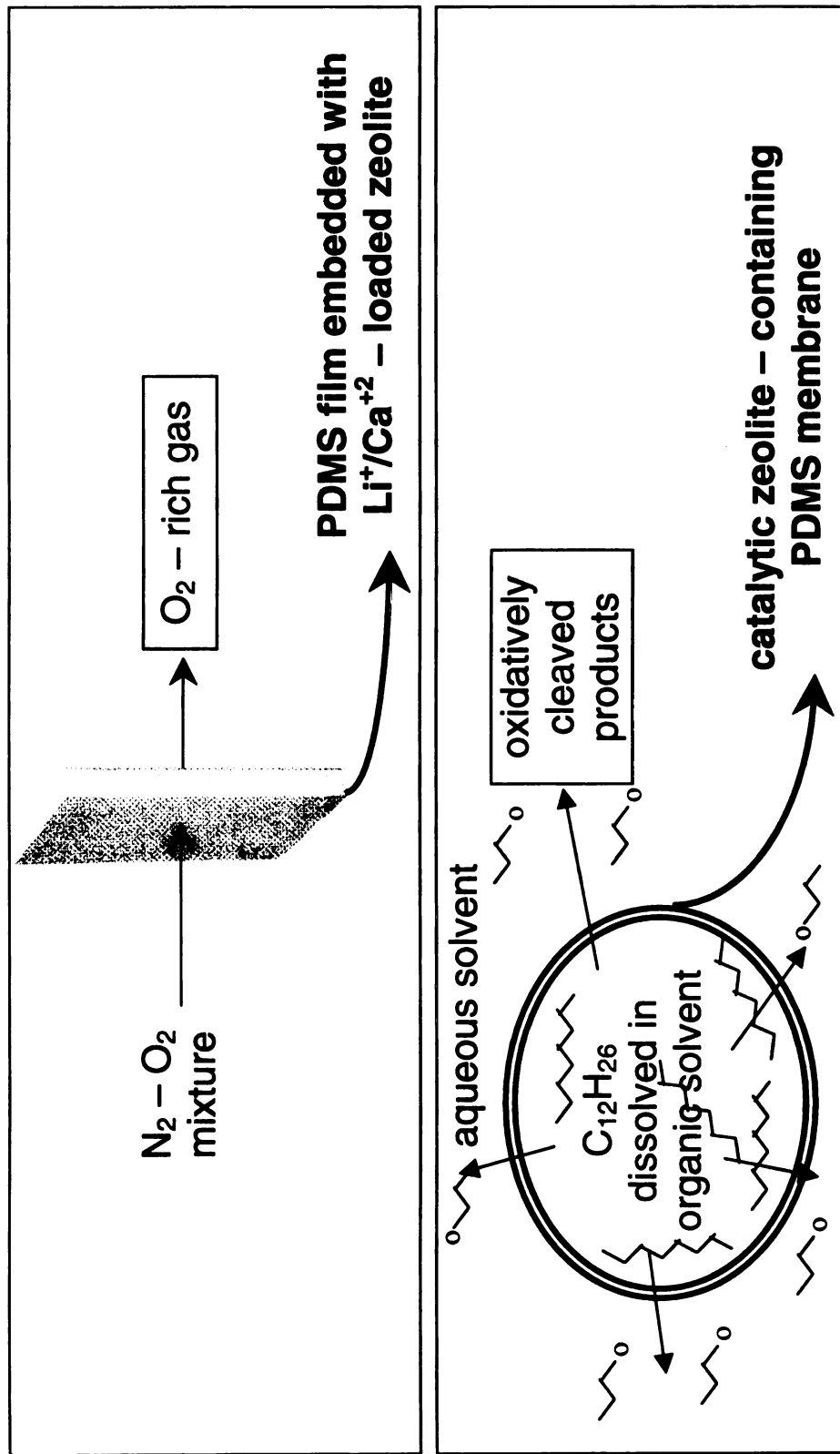


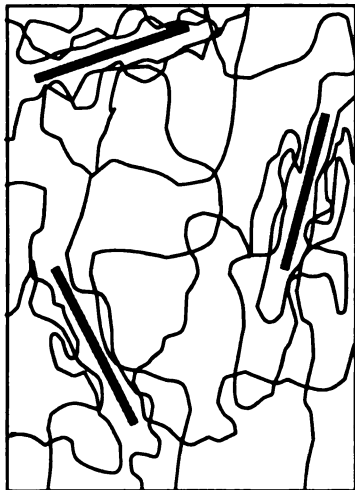
Figure 3.1 Schematics representing known reactive membrane and selective gas separation procedures using functionalized aluminosilicates.

This study involves introducing a copper salt delivered in tetrahydrofuran (THF) to the crosslinked silicone systems. Solvent choice is particularly important in achieving a post-cure ion exchange as ordinarily mutually exclusive solvation properties are needed to successfully complete the replacement of clay gallery cations within the silicone matrix. First off, the silicone polymer is highly non-polar and swells when exposed to typical organic solvents such as toluene, cyclohexane, chlorinated hydrocarbons and straight chain alkanes. Large amounts of solvent invade the crosslinked rubber and distend the samples to several times their original volume as alluded to earlier. The extent of sample expansion has been noted to vary directly with the amount and effectiveness of filler content. This swelling phenomenon in composite materials has been described by Kraus, who plotted the swelling ratio shown below versus the amount of filler.

$$V_r = \frac{\text{volume of unswollen polymer matrix}}{\text{volume of swollen polymer matrix}}$$

After accounting for the volume content of the unswellable filler, correlations between the curves of different filler types revealed that the better reinforcement phases also had the greatest effect of reducing solvent uptake. High surface area fillers having strong interfacial interactions with the polymeric phase matrix create regions in the matrix known as “bound polymer”. Here physisorbed or chemisorbed polymer in close proximity with the reinforcement phase has a more

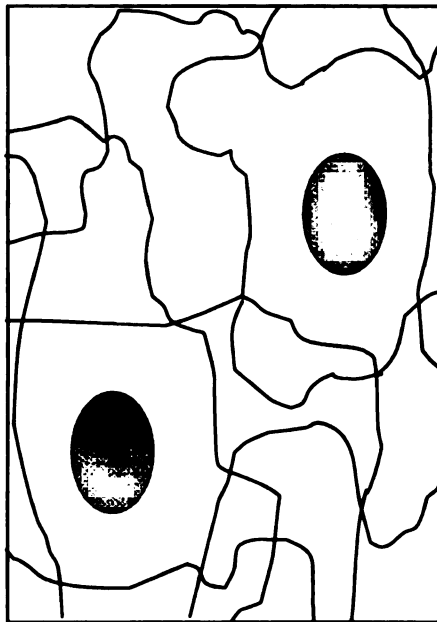
limited free volume and extendability, thus restricting the swelling capability. Non-reinforcing fillers lack the presence of significant amounts of bound polymer at the interface, and interestingly can actually undergo a greater solvent uptake than in the unfilled system. In this case, large vacuoles arise at the interface of the non-reinforcing filler and these rapidly fill with solvent and expand further. Conventionally filled elastomers, such as kaolin – filled styrene butadiene rubber, commonly swell more than the unfilled rubber due to this detaching polymer at the filler interface when exposed to solvent. A schematic representing the affect of bound polymer and the detrimental filling affect of a poor reinforcement phase is shown in figure 3.2.



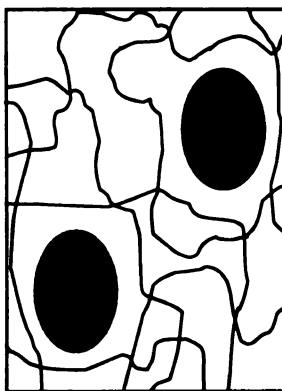
swelling solvent



Exfoliated nanocomposite with favorable interfacial interactions



swelling solvent



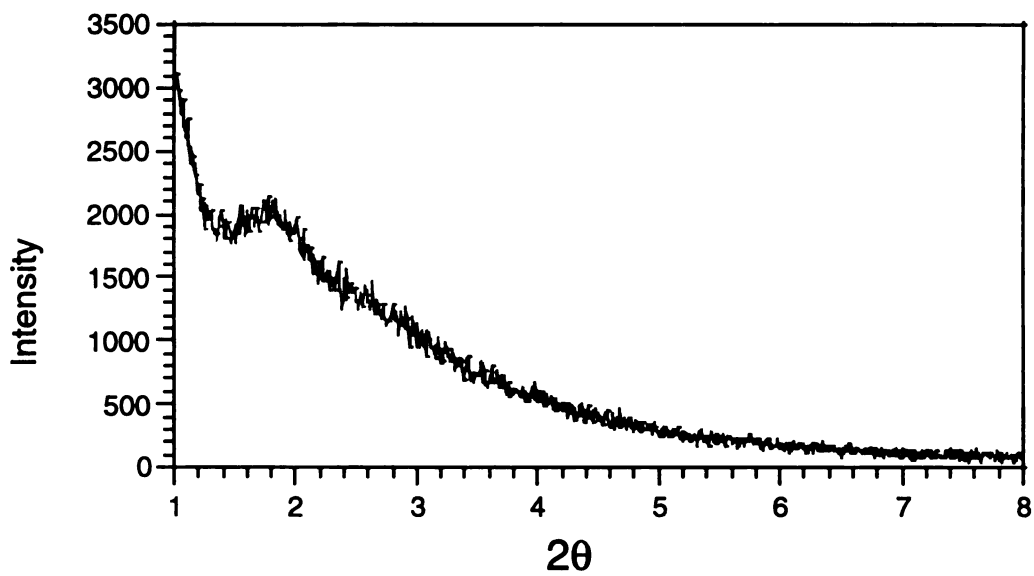
Conventional composite with poor interfacial interactions

Figure 3.2 Schematic showing the reduced swelling observed in nanocomposites due to the constrained polymer at the interface of the reinforcer.

The silicone nanocomposites synthesized in this work obey the indirect relationship between solvent - influenced volume increase and the nanocomposite clay content in accordance with favorable reinforcement phase – polymeric phase interfacial interactions. This supports the mechanical improvement evidence identified in chapter 2 that the nanolayers are not only well dispersed in the silicone matrix (influencing a larger portion of the polymer), but they are also having favorable interactions with the polymer at the interfacial region (leading to the bound polymer - driven reduced swelling). Indeed, even at clay loadings of 1-2% by weight, the nanocomposites exhibit a reduced swelling compared to the pristine silicone on the order of 10-20%. Rather uniquely, organofluorohectorite – synthesized nanocomposites generated with identical clay loadings, but cured under different conditions gave rise to a disparity in the amount of solvent equilibrated into their matrices. While all samples cured at room temperature under vacuum absorbed the same volume of solvent at particular clay loadings, those nanocomposites that were prematurely heated (~100°C) were capable of uptaking more organics. This can be understood by examining the X-ray diffraction patterns in the two dissimilarly cured samples. Amorphous patterns arise from all room temperature cured systems, indicating a more exfoliated nanocomposite, while rapid heating of the ungelled samples causes a premature gelation that immobilizes clay layers before they can be fully dispersed. Figure 3.3 shows two XRD patterns, one of the typically cured PDMS nanocomposite, the other of a prematurely heated nanocomposite that retains some registry between clay layers. Detrimental implications of non-exfoliated

clay tactoids arise from inefficient surface area exposure of the clay particles, and thus a limited reinforcing effect.

prematurely heated nanocomposite



room temperature cured nanocomposite

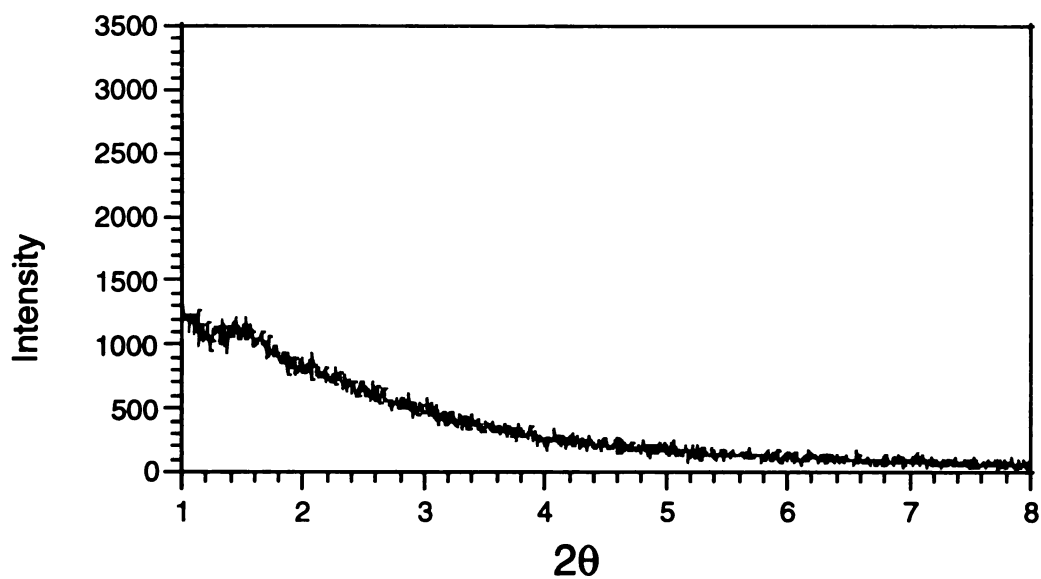


Figure 3.3 XRD patterns of silicone nanocomposites cured under different conditions. Accelerating the cure with premature heating (top pattern) leads to a lower degree of exfoliated clay layers.

Aside from the importance of swelling polydimethylsiloxane, which exposes the exfoliated clay layers to the liquid medium, the solvent also must be capable of dissolving the salt in order to allow for the solvated cations to penetrate into the silicone matrix and ultimately approach the clay exchange sites. The use of tetrahydrofuran as a post-cure ion exchange bath is an ideal choice as it both swells the organophilic silicone matrix and also has sufficient polarity and coordinative ability to allow for copper salt dissolution. Other solvents explored in achieving both the swelling of the silicone matrix and dissolution of various salts included acetone, ethanol, isopropanol, acetonitrile, chloroform, and mixtures thereof. While the copper salt has appreciable solubility in the more polar solvents, these solutions lack the capability of infiltrating the silicone rubber. Employing THF solves this problem, and therefore all post-cure ion exchanges were carried out in a THF – CuCl₂ bath. As touched upon later, copper was selected as the replacement cation for several reasons, however a variety of copper (II) salts were experimented with for delivering the cations. Although ordinarily not a discriminating factor, the balancing anions did affect the end ion exchanges in certain cases. Copper acetate is one such example where the persistence of significant amounts of acetate after several washings was detected by Infrared Spectroscopy. Though evidence for copper ion exchange was noted in these systems, it appeared that the cetyltrimethylammonium acetate salts formed after copper replacement were more soluble in and therefore less mobile through the silicone. Just as the THF was selected as the ideal solvent, the readily available and most successful copper source was determined to be halide salts. An illustration of the general post - cure ion

exchange procedure utilizing THF as the swelling agent, and CuCl_2 as the exchange salt is represented in figure 3.4.

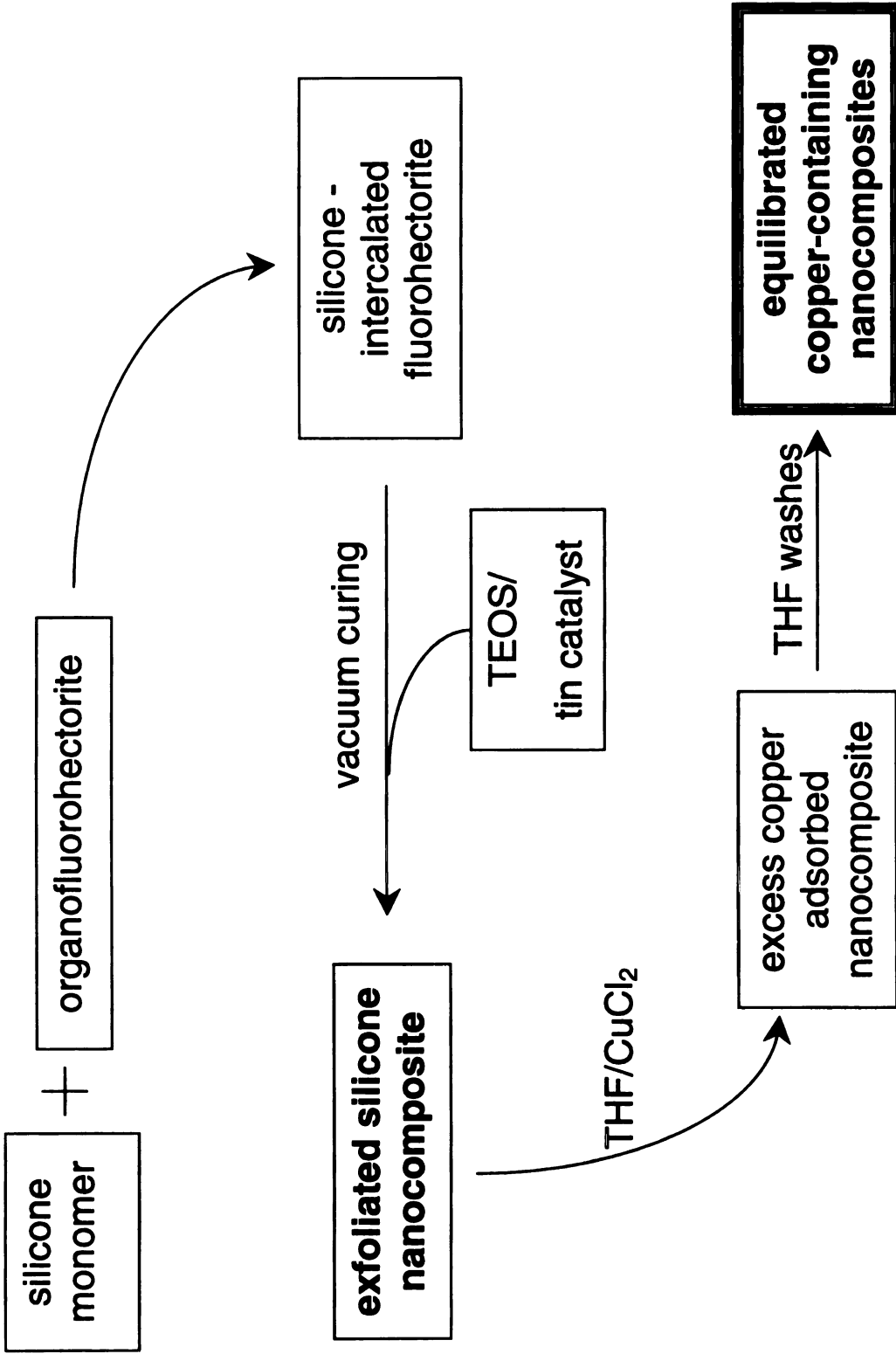


Figure 3.4 Schematic of the procedure involved in synthesizing and post-cure ion exchanging silicone nanocomposites.

This study represents the first demonstration involved in probing the clay exchange site accessibility of a polymer – clay nanocomposite. The potential contributions for examining the fluorohectorite - silicone hybrid system for this previously unexplored phenomenon were touched on above, but the main focus of this preliminary work is to first prove that the smectite surfaces can be accessed even when housed in an entangled polymer matrix. The challenges of such a procedure are obvious, however, the unique properties of silicone rubbers make the unconventional ion exchange achievable. The ability of silicone rubbers to absorb and transmit large molecules through the matrix hinted at the notion that a post-cure ion exchange was possible provided an adequate solvation medium could be isolated. It is the weak intermolecular interactions between neighboring polydimethylsiloxane chains that facilitate the migration of macromolecules into and through the matrix. Weak chain – to – chain forces create large free volumes not ordinarily associated with organic elastomers, nor any carbon based polymer systems. The lack of crystallinity does not discount silicones as dimensionally stable, physically robust elastomers, however. In fact, silicones have a more chemically inert and thermally stable Si-O backbone relative to carbon based polymers, and the bond strength is almost twice that of a carbon – carbon bond (160 kcal/mol versus 86 kcal/mol). The backbone also has a much lower barrier to rotation (1.0 kcal/mol versus 3.0 kcal/mol), and this, along with the reduced intermolecular interactions, creates a highly random crosslinked polymer that can uptake large amounts of solvent, thereby extending the siloxane chains and rendering the swollen matrix liquid-like. In this state the

desired migration of exchangeable cations to the exfoliated clay layer sites is quite feasible. Figure 3.5 schematically shows the influence on polydimethylsiloxane chains by equilibrating the crosslinked polymer network with an organic solvent.

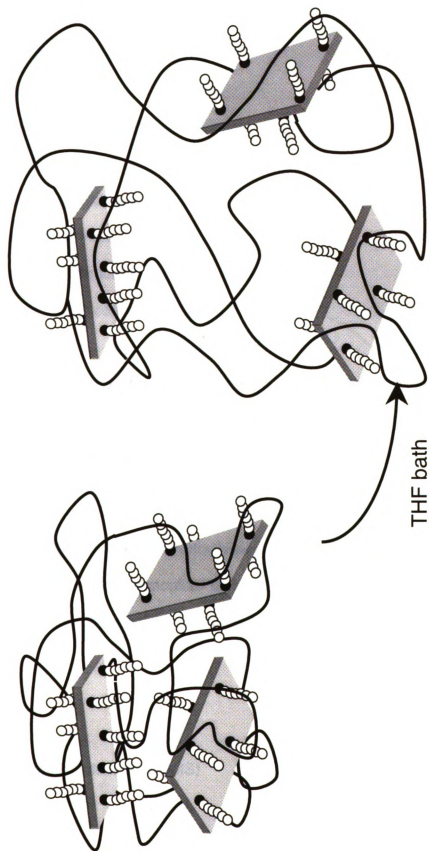


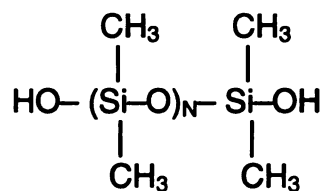
Figure 3.5 Representation of the crosslinked silicone nanocomposite before and after immersion in THF.

The occurrence of two distinct polymer regions, one at the interface and another in the bulk, gives rise to anisotropic swelling of the matrix. Although less solvent is partitioned into the bound polymer at the interfacial regions, the overriding permeability of polydimethylsiloxane still permits infiltration of the solvated copper, as described in the results section. When equilibrated with Cu/THF, the silicone samples take on the color of the THF – copper solution as described later. The nanocomposite color change when copper is present provided qualitative feedback and this, along with the added accuracy of monitoring copper metal content in particular via elemental analysis, made it a practical choice for the demonstration-of-concept experiments in silicone nanocomposite post-cure ion exchanges.

3.2 Experimental

Materials. PDMS polymers with average molecular weight values of 400, 1750 and 4200 and tin(II) 2-ethylhexanoate were obtained from Gelest, Inc. Hexadecyltrimethylammonium bromide and all other chemicals were purchased from Aldrich Chemical Co. and used without further purification.

Polydimethylsiloxane (PDMS)



Tetraethylorthosilicate (TEOS)

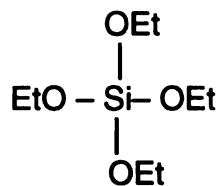


Table 3.1 Silanol Terminated PDMS Monomers

PDMS MW	N value (Si(CH₃)₂-O repeat)	Viscosity (cSt)
400	6	20
1500-2000	23	45-85
4200	57	90-120
18000	243	700-800

Organoclay Synthesis

Lithium fluorohectorite (Corning, Inc.) with an anhydrous unit cell formula of $\text{Li}_{1.12}[\text{Mg}_{4.88}\text{Li}_{1.12}](\text{Si}_{8.00})\text{F}_4$ was ion-exchanged with a two-fold stoichiometric excess of hexadecyltrimethylammonium bromide. A mixture of the surfactant cations and a 1.0 wt % aqueous suspension of the inorganic clay was stirred at room temperature for 12 hours. The flocculated organoclay was removed by vacuum filtration and the excess surfactant was washed from the clay by re-suspending the solid in water, filtering again, and then subjecting the solid to a final Soxhlet extraction in ethanol for 24 hours. The clay was then dried, crushed and sieved to a particle size $<106 \mu\text{m}$ prior to use in the intercalation and nanocomposite studies. The water and organic content of the air-dried organoclay, as determined by the weight loss at 150°C and 500°C , was 6 wt % and 24 wt %, respectively.

Nanocomposite Synthesis

The nanocomposites were synthesized through initial swelling of organofluorohectorite by the PDMS monomers, followed by addition of TEOS and tin octoate catalyst to commence crosslinking. A predetermined amount of organoclay was added to the desired PDMS pre-polymer and mixed for 12 hours. Agitation of the clay-PDMS mixture was accomplished by first manual stirring with a spatula followed by vortexing the suspension for several minutes. A stoichiometric amount of tetraethylorthosilicate (TEOS) as a crosslinking agent and tin(II) 2-ethylhexanoate as a catalyst (TEOS : Sn = 4 : 1 by volume) were added to the PDMS - organoclay mixture. The resulting thixotropic intercalate

was then transferred to an stainless steel mold and out gassed under vacuum. Crosslinking of the nanocomposite was carried out under vacuum at ambient temperature for 12 hours, followed by an additional 12 hours at 100 °C remaining under vacuum.

Post-cure Ion Exchange

Nanocomposite and pristine crosslinked silicone samples were exposed to a THF bath containing copper cations for the ion exchange of cetyltrimethylammonium present at the exfoliated clay surface. Nanocomposite immersion in copper salt-containing THF was carried out at a concentration of 6.0×10^{-3} mole per gram of silicate in the nanocomposite samples (10 fold excess calculated by clay CEC). This dark green solution was allowed to penetrate the samples and ultimately swell them to several times their initial volume once replete with solvent. The equilibrated samples remained in copper - THF solution for 24 hours, after which they were transferred to a pure THF wash. At this point the samples had taken on the dark green color of the copper - THF solution, and an immediate leaching of the excess adsorbed copper into the first THF wash was observed. Successive THF washes, each 10 ml per gram of silicone sample, were employed to remove the unbound copper and potentially exchanged quaternary alkylamine salts. Elemental analysis studies indicated that the removal of unbound copper was completed after roughly 2 washes, however a total of 10 THF washes were employed to ensure an equilibrated state.

imm

sar

ret

pri

the

res

ev

no

un

un

rel

se

na

3.3 Results and Discussion

Cured pristine silicone and silicone nanocomposite samples were fully immersed in a copper chloride – THF solution. Once equilibrated, the swollen samples had taken on the dark green color of the solution. This color was retained after allowing the solvent to evaporate (a process which destroyed the pristine silicone), indicating that strong coordination of THF to copper persisted in the samples even in the unswollen state. Washing the samples with pure THF resulted in rapid removal of the unbound copper salt, as noted above. Indeed, evaporation of THF after the third wash, unlike the first two, did not result in any notable residual copper/alkylammonium salt. Therefore, the high solubility of unbound copper chloride in THF is thought to promote the removal of unexchanged copper as well as potentially exchanged alkylammonium salts relatively efficiently. Figure 3.6 depicts the copper content present after sequential THF washings for pristine (0%), 5% and 10%wt. silicate nanocomposite samples.

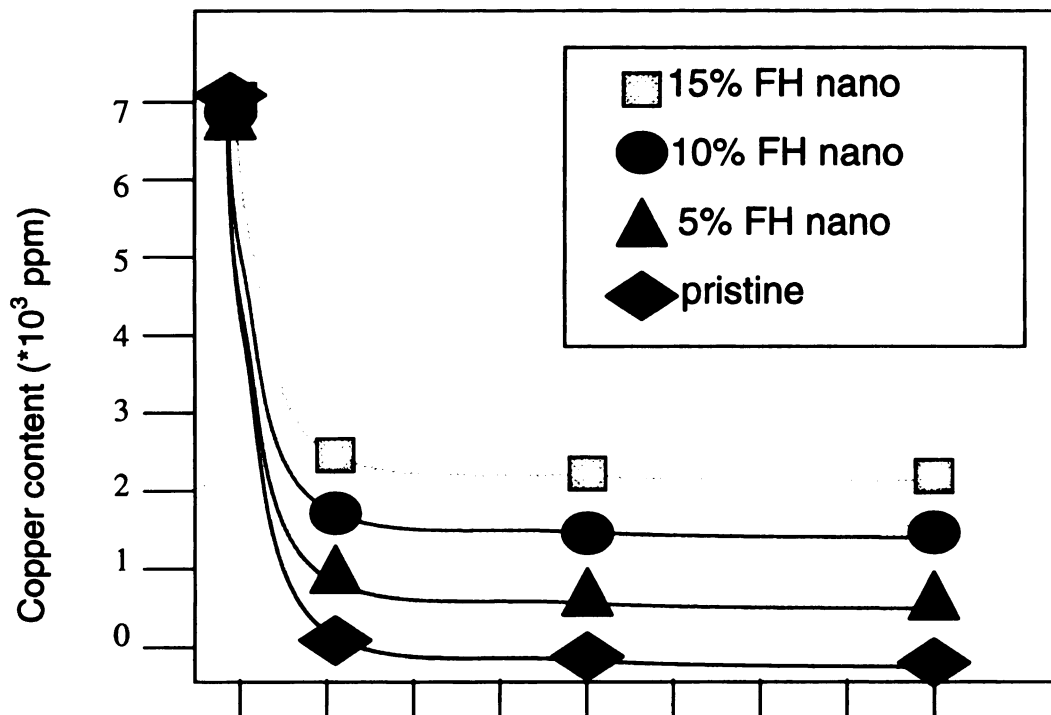


Figure 3.6 Copper content following post-cure ion exchanges for silicone nanocomposites examined after successive THF washes. Unleachable copper accounted for roughly 70% of the fluorohectorite ion exchange capacity in the filled systems, while pristine silicone retained almost no copper after washing.

The final nanocomposites retained a pale sky blue color after THF washings, identical to Cu^{+2} -exchanged fluorohectorite (synthesized for comparison), while the pristine silicones returned to their original transparent state. A brief depiction of this significant result is shown schematically in figure 3.7.

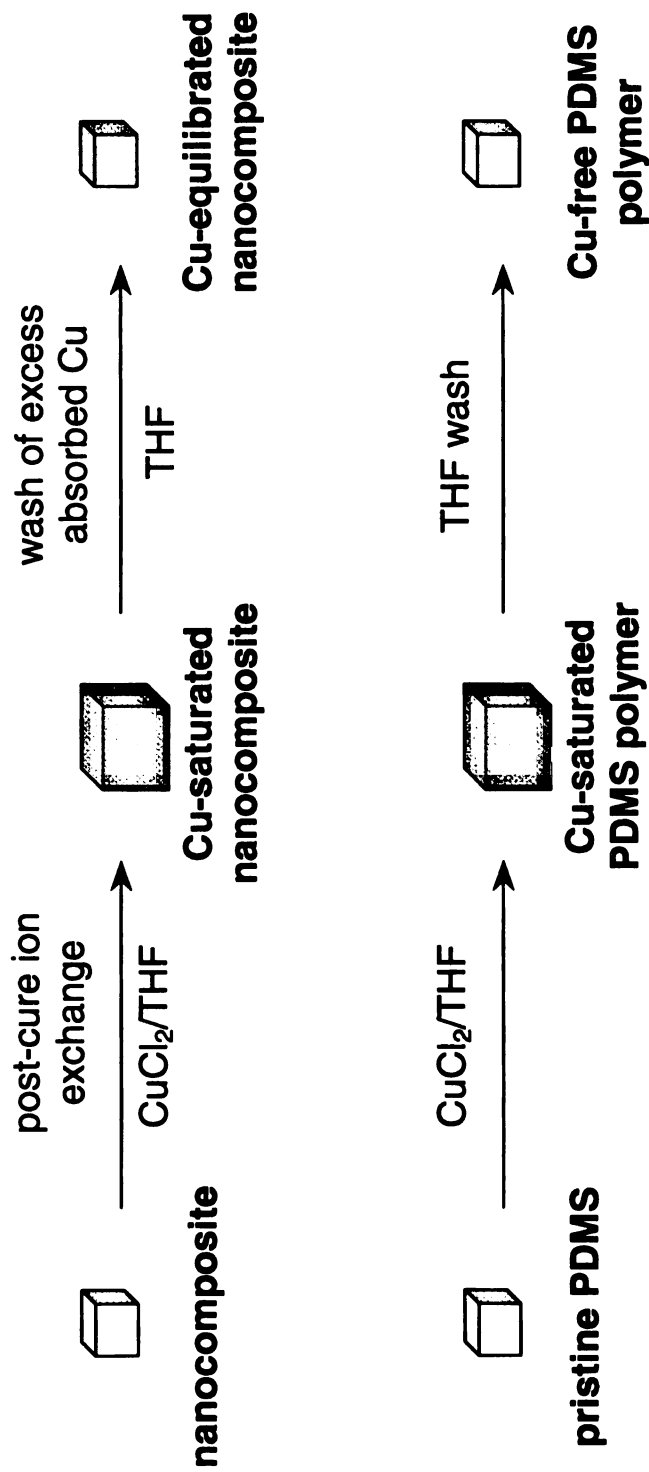


Figure 3.7 Schematic representation of the post-cure ion exchange using a CuCl_2/THF exchange bath and pure THF as the wash. Uptake of copper into both nanocomposite and pristine samples was observed, however upon purging with THF only the nanocomposites retained copper.

The predicted values, assuming complete ion exchange of Cu^{+2} based on a cationic exchange capacity of 121 meq/100g (experimentally determined) for fluorohectorite, are listed in Table 3.2 along with the observed final copper content for several nanocomposites.

Table 3.2 Copper Content Present After Post – Cure Ion Exchange

	Theoretical Cu (ppm) ^a	Actual Cu (ppm) ^b	% ion exchange
Pristine	0	53	–
5% FH	1330	891	67
10% FH	2660	1747	66
15% FH	3990	2884	72

a – theoretical Cu^{+2} content as calculated using an experimentally determined fluorohectorite CEC of 121meq/100g

b – residual copper content determined by ICP elemental analysis

The direct correlation between clay content and remnant copper concentration after THF soakings reveals the presence of strong copper to clay binding. The high solubility of cupric halides in THF dispels the possibility of insufficient washing giving rise to the residual, unleachable copper analyzed in the final clay containing samples. Unlike the reverse scenario, quantitative copper exchange for cationic alkylamines occupying the organoclay exchange sites is not

anticipated in any solvent. More generally, the attempted ion exchange of any inorganic cations for already present organic surfactant cations on high charge density surfaces is highly unfavorable. Here the van der Waals interactions between organic surfactant chains creates a more stable intercalated organoclay phase relative to the inorganic clay. This leads to an unfavorable displacement by the inorganic cations despite introducing a large excess of copper salt. The higher the charge density of the exchange medium, the denser the surfactant stacking, and thus the thermodynamically favorable organic entanglement becomes more difficult to infiltrate by alternative cations. In fact, attempting a cation exchange starting with pure cetyltrimethylammonium fluorohectorite suspended in THF, and introducing a 20 fold excess of copper salt (based on CEC of the clay) for 48 hours yields an identical XRD pattern to the original organoclay, and elemental analysis studies indicate only trace amounts of copper substitution into the final exchanged clay. However, THF is not to be precluded as a viable solvent for general smectite clay ion exchange as Cu^{+2} - fluorohectorite clays were successfully synthesized by introduction of 10 fold excess CuCl_2 to a parent inorganic fluorohectorite (Li^+ -exchanged) suspension in THF. As hypothesized, the persistence of bound copper in the post-cure nanocomposite ion exchanges occurs at a much higher fraction than pure organoclay exchanges, on the order of 70%, using a 10 fold equivalence of copper cations. The highly dispersed clay layers in exfoliated silicone nanocomposites appear to facilitate exposure of the incumbent quaternary surfactant cations to the copper – containing solvent relative to the exchange

performed with pure organoclay. Additionally, a more complete ion exchange of copper for alkylammonium ions in the post-cure nanocomposite could result from solvation of the C₁₆ surfactant chains by the silicone polymer. The favorable silicone – onium interactions (as supported by the large driving force for PDMS monomer intercalation into the organofluorohectorite) disrupt onium - onium contact at the silicate surface that, in the pure organoclay – copper exchange, likely limits the abstraction of surfactant ions. This onium – onium disruption is seen in certain solvated and intercalated organoclay species where the inclined paraffin arrangement (00l spacing of 27.4 Å for CTA-FH) is expanded to a completely vertical orientation (~32 Å solvated), and an interdigitated vertical orientation (38 Å intercalated with 400 MW PDMS). In the latter case, polydimethylsiloxane monomers solvate the onium chains and permit their enthalpic favorable contact with one another to be disrupted in favor of silicone – onium interactions. Silicone – onium contact is not restricted to the clay surface, therefore displacement of the organic cations by copper followed by subsequent migration of the surfactant salts ultimately out of the silicone matrix into the THF bath is a potential route not viable in the copper ion exchange of pure organoclay. After washing, the comprehensive copper extraction in the clay-free silicone, coupled with the direct correlation of clay content to the amount of bound copper, indicates that the copper found in the nanocomposites does not arise from residual incorporation or trapping in the polydimethylsiloxane matrix. A schematic representation of the biased ion exchange in the nanocomposite versus the pure organoclay, along with a depiction of the successful

fluorohectorite ion exchange of Li^+ for Cu^{+2} as carried out in THF is represented in figure 3.8.

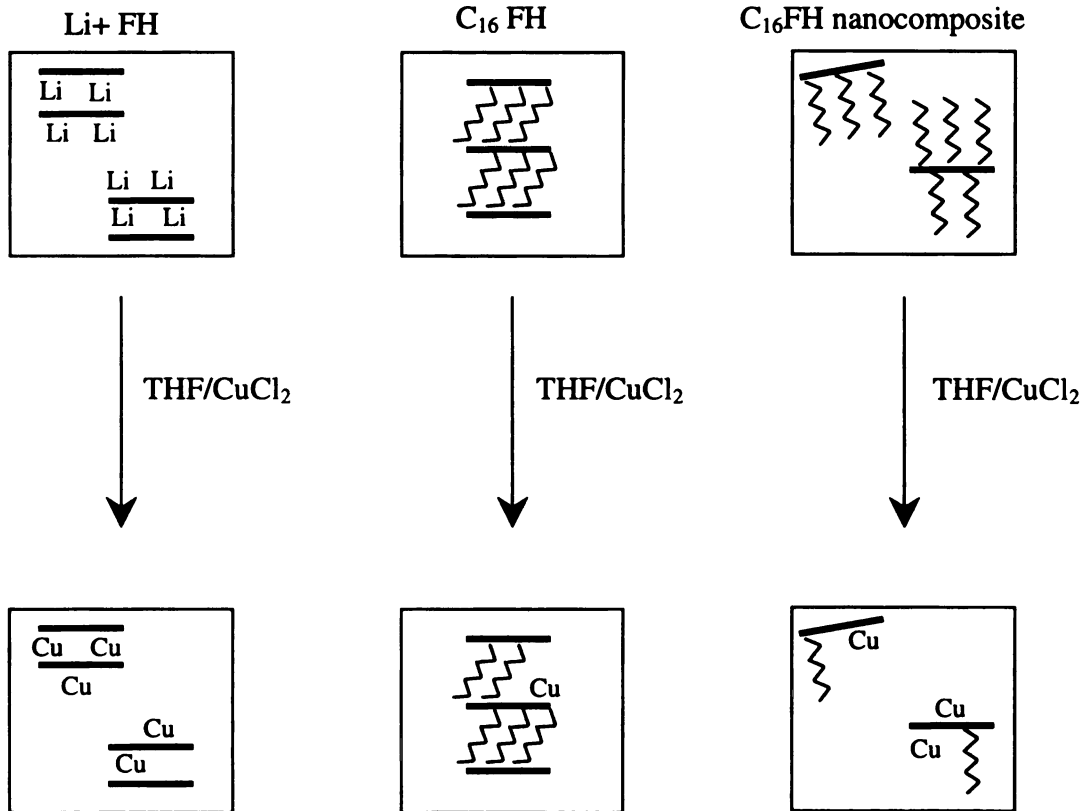


Figure 3.8 Schematic illustrating copper ion exchanges carried out in THF for different parent clay systems. Excess copper successfully substitutes for both the inorganic cations in lithium fluorohectorite as well as the majority of surfactant ions on organofluorohectorite exfoliated in a silicone matrix. However, despite increasing the copper concentration to 20 times the CEC of the clay, organic cations could not be appreciably displaced by Cu⁺² in THF.

3.4 Conclusions

In summary, crosslinking of a PDMS - swollen cetyltrimethylammonium fluorohectorite clay–silicone suspension yields exfoliated nanocomposites as outlined in chapter 2. Utilizing the high free volume and large diffusion coefficient inherent in silicones, post-cure ion exchanges of the dispersed nanolayers were performed. Post-cure ion exchange was accomplished by immersion of the nanocomposites in a CuCl_2/THF solution, followed by pure THF purging of the distended samples in order to remove unbound copper and potentially exchanged alkylamine salts. The amount of unleachable copper varied directly with clay content of the nanocomposites, while pristine silicone samples retained essentially no copper after washing. In the clay containing samples, remnant copper concentration accounted for roughly 70% of the predicted ion exchange capacity for the exfoliated clay layers. Performing ion exchanges of the identical clay (CTA-FH) outside the silicone matrix in THF resulted in only trace exchanges of copper. While inorganic – inorganic ion exchanges were successfully completed in THF, organic cations could only be exchanged for inorganic cations (copper) when the organoclay was exfoliated in a PDMS matrix. The accessible cationic clay sites in a crosslinked nanocomposite afford an opportunity to explore selective membrane and flow-through gas or liquid separation chemistry formerly unavailable with typical organo-functionalized silicate nanocomposites. The success of a post-cure ion exchange with silicone

nanocomposites likely stems from both the high permeability of the matrix, allowing a relatively unhindered influx of exchangeable solvated cations, along with the highly exposed exfoliated nanolayers, limiting confined galleries that would inhibit accessibility of the cationic clay sites. Extension of post-cure nanocomposite ion exchanges into other polymer systems will be dependant upon how permeable and swellable the polymer matrix is, and also how well exfoliated (and thus exposed to the exchange medium) the clay layers are in the final nanocomposite.

3.5 References

- (1) Pinnavaia, T. J. *Science* **1983**, *220*, 365-371.
- (2) Messersmith, P. B.; Stupp, S. *J. Mater. Res.* **1992**, *7*, 2599.
- (3) Okada, A.; Usuki, A. *Mater. Sci. Eng. C-Biomimetic Mater. Sens. Syst.* **1995**, *3*, 109-115.
- (4) Giannelis, E. P. *Adv. Mater.* **1996**, *8*, 29-&.
- (5) Wang, S.; Long, C.; Wang, X.; Li, Q.; Qi, Z. *J. Appl. Polym. Sci.* **1998**, *69*, 1557-1561.
- (6) Burnside, S. D.; Giannelis, E. P. *Abstr. Pap. Am. Chem. Soc.* **1996**, *212*, 19.
- (7) Burnside, S. D.; Giannelis, E. P. *J. Polym. Sci. Pt. B-Polym. Phys.* **2000**, *38*, 1595-1604.
- (8) LeBaron, P. C.; Pinnavaia, T. J. *Chem. Mater.* **2001**, ACS ASAP.

- (9) Shi, H.; Lan, T.; Pinnavaia, T. J. *Chem. Mater.* **1996**, *8*, 1584-1587.
- (10) Balazs, A. C.; Singh, C.; Zhulina, E. *Macromolecules* **1998**, *31*, 8370-8381.
- (11) Lyatskaya, Y.; Balazs, A. C. *Macromolecules* **1998**, *31*, 6676-6680.
- (12) Coe, C. G. *Access Nanoporous Mater., [Proc. Symp.]* **1995**, 213-229.
- (13) Langhendries, G.; Baron, G.; Vankelecom, I.; Parton, R.; Jacobs, P. *Catal. Today* **2000**, *56*, 131-135.

Chapter 4

EXFOLIATION OF DIAMINE – MODIFIED CLAYS IN A GLASSY EPOXY MATRIX

4.1 Introduction

Polymer layered silicate nanocomposites (PLSNs) represent one of the most interesting classes of organic – inorganic hybrid materials, with an increasing potential both in fundamental research and in commercial applications.¹⁻¹⁵ The PLSNs exhibit improved physical and performance properties compared to the unmodified polymers and the conventional composites, mainly due to their unique phase morphology and interfacial properties induced by the highly dispersed silicate nanolayers in the polymer matrix. These effects are minimized in the conventional composites where the inorganic additives have dimensions in the macroscopic (μm) length scale. As a result greater improvement of the polymer's properties can be achieved at a considerably lower concentration of the inorganic reinforcement phase in PLSNs compared to conventional composites. Loadings of only up to ~5 wt. % exfoliated silicate nanoparticles in PLSNs generally result in significant enhancement of a number of physical properties, including mechanical properties (modulus, strength, thermal expansion coefficient), barrier properties, thermal stability, resistance to solvent swelling, flammability resistance and ablation performance.

A wide variety of layered materials are potentially well suited for the formation of organic – inorganic nanocomposites because their lamellar elements have high in-plane strength and stiffness accompanied with a high aspect ratio. However, the smectite clays¹⁶ (e.g. montmorillonite, hectorite and synthetic smectites) along with other layered silicates are the materials of choice for polymer nanocomposite design, mainly because of their rich intercalation chemistry which allows them to be chemically modified and to become compatible with the polymer precursors. Many robust reinforcement fillers, including high surface area silicas and various aluminosilicates, certainly have the facility of strengthening a polymeric matrix, however, their lack of ion exchange capability renders such materials highly limited as universal polymer fillers. Additionally, even though they can be readily synthesized, layered smectites occur ubiquitously in nature and can be purified at relatively low cost.

Toyota researchers demonstrated the first example in which an organic montmorillonite clay was exfoliated in a thermoplastic nylon-6 polymer, resulting in a commercialized product with enhanced thermo-mechanical properties. The organic clay was synthesized by ion-exchanging the cations of the parent clay with more hydrophobic organic onium ions.¹⁷⁻¹⁹ In the next 10 years research focused on issues relating to the most suitable organic modifier for the clay and the best conditions for the formation of the nanocomposites. A major portion of this research was explored in studying nanocomposites formed by thermoset polymers, more specifically epoxy resins, and modified smectite clays,^{8,10,12,15,20-29} along with other layered silicates, such as silicic acids (e.g. magadiite).³⁰ It has

been previously shown that acidic primary onium ions, when they are ion-exchanged for the inorganic cations of the parent layered silicates, catalyze the intragallery epoxide polymerization process in the presence of diamine curing agent.^{25,30} Parameters like the chain-length of the organic onium ion, the relative acid strength (primary, secondary, tertiary) and the clay layer charge density, which dictates the concentration of the organic modifier in the galleries, play an important role in achieving optimum nanolayer intercalation by, and ultimately exfoliation in the polymer. The catalytic activity of the acidic onium ions is more pronounced when the alkyl chain is of particular size and functionality to intercalate the largest amount of monomer. Matching the polarity of the intragallery region with the polymer in this way provides a compatibilized environment that promotes a maximum polymerization rate between the clay layers by permitting a sufficient concentration of reactive monomers to exist within the acid catalyzed region between clay layers. In a recently reported study,²² it was shown that the use of a hydroxyl - substituted quaternary ammonium modifier in a montmorillonite clay resulted in a high degree of clay layer exfoliation. In this case the strong hydrogen bonding between the surfactant hydroxyls and the oxirane ring in the resin provided a similar intragallery reaction rate bias that facilitated the dissemination of the organofunctionalized clay particles. Figure 4.1 schematically represents the influential role of acidic surfactant molecules found in the intragallery regions.

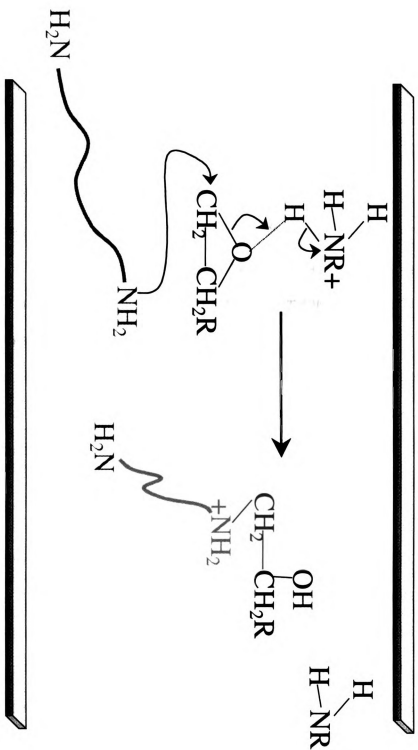


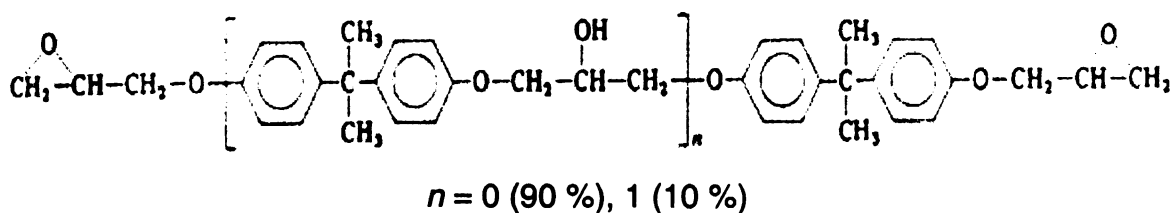
Figure 4.1

Acid catalyzed intragallery ring – opening of an epoxy resin.

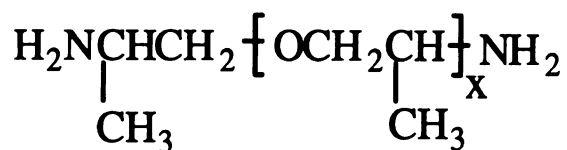
In an effort to optimize the overall formation process of the of thermoset epoxy – clay nanocomposites, the work presented in this chapter focuses on the synthesis of a new type of potentially advantageous organic smectite clays. The direct incorporation of Jeffamine (multifunctionalized primary amines provided by Huntsman Chemical) curing agents inside the galleries of montmorillonite and fluorohectorite clays in the form of diprotonated diamines through an ion-exchange process, is presented as an alternative, commercially attractive way of preparing epoxy – clay nanocomposites. Different degrees of clay nanolayer intercalation/exfoliation could be achieved, depending mainly on the chain-length and the concentration of the diamine surfactant molecules in the clay galleries. While a substantial improvement in the mechanical properties of all nanocomposites synthesized via this route was found, the ultimate goal of achieving the highest degree of clay exfoliation is stressed, as these materials should be most functional commercially in replacing heavier glass – reinforced engineering plastics.

4.2 Experimental

Materials. The epoxide resin used for synthesis of the pristine glassy epoxy polymer and the epoxy – clay nanocomposites was a diglycidyl ether of bisphenol A (DGEBA), more specifically, Shell EPON 826 with MW ~369 and epoxy equivalent weight ~182:



The curing agent was a polyoxypropylene diamine, Jeffamine D230 (Huntsman Chemical) with MW ~230:



$$n = 2.6$$

Jeffamines D2000 (MW ~2000, $n=33.1$), D400 (MW ~400, $n=5.6$) and D230 (MW ~230, $n=2.6$) were used for the synthesis of the organic clays, as is outlined below. All other chemicals used in this work were purchased from Aldrich Chemical Co. and used without further purification.

Organic Clay Synthesis

An industrially purified Na^+ -montmorillonite clay (PGW, Nanocor Inc.) with CEC = 120 meq/100 g, was used to produce the H^+ and Li^+ forms of the montmorillonite clay by typical ion-exchange procedures with diluted HCl (for H^+ -clay) or LiCl (for Li^+ -clay) aqueous solutions. A synthetic Li^+ -fluorohectorite clay (FH, Corning Inc.) with CEC similar to that of the PGW montmorillonite was used as the parent fluorohectorite clay in this study.

The organic clays were prepared by ion-exchanging the inorganic clay with diprotonated diamines, Jeffamines D2000, D400 and D230. Jeffamines in

slight excess of the stoichiometric ion-exchange of the clay were diluted in aqueous HCl solution; a small excess of H⁺ was also used to ensure the formation of diprotonated diamines. The acidic Jeffamine solution was then blended for 1-2 min with an aqueous inorganic clay suspension. The blended mixture was further stirred for 48 hrs at ambient temperature. In the case of D230, a second sample was prepared by ion-exchanging the parent clay using double the stoichiometric amount of diamine, in order to achieve higher degree of ion exchange. The ion-exchanged clays were separated by centrifugation, washed 3-4 times with deionized water (until free of Cl⁻) and once with EtOH, previous to air-drying at room temperature. The dried products were ground and sieved to a particle size < 270 mesh (53 μm). All the inorganic and organic montmorillonite (PGW) clays prepared are listed in Table 1, together with compositional and structural data.

Preparation of Epoxy – Clay Nanocomposites

The pristine glassy epoxy polymer was formed by mixing the epoxy monomer (EPON 826) with the curing agent (Jeffamine D230) at 50°C for ~30 min, outgassing of the liquid mixture at room temperature and curing in RTV silicone rubber molds at 75°C for 3 hrs and, subsequently, at 125°C for an additional 3 hrs, under nitrogen (to avoid oxidation and browning of the polymer at the higher cure temperatures).

In the preparation of the epoxy – clay nanocomposites, the modified clay was added to EPON 826 - curing agent D230 mixture at 50°C by stirring for 30 min,

before outgassing and curing at 75°C and 125°C (procedure *P-1*), similar to the pristine polymer formation. Alternatively, the epoxy EPON 826 was initially mixed with the clay at 50°C for a certain period of time and then the curing agent D230 was added (procedure *P-2*). In the case of the organic clays synthesized with the three different Jeffamines (D2000, D400, D230), the moles of onium ions present in the organic clay were counted as contributing crosslinking agents to the curing process, supplementary to the amine groups of Jeffamine D230 (the main curing agent for the formation of the glassy epoxy polymers). The amount of diamine crosslinker arising from the organic modifier of the clays was always less than 4 % of the total amine groups necessary for complete cross-linking of the epoxy monomers. The clay loadings of the nanocomposites prepared were 1, 3 and 6 wt. % silicate (meaning the content of organic in the functionalized clays was normalized and actual reinforcing silicate weights were reported).

Physical Measurements

X-ray diffraction (XRD) patterns were obtained on a Rigaku rotaflex 200B diffractometer equipped with Cu K α X-ray radiation and a curved crystal graphite monochromator, operating at 45 KV and 100 mA. The diffraction patterns were collected between 1 and 12° at a scanning rate of 1°/min. Samples of the liquid (gel-like) epoxy - clay mixtures or of the uncured epoxy/curing agent - clay mixtures were prepared by applying a thin film on filter paper mounted on glass slide. Cured composite samples were prepared by mounting a rectangular flat specimen into an aluminum holder.

Transmission Electron Microscopy (TEM) images were obtained on a JEOL JEM-100CX II microscope with a CeB₆ filament and an accelerating voltage of 120 kV, a beam diameter of ~5 μm and an objective aperture of 20 μm. The TEM samples were prepared by supporting thin sections (80-100 nm) of the nanocomposite samples onto 300 mesh nickel grids.

Dynamic Mechanical Analysis tests were performed on a DMA 2980 Dynamic Mechanical Analyzer (TA instruments) in the Three Point Bending mode at a frequency of 1 Hz and amplitude of 20 μm, from 25°C to 140°C at a heating rate of 4°C/min. The pristine epoxy polymer and the nanocomposite specimens were rectangular bars with dimensions 60 mm x 13 mm x 3 mm.

Thermogravimetric analyses (TGA) were performed using a Cahn TG System 121 Analyzer. The powdered clays, the pristine epoxy polymer and the nanocomposite samples tested, were heated to 800°C at a heating rate of 5°C/min under N₂ flow.

The composition of the inorganic and the organic clays was determined by a combination of Energy Dispersive Spectroscopy (EDS), CHN and TGA analysis.

4.3 Results and Discussion

Synthesis of Diamine Smectite Clay Intercalates.

Insertion of organic onium ions in the layered silicates by ion - exchange procedures results in an expansion of basal separation between the silicate nanolayers. Various potential configurations of the organic modifier give rise to an array of observed basal distances as outlined in chapter 1, and noted by Legaly and Giannelis.^{31,32} When alkylammonium ions with a C12-C18 carbon

chain are ion - exchanged for the inorganic cations in typical montmorillonite clays (CEC ~90-100 meq/100 g), they adopt a lateral bilayer (~18 Å) intragallery structure. The same surfactant molecules present in the higher charge density synthetic fluorohectorite clay (CEC ~120-130 meq/100 g) gives rise to an inclined paraffin - like structure (~20-30 Å, depending on the alkyl length). The pseudo - trilayer structure shown in chapter 1 is also a possible intermediate surfactant orientation, however, due to the regular basal increase witnessed when moving to larger exchanged alkyl chains in fluorohectorite, it is more likely an inclination of consecutively steeper angles accounting for the incremental clay layer expansion noted. A lipid bilayer configuration at higher onium ion concentrations, perhaps induced upon the introduction of excess neutral amines, is also possible.^{4,33} However, synthesizing nanocomposites using clays containing these relatively high concentrations of alkylammonium ions yields undesirable dangling alkyl chains in the final matrix. Here the gallery – contained onium ions contribute to the crosslinking stoichiometry of the epoxy groups, and have a detrimental effect on the final properties by rubberizing and solvating the resin with the low molecular weight, mono-functionalized amines ordinarily employed in epoxy nanocomposites.³⁰

The utilization of the diprotonated primary diamines (Jeffamines) as organic modifiers of the clay instead of typical octyl and dodecyl amines eliminates this undesirable “polymeric dead end” effect. The XRD patterns of the fluorohectorite clay exchanged by diprotonated Jeffamines D230, D400 and D2000 are shown in figure 4.2 (organoclays denoted D230-FH, D400-FH,

D2000-FH). Similar XRD patterns of the respective PGW - diamine exchanged clays were observed, though not shown here.

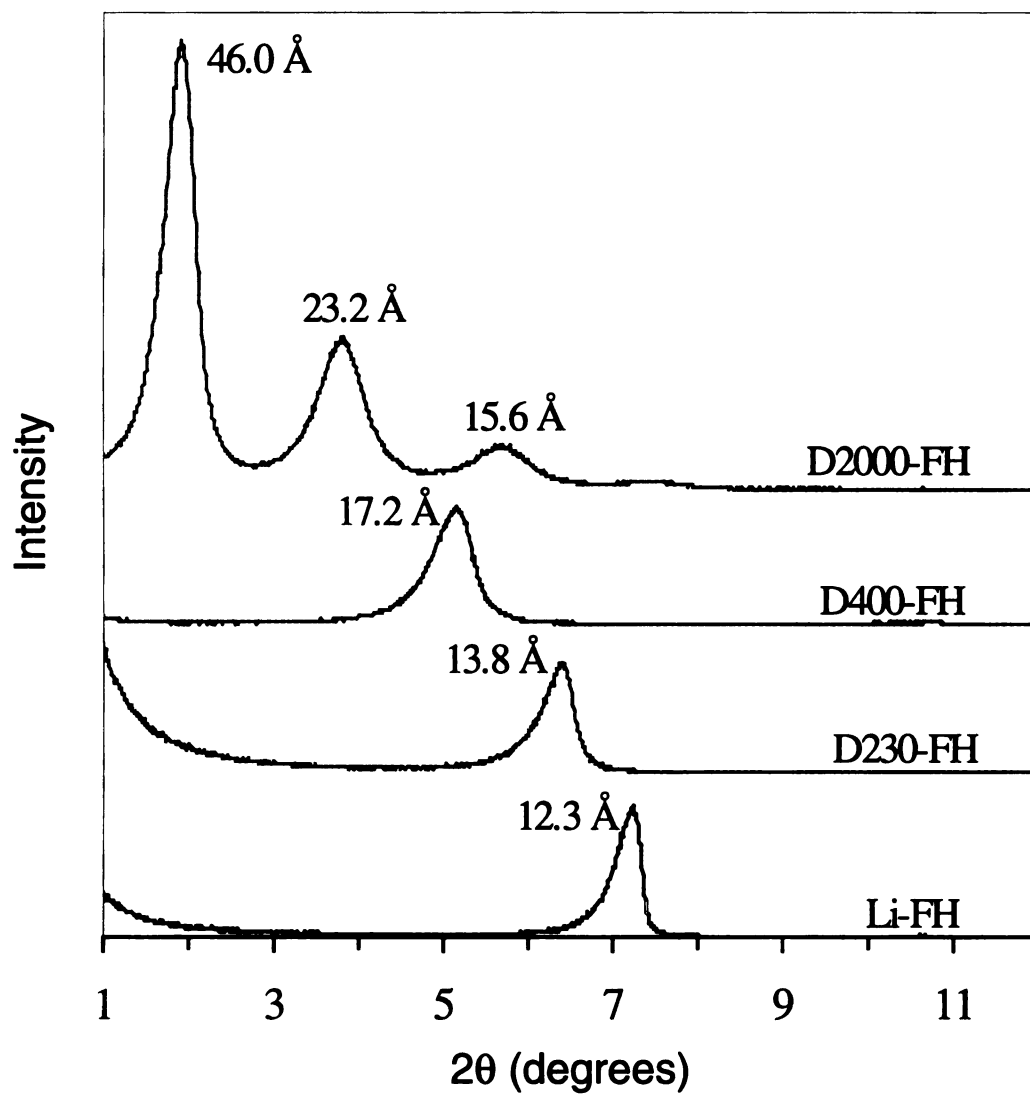


Figure 4.2 X-ray diffraction patterns of the Li^+ -Fluorohectorite (Li-FH) and organically modified FH-clays (with diprotonated diamines D230, D400, D2000).

From the spacings of the d_{001} basal reflection it can be suggested that the short chain, low molecular weight Jeffamine D230 ($n=2.6$, the average number of polypropylene oxide units in the chain) adopts a lateral monolayer structure (13.8 Å), as expected from the short end – to – end distance in the diamine. When the slightly longer polypropylene oxide chain - containing Jeffamine D400 ($n=5.6$) was used, the basal spacing of the exchanged fluorohectorite was ~17.5 Å. This spacing could be either explained by a lateral bilayer orientation, or with a more complex argument that will be addressed in chapter 5. Ion - exchange of the parent clay with the high molecular weight diprotonated Jeffamine D2000 ($n=33.1$) resulted in a d-spacing of ~46 Å, indicative of a structure where the long alkyl oxide chains of D2000 adopt an inclined paraffin - like configuration. Unlike their purely carbon backbone – containing cousins, the polypropyleneneoxide (PPO) diamines do not have the same solubility properties, nor conformational restrictions most clay chemists are accustomed to. For example, neutral alkyl chain diamines are not soluble in water, while the clear solutions obtained from aqueous dissolution of D230 and D400 give off noticeable heats of mixing. The high solubility of these PPO diamines results in a lowered micellular driving force, meaning complete organic insertion into all of the clay exchange sites is less likely than if synthesizing typical organoclay with purely carbon – containing surfactants. Typically the ion exchange of cationic alkyl surfactant in smectite clays involves the simultaneous influx of large quantities of onium ions, as observed in the instantaneous flocculation of formed hydrophobic clay tactoids upon surfactant addition. In the PPO case, there are not sufficient chain – to –

chain interactions in solution to permit the rapid and complete ion exchanges ordinarily anticipated in synthesizing organoclays. For this reason, somewhat incomplete ion exchanges are the norm for PPO – based cations, as indicated in the compositional and basal spacing data of the diamine - exchanged clays given in table 4.1.

Table 4.1 Composition and Basal Spacings of the Inorganic and Organic Clays used for the Preparation of the Nanocomposites

inorganic – organic clays	parent inorganic clay	organic modifier ^a		basal spacings	
		onium ion (%)	diprotonated diamine	d_{001} (Å)	d_{002} (Å)
H-PGW	Na-PGW	-	-	13.4	-
Li-PGW	Na-PGW	-	-	12.4	-
Li-FH	Li-FH	-	-	12.3	-
D2000-PGW	Na-PGW	80	D2000	45.5	21.8
D400-PGW	Na-PGW	90	D400	17.2	-
D230-PGW	Na-PGW	85	D230	13.8	-
D230/high-PGW ^b	Na-PGW	95	D230	13.8	-
D2000-FH	Li-FH	80	D2000	46.0	23.2
D400-FH	Li-FH	85	D400	17.2	-
D230-FH	Li-FH	80	D230	13.8	-
D230/high-FH ^b	Li-FH	95	D230	14.0	-

^a The inorganic clays were ion-exchanged with diprotonated diamines D2000, D400 and D230 (Jeffamines, Huntsman Chemical); the Na⁺ content of all the ion-exchanged clays was below 5 %

^b The amount of D230 used for the ion-exchange was twice the amount necessary for stoichiometric exchange of Na⁺ or Li⁺ ions with onium ions

Epoxy-Clay Nanocomposite Formation from Diamine Smectite Clay Intercalates. The complexity of a three - component system in making a

thermoset epoxy – clay nanocomposite has been well described recently by Vaia and his co-workers.²² The preferred sequence of component mixing, the use of solvents to reduce the viscosity of the system, the temperature and time of curing, and finally the fabrication techniques could have a significant effect on the quality of the final nanocomposite material. With regard to the preparation of the mixture before curing, the compatibility of the organic modifier with both the epoxy monomers and the curing agent should be considered. Strong cases can be made for both addition of pure epoxy resin to the clay (followed finally by Jeffamine), and also for premixing the curing agent and resin prior to organoclay addition. Epoxy resin by itself will only be available to react with the diamines present between the clay layers, therefore a longer mixing time with smaller polymer domains will be possible. Contrarily, premixing both polymeric components before adding the organoclay lowers the viscosity initially (allowing for easier mixing), and ensures sufficient curing agent content in the interclay regions. In the case of the diprotonated diamines used in this study, successful intercalation by the pre-polymer, and exfoliation of the clay in the final polymer were accomplished via both routes. Therefore, it appears that the conditions are optimum for the epoxy monomers not only to migrate inside the galleries, as evidenced by the intercalated X-ray patterns, but also the protonated alpha - omega diamines effectively catalyze the intragallery polymerization. However, in order to avoid gelling in the premixed epoxy – curing agent scenario, care should be taken that the mixing of the polymeric components is not overly lengthy or heated. An alternative way to achieve premixing could be the use of low - boiling

point solvents for viscosity reduction and facilitation of the epoxy monomers intercalation in the clay galleries.

The above described reaction pathways between the epoxy and the onium ions of the diprotonated diamines require the polymer precursors to diffuse inside the clay galleries. This was clearly the case for both the D2000-PGW and the D2000-FH organic clays, as indicated in the alluded to intercalation studies. Figure 4.3 represents XRD patterns of D2000-FH clay in which the epoxy monomer was progressively intercalated resulting in d-spacing values of ~ 59 Å after 6 hrs of mixing and ~ 64 Å after 24 hours mixing at 50°C . After addition of the short chain diamine D230 curing agent necessary for the formation of the rigid epoxy matrix, gelation of the epoxy matrix occurs and polymer domains become larger, thus forcing apart the clay layers. A broad second order peak with d-spacing of ~ 30 Å dominated in the XRD pattern after heating the mixture at 75°C for 30 minutes. As crosslinking continued, the basal reflection continued to expand, noted in the second order peak as it became broader and shifted towards lower angle 2θ . The XRD pattern of the final, cured nanocomposite becomes completely amorphous, revealing the loss of registry between clay layers. As a check to ensure that the clay is still perceptible to the X-rays, the in – plane 060 reflection given off by individual clay layers is also included in figure 4.3 as an inset peak near $60^{\circ} 2\theta$.

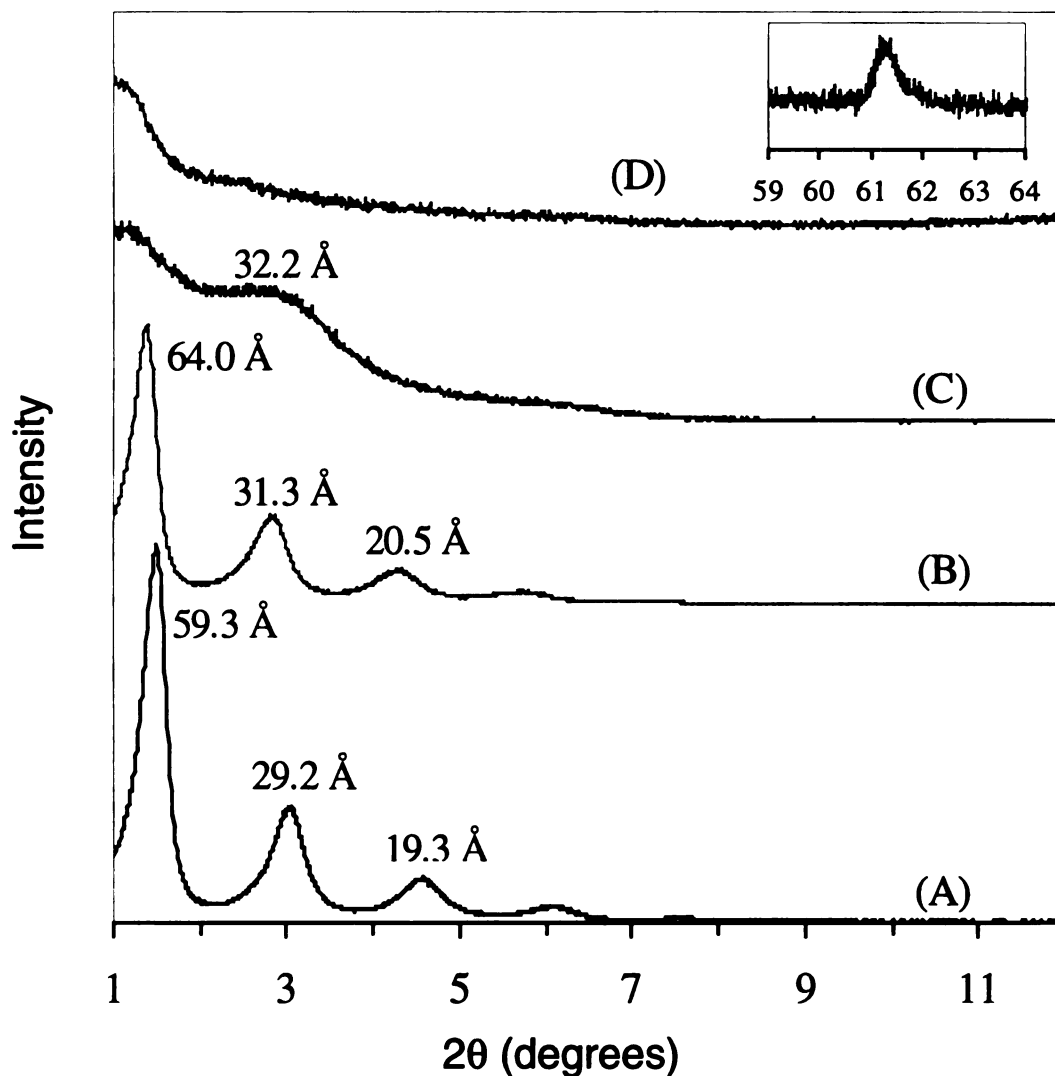


Figure 4.3 X-ray diffraction patterns of mixtures of the organic clays D2000-FH, the epoxy monomer EPON 826 and the curing agent D230: (A) after intercalation of EPON 826 in D2000-FH at 50°C for 6 hrs, (B) after intercalation of EPON 826 for 24 hrs, (C) after addition of D230 in the mixture of step C, outgassing and heating at 75°C for 0.5 hrs, (D) after curing at 75°C, 3 hrs and 125°C, 3hrs (the clay loading was 6 wt. % silicate basis). The inset shows the presence of an in-plane 060 clay reflection in the cured nanocomposite.

It is interesting to note that after pre-intercalation of the epoxy monomer the lamellar ordering of the D2000-FH organic fluorohectorite-clay was not damaged, although the increase in d-spacing ($\sim 20 \text{ \AA}$) resulted in a relatively high value ($\sim 65 \text{ \AA}$) compared to other organic layered silicates in similar epoxy resins.^{22,30} This could be attributed to electrostatic interactions between the onium ions of the alpha-omega diamine (in a paraffin-like arrangement) and the negatively charged clay layers, capable of retaining the integrity of the nanolayer tactoids. In the case of the D2000-PGW organic montmorillonite clay, the degree of lamellar ordering was lower upon mixing with the epoxy monomers, since both the (001) and (002) reflections in the XRD pattern (not shown) were relatively broad compared to those in the XRD pattern of D2000-FH. The lower aspect ratio of PGW (~ 200) compared to FH (~ 2000) also likely accounts for the higher tendency of the montmorillonite nanolayers to lose higher orders of reflection more easily, even during pre-intercalation of the epoxy monomers. Also important to note is the fact that synthetic clays have a very uniform distribution of charge compared to naturally occurring clays, and this can lead to a more regular arrangement of ion exchanged surfactants and intercalated pre-polymers between the layers. Regardless, the initial organoclay basal spacing and ease of intercalating epoxy resin for both types of clays examined are promising results which should not discount either as potential nanoscaled fillers for reinforcement of an epoxy polymer.

The above suggested mechanism of nanolayer exfoliation is in accord with the findings from the TEM images of the nanocomposites prepared from D2000-

FH (figures 4.4a and b) and D2000-PGW (figures 4.4c and d), at clay loading of 6 wt. % silicate.

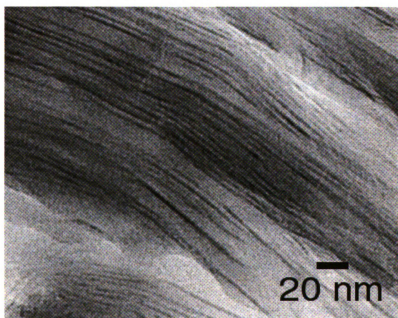
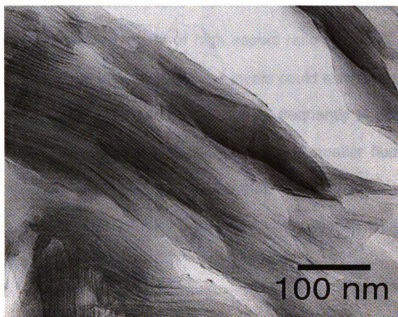


Figure 4.4 TEM images of thin sections of the glassy epoxy nanocomposites prepared from D2000-FH. The clay loading of the nanocomposite samples was 6 wt. % silicate.

The D2000-FH nanocomposite consisted mainly of tactoids with disordered, highly intercalated layers of high aspect ratio (≥ 2000), with basal spacing between 5–15 nm. Individual, shorter layers could also be found on the edges of the primary dispersed particles and most frequently in domains with relatively low number of layers. It appeared that the smaller fluorohectorite layers were more easily disseminated into the matrix, and accordingly it would seem that that much smaller naturally occurring montmorillonite should show a better dispersion of the clay layers.

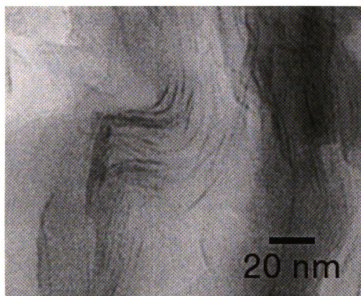
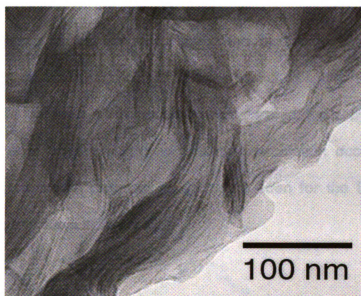


Figure 4.5 TEM images of thin sections of the glassy epoxy nanocomposites prepared from D2000-PGW. The clay loading of the nanocomposite samples was 6 wt. % silicate.

Indeed, the nanolayers of the lower aspect ratio D2000-PGW clay were more randomly dispersed in the polymer matrix and existed in a more exfoliated arrangement.

The XRD patterns of nanocomposites formed from D230 and D400 exchanged clays indicated that no significant intercalation occurred before or during the polymerization process, as it can be seen for the D230-PGW and D400-PGW organic clays in figure 4.6.

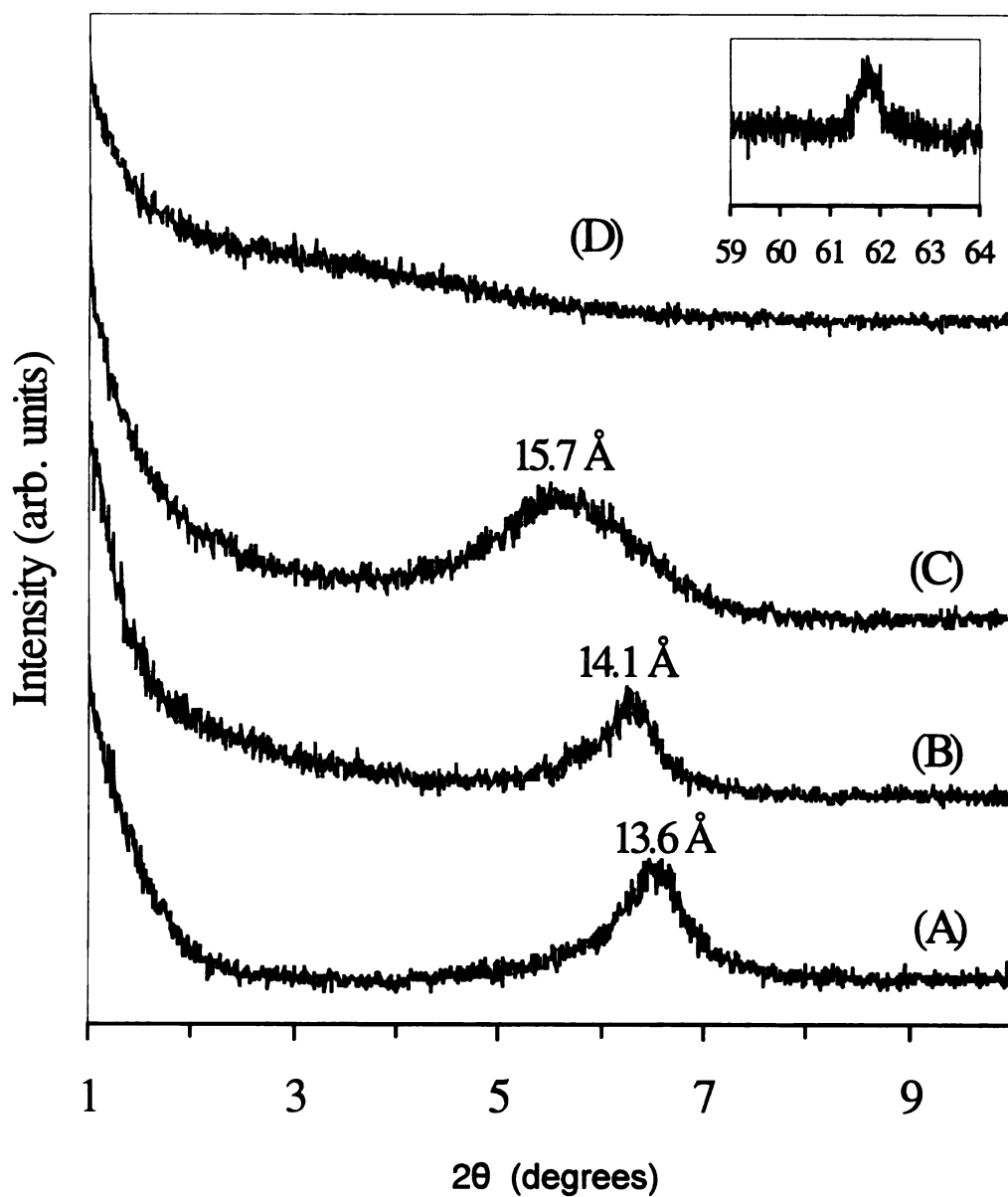


Figure 4.6 X-ray diffraction patterns of EPON 826 – montmorillonite PGW clay composites and nanocomposites using: (A) H-PGW, (B) D230-PGW, (C) D400-PGW and (D) D2000-PGW clays. No intercalation occurred for the inorganic, nor the D230 and D400-PGW clays. The inset shows the presence of an in-plane 060 clay reflection in the cured D2000-PGW nanocomposite.

This behavior is expected for D230-clays due to the relatively short PPO chain of the 230 molecular weight diamine, as there is little driving force for solvation by epoxy resin into the more polar galleries. However, in the case of D400, the d-spacing of both organic clays was $\sim 17.5 \text{ \AA}$, similar to that of a primary C18 alkylammonium exchanged montmorillonite, hinting that there may be sufficient driving force to permit intercalation of the epoxy resin. Octadecyl primary amine - montmorillonites have been shown in other work, and also positively tested here for comparison, to readily intercalate 826 resin. The fact that D400-clays do not allow for epoxy intercalation could be attributed to the situation alluded to above where the electrostatic interactions between either end of the two protonated amines in each diamine and the clay layers are strong enough to inhibit any significant swelling by essentially pinning the galleries shut. Somewhat surprisingly, the composite samples prepared by D230-PGW and D400-PGW clays exhibited very good modulus properties and the 3 mm thick specimens which were prepared for DMA tests had a light brown color and were optically transparent, despite retention of the organoclay basal spacing. This indicates that while epoxy resin was unsuccessful at penetrating between the layers, the separation and suspension of small PGW tactoids could be accomplished. The larger particle size fluorohectorite clays were not as easily separated into individual tactoids, and the composites showed a distinct separation of the phases, causing them to be opaque.

In contrast to the non-intercalated composite samples formed from D230- and D400-exchanged PGW, the use of the inorganic H^+ - and Li^+ -clays resulted in



samples where nearly 20 wt. % of the added clay (6 wt. % silicate) settled at the bottom of the composite specimen. Inorganic clay, it seems, even in the small particle sized PGW, does not become separated into smaller tactoids as in the case of D-230 and D-400 PGW.

As aforementioned, the nanolayers of a D2000-clay intercalate could be exfoliated in a glassy epoxy matrix first through intercalation by the resin, followed by the crosslinking reaction. Moreover, pre-intercalating the 2000 molecular weight diamine in an inorganic H⁺-clay before the addition of the epoxy resin was a viable means to synthesize the effective D2000-organoclay avoiding the costly and time - consuming step of synthesizing the organic clay in solution and washing. Here the acid – base reaction provides the driving force for insertion of the large Jeffamine D2000, creating an *in situ* organic clay synthesis that can be accomplished by using an otherwise inactive H⁺-clay.

Properties of the Nanocomposites. The affects of clay nanolayer reinforcement on the mechanical properties of the D230 – cured 826 glassy epoxy polymer were investigated by Dynamic Mechanic Analysis (DMA). DMA is a powerful analysis tool for probing the stiffness, glass transition temperature and heat dependant behavior of polymeric materials. While DMA can be used to analyze complex dynamic rigid and viscoelastic polymer chain behavior, it can be described simply as monitoring a material's response to an applied oscillatory force.³⁴ Using a three point bending mode, the sample is supported at either end and a constant force is applied at the center of the material. In conjunction with

the steady force, a dynamic pulsed load is also applied at a known frequency and amplitude. Through monitoring the deflection of the material, the delay of deflection and the resistance to deflection one can plot temperature – dependant curves that track two different stiffness, or moduli, of the material. The DMA technique provides two different moduli, an elastic modulus (E') which is called storage modulus and is related to the ability of the material to return or store energy and an imaginary (loss) modulus (E'') which relates to the ability of the material to lose or disperse energy. In simple terms, one can envision dropping a ball, and measuring the height that the ball returns on the rebound, its storage modulus, and the difference of the dropped height to the returned height, the loss modulus. The ratio E''/E' is called tan delta ($\tan\delta$) and typically reaches a maximum at the glass transition (T_g) of the polymer. The following schematic, figure 4.7, depicts the sample orientation, the three point bending sample holder and the curves describing the energy applied, lost and returned in the DMA test.

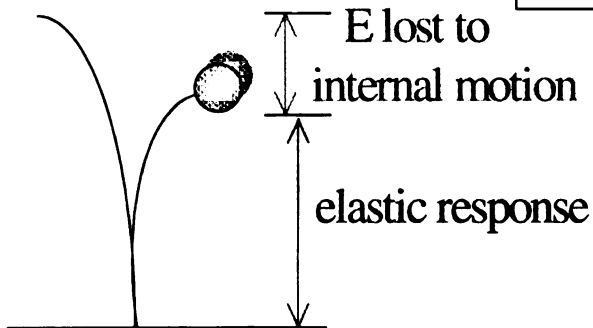
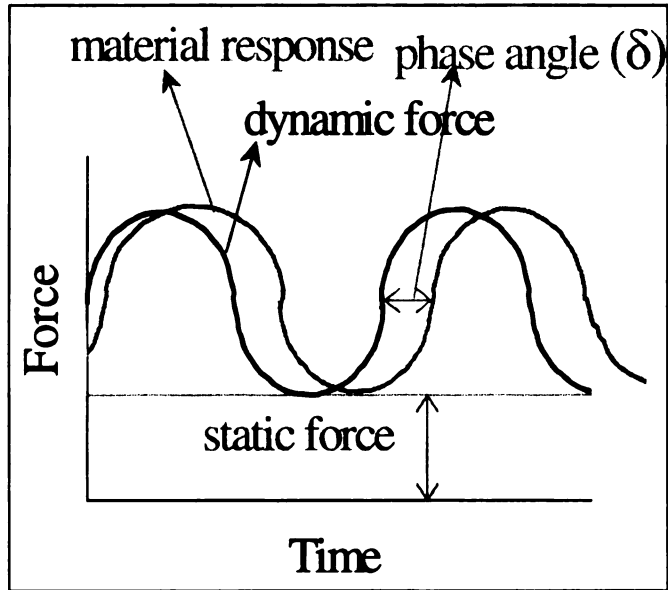
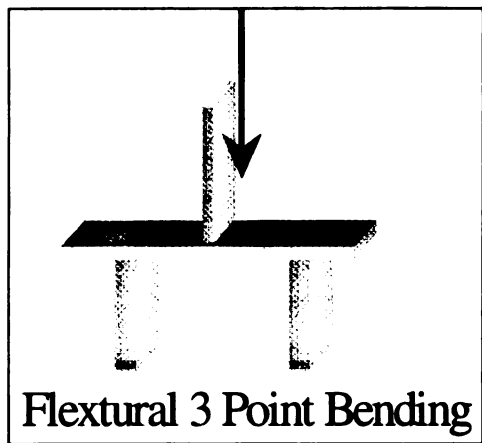


Figure 4.7 Schematic portraying the three point bending device used in obtaining DMA data and the plot of DMA testing parameters. The amount of energy the material returns is related to its storage modulus, the energy dissipated in the internal motions of the polymer chains is related to its loss modulus and the actual measured material lag in experiencing the oscillatory force is the phase angle.

Care should be taken when independently acquired DMA data are compared since different DMA modes can be applied, such as the flexural (ie. three point bending) or torsional mode. The curves in figures 4.8 and 5b show the dependency of the storage modulus and the $\tan\delta$ (E'/E'') on temperature obtained from the three point bending DMA tests performed on the nanocomposite samples of this study. As would be expected, increasing the heat makes a glassy matrix more plastic, and, as the chains become more mobile, the dampening effect on the applied force is increased, giving a rise in the loss modulus. Coincident with the increase in loss modulus is a reduction in storage modulus with increased heating as the material loses stiffness (resistance to a load) and becomes more deformable. The data in Table 2 refers to the storage modulus values of the pristine polymer and the nanocomposite samples at 40°C (glassy region below T_g) and at 120°C (rubbery region above T_g), and to the T_g values of the samples.

Table 4.2 Dynamic Mechanical Analysis and thermal analysis data of the pristine epoxy polymer and the clay-polymer nanocomposite samples ^a

samples	storage modulus (E')		T_g	Thermal stability ^d
	at 40°C (GPa), ± 10%	at 110°C (MPa), ± 10%	(tan δ) (°C), ± 2	(TGA data) (°C)
Pristine epoxy-A	2.9	18.4	82.6	373
Pristine epoxy-B ^b	3.0	20.1	75.5	361
H-PGW	2.9	22.1	82.8	354
Li-PGW	2.7	19.9	82.3	356
Li-FH	3.1	25.2	85.2	351
D2000-PGW (1 wt. % clay)	3.5	21.5	81.2	345
D2000-PGW (3 wt. % clay)	3.6	22.1	76.8	341
D2000-PGW	3.8	21.5	69.8	336
D2000-PGW ^c	3.6	24.0	75.1	339
D400-PGW	3.6	23.2	84.2	346
D230-PGW	3.5	28.3	84.5	358
D2000-FH	3.9	30.5	73.7	323
D400-FH	3.9	32.1	79.1	340
D230-FH	4.0	45.4	84.7	345

^a The nanocomposite samples were named from the organic clay used; the clay loading of the samples was 6 wt. % silicate basis, unless otherwise stated

^b Substitution of 4 % mole D2000 (organic modifier of clays) for D230 (curing agent) in the pristine epoxy polymer

^c Nanocomposite sample prepared by pre-mixing of epoxy monomers with the organic clay (*P-2*); all the rest of the nanocomposite samples in Table 2 were prepared by direct addition of the clays in the epoxy – curing agent mixture (*P-1*)

^d Temperature at which the weight loss in TGA was 1.5 %

The storage modulus in both the glassy and rubbery regions is higher for the nanocomposite samples prepared from the diamine exchanged organic clays (6 wt. % silicate loading), compared to the pristine epoxy polymer. The storage modulus data for a selected portion of the nanocomposites studied is shown in figure 4.8.

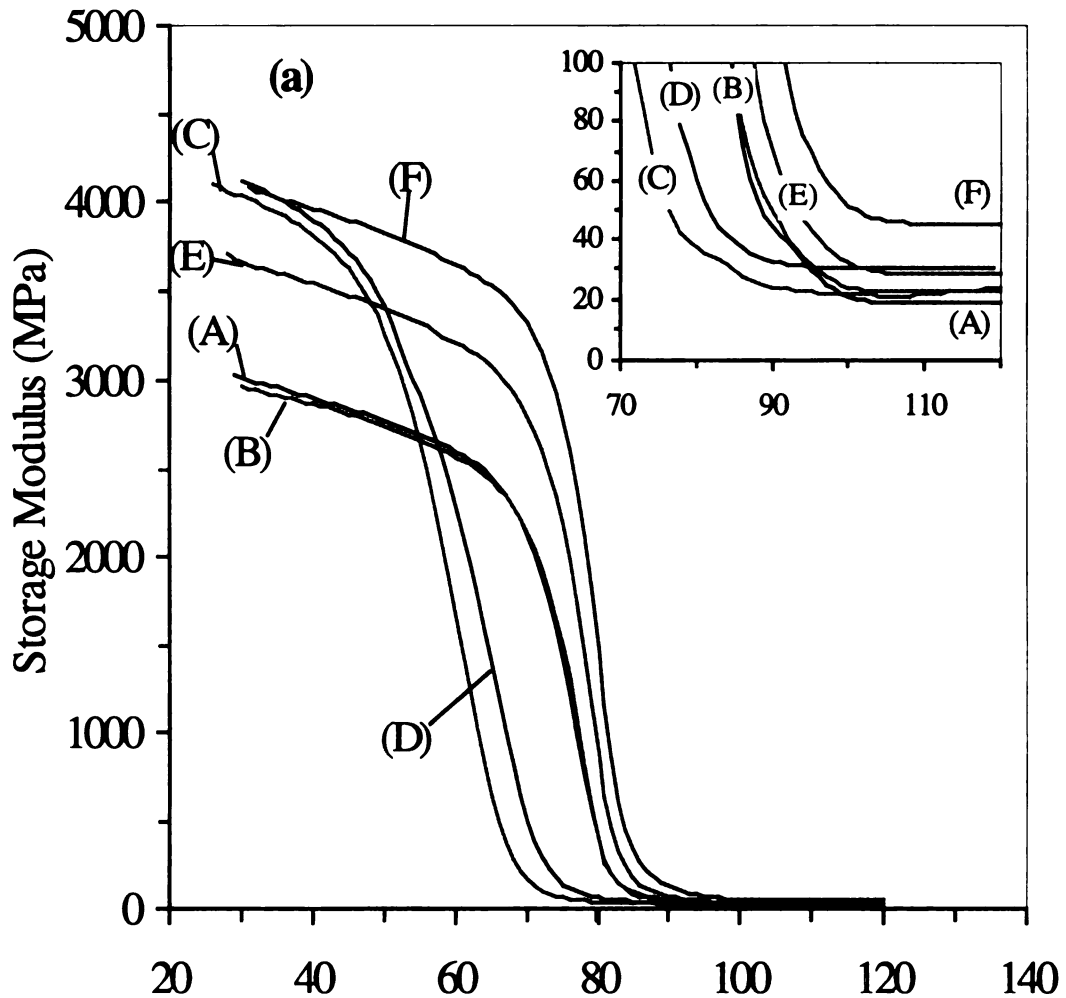


Figure 4.8 Dynamic Mechanical Analysis measurements indicating storage modulus vs. temperature curves for (A) Pristine-A epoxy polymer and for the nanocomposite samples prepared from (B) H-PGW, (C) D2000-PGW, (D) D2000-FH, (E) D230-PGW, (F) D230-FH. The clay loading of the nanocomposite samples was 6 wt. % silicate basis.

The most commonly accepted means for obtaining the glass transition temperature of a plastic material is by taking the maximum value of the loss to storage modulus ratio. This ratio, denoted $\tan \delta$, is plotted in figure 4.9.

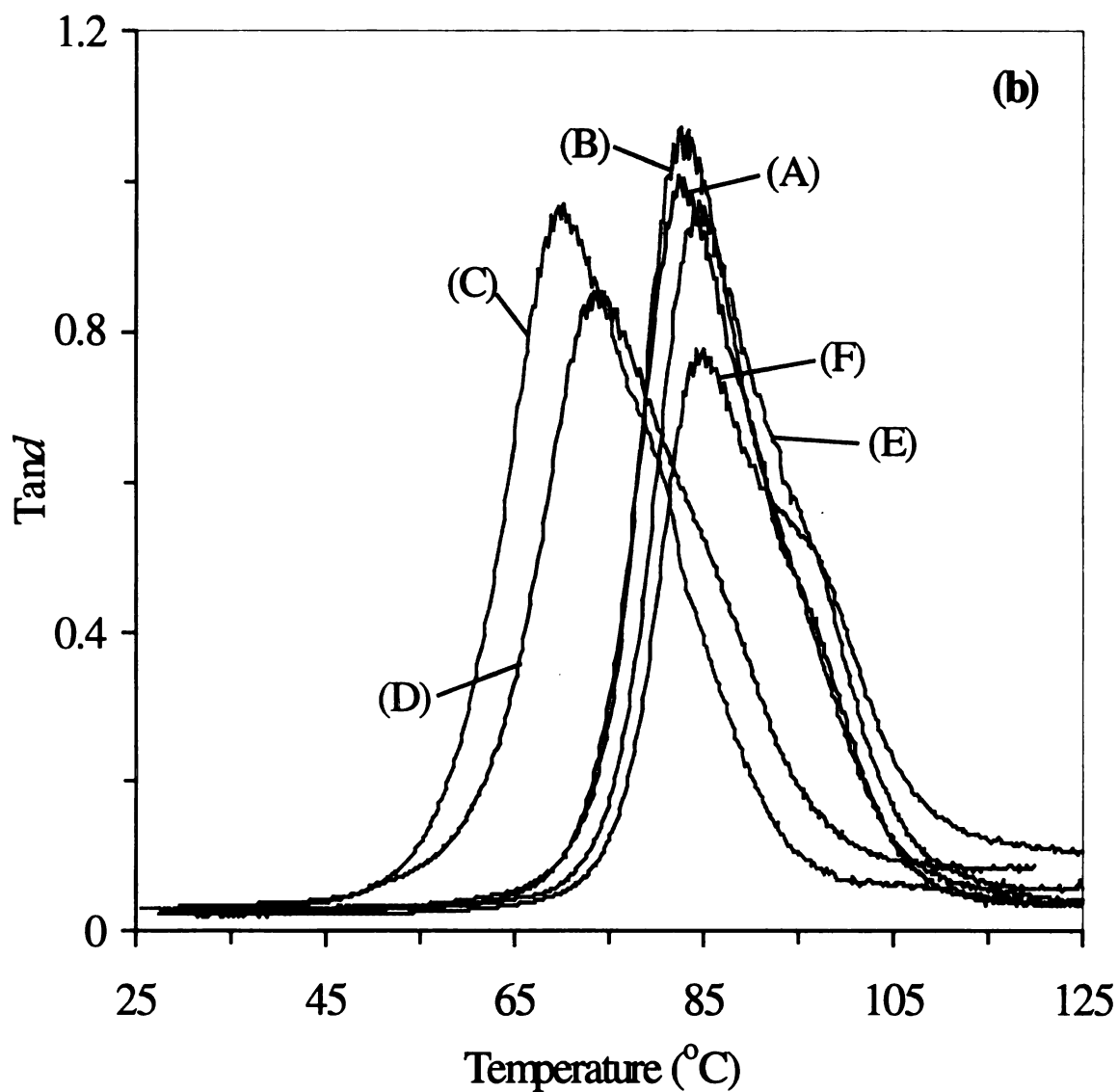


Figure 4.9 Dynamic Mechanical Analysis measurements indicating $\tan \delta$ vs. temperature, for (A) Pristine-A epoxy polymer and for the nanocomposite samples prepared from (B) H-PGW, (C) D2000-PGW, (D) D2000-FH, (E) D230-PGW, (F) D230-FH. The clay loading of the nanocomposite samples was 6 wt. % silicate basis.

As for the D2000-PGW nanocomposite, a 25 % increase in storage modulus was noted in both glassy and elastomeric regions. The composite samples formed from the D230-PGW and D400-PGW clays showed similar increase of the storage modulus, although the clays in those samples were not intercalated by epoxy resin. A 35 % (glassy region) and 65 % (rubbery region) increase in storage modulus was measured for the D2000-FH nanocomposite sample, while the increase was even higher for the non-intercalated D230- and D400-FH composite samples, especially in the rubbery region at 75-150 % in the increase. It is important to note that while the D230 and D400 clays did not form ideal exfoliated nanocomposites, drastic improvements in storage modulus, particularly in the higher temperature regime, are to be expected relative to the D2000 clays. This is due to the fact that even though intercalated, and ultimately exfoliated, the D2000 clays contain approximately 4% mol 2000 molecular weight Jeffamine molecules along with the D230 curing agent added to crosslink the matrix. While the large D2000 diamines compatibilize the intragallery region with the epoxy resin and permit intercalation, they also crosslink with the epoxy and create rubbery regions in the glassy matrix. While this likely toughens the epoxy polymer, especially due to the locale of the D2000 molecules near the reinforcing platelets, the storage modulus and general stiffness of the materials will be reduced at higher temperatures. Also, the T_g of the polymer will be sacrificed with increasing D2000 content for similar reasons.

The increase in storage modulus is in the same range found in previous related works,^{22,28,29} but it should be mentioned that the absolute modulus values

of the pristine epoxy polymer of this work (e.g. ~3 GPa below T_g and ~18 MPa above T_g) are higher than those previously reported.

The glass transition temperature (T_g) of the nanocomposites remained nearly the same compared to the pristine epoxy polymer. The small amount of D2000 introduced to the matrix from the onium ions of the clay galleries acted as a rubberizer and caused a small decrease in T_g , as alluded to earlier, however, when the nanocomposites formed from the D2000-exchanged clays were compared to a pristine polymer in which the same amount of D2000 was used as curing agent (~ 4 % mole of the total curing agent) the T_g remained relatively unchanged.

One interesting and unexpected find that may reveal information about the crosslinking and mobility of reactants in a gelling epoxy network pertains to the drop in T_g (5°C) noted between the same nanocomposites synthesized by different procedures (P1 versus P2). By first allowing the pure epoxy resin to mix with the D2000 organoclay, followed by addition of the D230 curing agent, and even distribution of curing agent throughout the entire system will occur. This is different than if the epoxy and D230 are premixed prior to organoclay addition. In the latter case, an equal distribution of diamine will be found prior to clay addition, however once clay is added, the intercalation of stoichiometric amounts of 826 and D230 results in a Jeffamine – heavy mixture in the regions between the clay layers. Here uncrosslinked chains can result when an anisotropic partitioning of curing agent occurs in the samples. An alternative explanation for the significant T_g drop in the premixed D230 – 826 is that the polymer has begun

to react prior to clay addition, and although XRD patterns indicate intercalation still occurs, the driving force for exfoliation of the layers could be reduced as the bulk polymerization already has been initiated.

Thermogravimetric analyses of the samples provided additional information on the structural characteristics of the nanocomposites. From the TGA curves in Figures 4.10 and 4.11 and the related data in Table 2, it is evident that the thermal stability of the nanocomposites was not sacrificed by the presence of the long chain D2000-organic modifier. This verifies that the surface onium ions of the diamine are crosslinking with the epoxy and being incorporated into the polymer network, unlike free protonated primary amines that ordinarily undergo thermal decomposition several hundred degrees before the crosslinked epoxy matrix. Interestingly, the stability of the composites with the non-intercalated D230- and D400-exchanged clays was also high, indicating that possibly small amounts of epoxy molecules were able to crosslink within the clay galleries, although swelling was not detected in these clays by XRD.

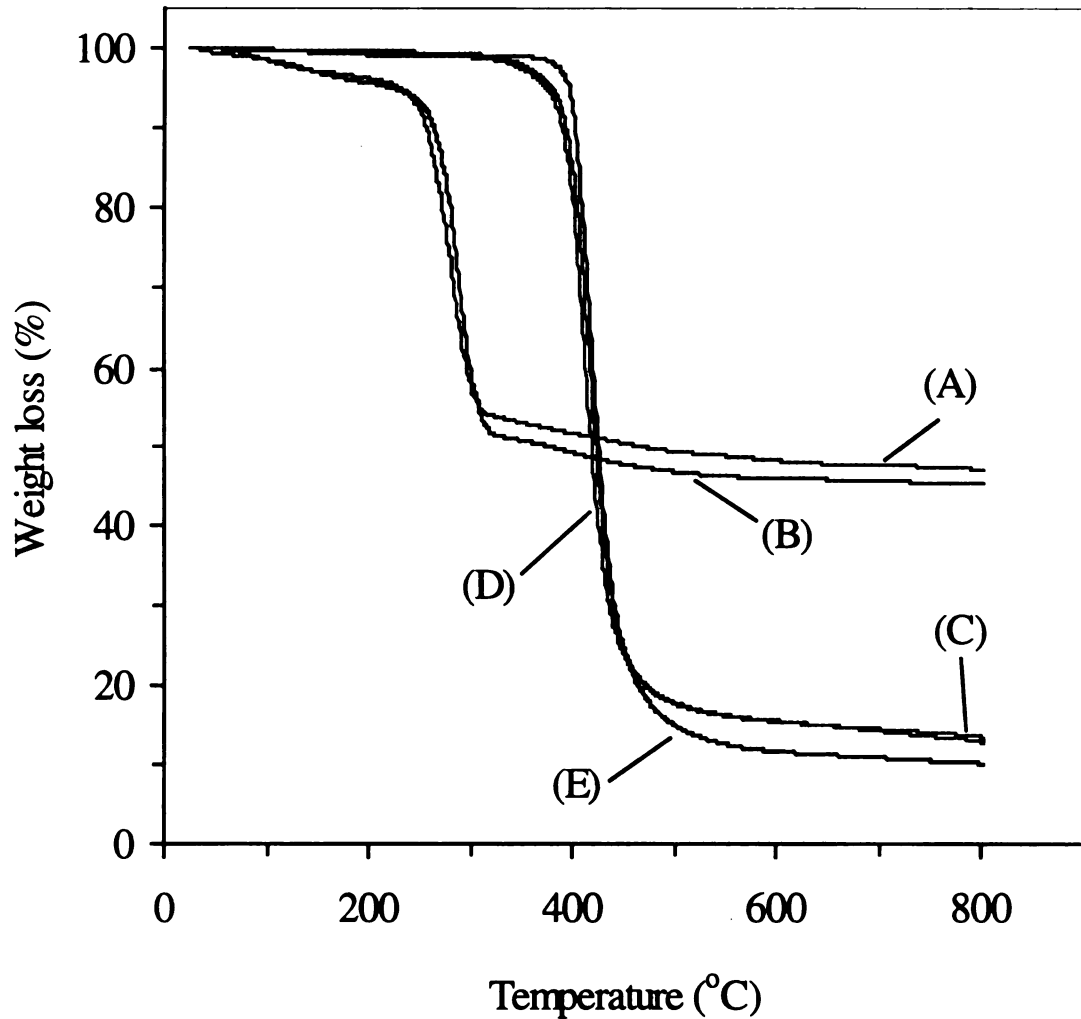


Figure 4.10 TGA curves of the organic clays (A) D2000-PGW and (B) D2000-FH, of the nanocomposites prepared from (C) D2000-PGW and (D) D2000-FH clays, and of the Pristine-A epoxy polymer (E). The clay loading of the nanocomposite samples was 6 wt. % silicate basis.

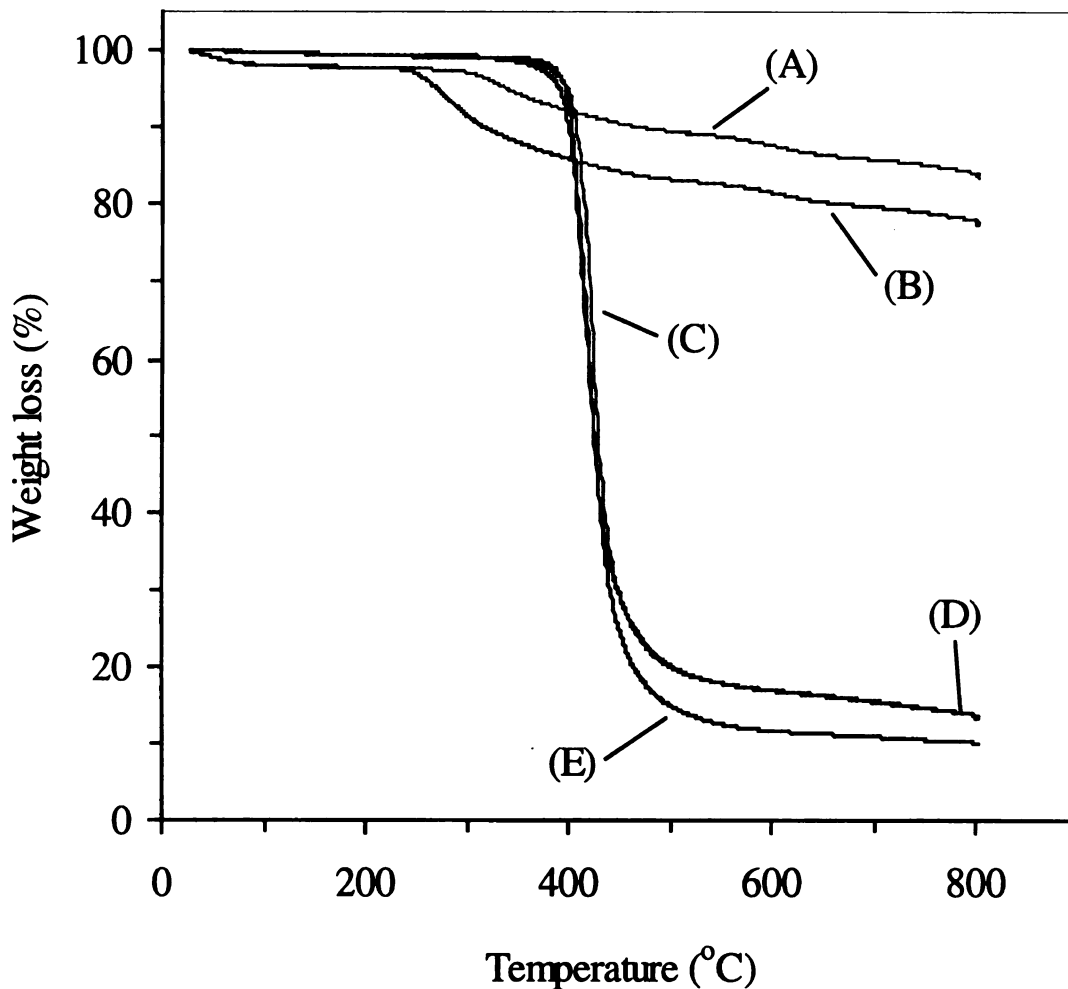


Figure 4.11 TGA curves of the organic clays (A) D230-PGW and (B) D400-PGW, of the nanocomposites prepared from (C) D230-PGW and (D) D400-PGW clays, and of the Pristine-A epoxy polymer (E). The clay loading of the nanocomposite samples was 6 wt. % silicate basis.

4.4 Conclusions

In summary, the use of Jeffamine – modified clays have been successful in synthesizing glassy epoxy nanocomposites. In particular, the D2000-clays were the first example of a difunctionalized organic – modified layered silicate capable of intercalating epoxy resin. Typical diprotonated diamine clays are limited in their capability due to the affect they can have in electrostatically pinning neighboring clay layers by bridging the gallery. Partial reaction XRD analysis revealed the basal expansion that occurred upon epoxy crosslinking. Final nanocomposites were determined by XRD to be partially exfoliated, and as a result significant improvements in the mechanical properties due to the dispersed nanolayers was determined by DMA. Nanocomposites containing 6% wt. silicate showed marked improvement in storage modulus (35% at 40°C). Also important to note is that although diamine – modified organoclays thermally degrade at 250°C, when crosslinked into the epoxy network, the premature degradation of primary amines is no longer detected and the nanocomposites do not lose any thermal stability. While typical syntheses of the organoclays used in this work are problem-free, commercially significant shortcuts can be taken in producing the epoxy – swellable clay powder. XRD studies indicate that addition of the neat liquid D2000 to proton – exchanged inorganic clay powders results in an uptake of the basic diamines into the acidic clay galleries, thus negating the need for solvent, filtering and washing. The use of primary diamines both as organic modifiers of clays and as curing agents provide an alternative,



commercially attractive way of fabricating epoxy – clay nanocomposites with improved interfacial and thermo/mechanical properties.

4.5 References

- (1) Vaia, R. A.; Giannelis, E. P. *MRS Bull.* **2001**, *26*, 394-401.
- (2) Pinnavaia, T. J., Beall, G.W., eds. *Polymer - Clay Nanocomposites*; Jonh Wiley & Sons Ltd, New York, 2000.
- (3) Vaia, R. A., Krishnamoorti, R., eds. *Polymer Nanocomposites*; American Chemical Society: Washington, DC, 2001.
- (4) LeBaron, P. C.; Wang, Z.; Pinnavaia, T. J. *Appl. Clay Sci.* **1999**, *15*, 11-29.
- (5) Giannelis, E. P. *Adv. Mater.* **1996**, *8*, 29-&.
- (6) Okada, A.; Usuki, A. *Mater. Sci. Eng. C-Biomimetic Mater. Sens. Syst.* **1995**, *3*, 109-115.
- (7) Lagaly, G. *Appl. Clay Sci.* **1999**, *15*, 1-9.
- (8) Chin, I. J.; Thurn-Albrecht, T.; Kim, H. C.; Russell, T. P.; Wang, J. *Polymer* **2001**, *42*, 5947-5952.
- (9) Hsiue, G. H.; Liu, Y. L.; Liao, H. H. *J. Polym. Sci. Pol. Chem.* **2001**, *39*, 986-996.
- (10) Kommann, X.; Lindberg, H.; Berglund, L. A. *Polymer* **2001**, *42*, 4493-4499.

- (11) Ahuja, S. K.; McGriff, R. B. *Abstr. Pap. Am. Chem. Soc.* **2000**, *220*, 61-COLL.
- (12) Lu, J. K.; Ke, Y. C.; Qi, Z. N.; Yi, X. S. *J. Polym. Sci. Pt. B-Polym. Phys.* **2001**, *39*, 115-120.
- (13) Curliss, D. B. *Abstr. Pap. Am. Chem. Soc.* **2000**, *219*, 43-POLY.
- (14) Gam, K. T.; Sue, H. J. *Abstr. Pap. Am. Chem. Soc.* **2000**, *219*, 223-PMSE.
- (15) Kang, J. H.; Lyu, S. G.; Sur, G. S. *Polym.-Korea* **2000**, *24*, 571-577.
- (16) Pinnavaia, T. J. *Science* **1983**, *220*, 365-371.
- (17) Usuki, A.; Kawasumi, M.; Kojima, Y.; Okada, A.; Kurauchi, T.; Kamigaito, O. *J. Mater. Res.* **1993**, *8*, 1174-1178.
- (18) Usuki, A.; Kojima, Y.; Kawasumi, M.; Okada, A.; Fukushima, Y.; Kurauchi, T.; Kamigaito, O. *J. Mater. Res.* **1993**, *8*, 1179-1184.
- (19) Kojima, Y.; Usuki, A.; Kawasumi, M.; Okada, A.; Fukushima, Y.; Kurauchi, T.; Kamigaito, O. *J. Mater. Res.* **1993**, *8*, 1185-1189.
- (20) Zerda, A. S.; Lesser, A. J. *J. Polym. Sci. Pt. B-Polym. Phys.* **2001**, *39*, 1137-1146.
- (21) Ke, Y. C.; Wang, L.; Qi, Z. N. *Acta Polym. Sin.* **2000**, 768-773.
- (22) Brown, J. M.; Curliss, D.; Vaia, R. A. *Chem. Mat.* **2000**, *12*, 3376-3384.
- (23) Kommann, X.; Lindberg, H.; Berglund, L. A. *Polymer* **2001**, *42*, 1303-1310.

- (24) Ke, Y. C.; Lu, J. K.; Yi, X. S.; Zhao, J.; Qi, Z. N. *J. Appl. Polym. Sci.* **2000**, *78*, 808-815.
- (25) Lan, T.; Kaviratna, P. D.; Pinnavaia, T. J. *Chem. Mat.* **1995**, *7*, 2144-2150.
- (26) Lan, T.; Pinnavaia, T. J. *Chem. Mat.* **1994**, *6*, 2216-2219.
- (27) Wang, M. S.; Pinnavaia, T. J. *Chem. Mat.* **1994**, *6*, 468-474.
- (28) Massam, J.; Pinnavaia, T. J. *Material Research Society Symposium Proceedings* **1998**, *520*, 223-232.
- (29) Messersmith, P. B.; Giannelis, E. P. *Chem. Mat.* **1994**, *6*, 1719-1725.
- (30) Wang, Z.; Pinnavaia, T. J. *Chem. Mat.* **1998**, *10*, 1820-1826.
- (31) Lagaly, G. *Solid State Ion.* **1986**, *22*, 43-51.
- (32) Hackett, E.; Manias, E.; Giannelis, E. P. *J. Chem. Phys.* **1998**, *108*, 7410-7415.
- (33) Wang, Z., Massam, J., Pinnavaia, T.J. In *Polymer - Clay Nanocomposites*; Pinnavaia, T. J., Beall, G.W., eds., Ed.; John Wiley & Sons Ltd, New York, 2000, pp 127-149.
- (34) Menard, K. P. *Dynamic Mechanical Analysis: A Practical Introduction*; CRC Press LLC, 1999.

Chapter 5

REDUCING THE ORGANIC MODIFIER CONTENT IN EPOXY NANOCOMPOSITES: MIXED-ION INORGANIC/ORGANIC MONTMORILLONITE AND FLUOROHECTORITE HOMOSTRUCTURES

5.1 Introduction

The remarkable enhancement in performance properties of engineering plastic nanocomposites over conventional and non-filled systems provided the polymer industry with a new perspective of reinforcement in thermoplastic and thermoset polymers for a variety of practical applications. The rich intercalation and ion-exchange chemistry of the smectite clay layered silicates enabled them to be successfully used as polymer - strengthening additives through organo-functionalization of the gallery regions, diversifying their industrial applications beyond water-based thickeners, cation-exchangers, catalysts, adsorbents, rheological modifiers, lubricants, etc. Polymer Layered Silicate Nanocomposites (PLSNs) exhibit improved mechanical properties (modulus, strength, heat distortion temperature, thermal expansion coefficient), barrier properties, thermal stability, resistance to solvent swelling, flammability resistance and ablation performance compared to unmodified polymers and conventional composites, mainly due to their unique interfacial properties induced by the highly dispersed, comparatively diminutive sized silicate nanolayers throughout the polymer matrix.¹⁻¹⁵

The beneficial high in-plane strength and high aspect ratio of the lamellar layered materials on the nanocomposite properties can be maximized by the use of smectite clays¹⁶ (e.g. montmorillonite, hectorite) in part due to their ease of organic modification. This invokes a highly compatible, hydrophobic intragallery environment that allows for insertion of polymer precursors, leading to an ideal situation for optimum nanolayer exfoliation upon polymerization. Additionally, even though they can be readily synthesized, smectite clays are ubiquitous in nature and can be purified at relatively low cost.

The pioneering work of Toyota researchers in the early 90's demonstrated the first practical application of a nylon – montmorillonite clay nanocomposite. In this case the modified materials had highly improved mechanical properties, including a near 80°C increase in heat deformation temperature, and this permitted their use as a timing belt cover for the automotive industry.¹⁷⁻¹⁹ In the original Toyota approach, the hydrophilic inorganic cations on the clay nanolayer surface were ion-exchanged with a protonated amino acid in order to both match the polarity of the caprolactam polymer precursor and provide an acidic gallery region to catalyze the ring opening polymerization. In the next 10 years, the *in situ* polymerization of pre-polymers in organoclay galleries has been successfully applied for the preparation of exfoliated clay nanocomposites of polyimide, epoxy, acrylonitrile rubber, polypropylene, polystyrene, polyether and polysiloxane matrices.²⁰⁻³⁰ Epoxy – clay nanocomposites have attracted the majority of research interest amongst the thermoset polymers while modified

smectite clays^{8-15,20,25-27,31-34}, and layered silicic acids, such as magadiite,³⁵ were found to be the most appropriate inorganic additives for this system.

Organic alkylammonium ions have been used as effective modifiers of the inorganic clays acting both as compatibilizing agents for the intercalation of the epoxy monomers and as acidic catalysis sites for facilitating the epoxy ring-opening with amine curing agents.^{20,35} In general, the chain-length of the organic onium ion, the relative acid strength (primary, secondary, or tertiary amines) and the clay layer charge density, which dictates the concentration of the organic modifier in the galleries, all play an important role in achieving optimum nanolayer exfoliation. In a recently reported work,³² it was shown that a hydroxyl-substituted quaternary ammonium modifier in a montmorillonite clay also induces a high degree of clay layer exfoliation, behaving in this system much like the acidic amines in forming hydrogen bonds with the epoxy rings.

While the use of fully exchanged organoclays has been successful in improving the desired epoxy properties, the goal of this work was to find new avenues for achieving even better mechanical behavior with more advanced and cost effective organo-functionalized clays. The previous chapter focused on the first diamine – modified clays as successful swelling and ultimately exfoliating agents in synthesizing a thermoset nanocomposite. The next step, which will be addressed in this chapter, was eliminating the need for large amounts of organo-modifiers in the smectite clays. One way of reducing the amount of the costly organic cations (alkyl amines) is to have the charge balancing cations consist of mixtures organic and inorganic cations within the same clay galleries. Such

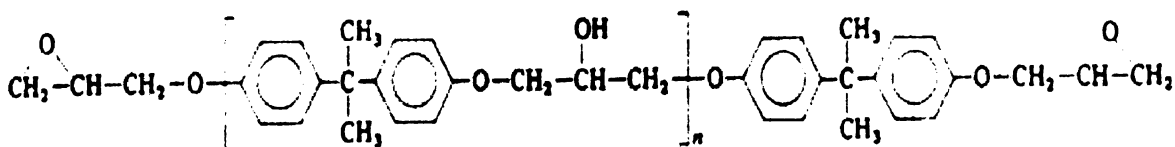
mixed exchange cation forms have been termed “homostructured” by the Pinnavaia group, as each gallery is compositionally equivalent (exhibiting uniform XRD patterns and intercalation properties). Mixed-ion homostructure synthesis using alkylammonium ions and Na⁺ or H⁺ cations was first described by Pinnavaia and his co-workers in a series of related patents.³⁶⁻³⁸ The clays used in the examples of the referenced patents were mainly of montmorillonite and hectorite-type, while the organic modifiers consisted of various amines, mainly primary octadecylamine (ODA). It was shown that an onium ion to proton ratio of 65:35 in montmorillonite clay was sufficient to induce similar epoxy resin swelling properties as with the homonionic organic clay.

As alluded to previously, chapter 4 reports the use of diamine smectite clay as advantageous fillers in epoxy – clay nanocomposites. Here the primary diamine played a dual role as organic modifier of the clay and cross-linking agent in the nanocomposite, thus eliminating the negative effects ordinarily introduced by monofunctionalized amine modifiers³⁹. The use of diprotonated diamines as an organic modifier nullifies the “dangling chains”³⁵ caused by the monofunctionalized amines via inducing polymeric dead ends as the surfactants ring-open the epoxy monomer. However, nanolayer exfoliation was accomplished only when a sufficient long-chain diamine (molecular weight ~2000) was employed as the clay modifier. As the D2000 diamine (Jeffamine, provided by Huntsman Chemical) was the only difunctionalized organic modifier to permit epoxy resin intercalation, this was selected as the primary surfactant of choice in synthesizing clay homostructures. The mixed-ion clays were

characterized and tested as fillers in a thermoset glassy epoxy polymer matrix (Shell epoxy resin 826 cured with Jeffamine D230). The observed improvement of mechanical properties (monitored by Dynamic Mechanical Analysis) and the high thermal stability of the nanocomposites formed from a mixed-ion clay with an onium ion to proton ratio of ~1:3, along with the clearly shown nanolayer exfoliation of a 1:1 mixed-ion clay supported the notion that minimization of the organic modifier content in clays used for nanocomposite synthesis is readily obtainable. Mixed-ion clays allow for the synthesis of more cost-effective nanocomposites that have reduced long chain diamine crosslinker content, thus resulting in higher glass transition temperature materials.

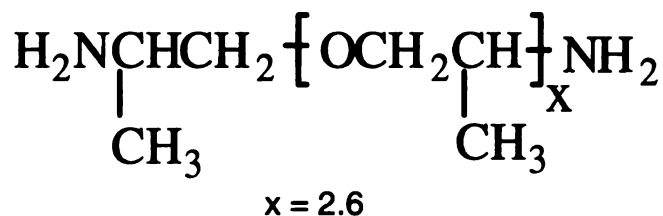
5.2 Experimental

Materials. The epoxide resin used for the formation of the pristine glassy epoxy polymer and the epoxy – clay nanocomposites was a diglycidyl ether of bisphenol A (DGEBA), more specifically, Shell EPON 826 with MW ~369 and epoxy equivalent weight ~182:



$$n = 0 (90 \%), 1 (10 \%)$$

The curing agent was a polyoxypropylene diamine, Jeffamine D230 (Huntsman Chemicals) with MW ~230:



Jeffamines D2000 (MW ~2000, $x=33.1$), D400 (MW ~400, $x=5.6$) and D230 (MW ~230, $x=2.6$) were used in the synthesis of the homoionic and mixed-ion inorganic/organic clays, as is described below. All other chemicals used in this work were purchased from Aldrich Chemical Co. and used without further purification.

Synthesis of Homoionic and Mixed-ion Inorganic/Organic Clays. An industrially purified Na^+ -montmorillonite clay (PGW, Nanocor Inc.) with CEC = 120 meq/100 g, was used as a precursor to the H^+ and Li^+ forms of the montmorillonite clay by typical ion-exchange procedures with diluted HCl (for H^+ -clays) or LiCl (for Li^+ -clays) aqueous solutions. A synthetic Li^+ -fluorohectorite

clay (FH, Corning Inc.), with similar CEC to that of the PGW montmorillonite was used as the parent fluorohectorite clay in this study.

The homoionic organic clays and the mixed-ion inorganic/organic clays were prepared by ion-exchanging the inorganic clays with diprotonated diamine (Jeffamine) D2000. Typically, an aqueous inorganic clay suspension was blended for 1-2 min with an acidic HCl aqueous solution of the Jeffamine, using a small excess of H^+ to ensure the formation of diprotonated diamines. The blended mixture was further stirred for 48 hrs under ambient conditions with a magnetic stirrer. For the homoionic organic clays, the amount of D2000 used was in small excess of the stoichiometric ion-exchange of the inorganic clay, while for the mixed-ion clays the mole ratio of onium ions to inorganic cations in the mixture was gradually reduced in order to prepare clays with different degrees of organic ion-exchange. For comparison purposes, a mixed-ion PGW clay was synthesized by ion-exchanging the H^+ -PGW with ODA, as this was the primary clay of choice in prior epoxy work. The ion-exchanged clays were separated by centrifugation, washed 3-4 times with deionized water (until free of Cl^- , as noted by lack of $AgCl$ precipitate when $AgNO_3$ was added to the supernatant) and washed once with EtOH prior to air-drying at room temperature. The dried clay products were ground and sieved to a particle size <270 mesh ($53 \mu m$). The percent ion-exchange of the inorganic cations by onium ions and the basal spacing of all the homoionic and mixed-ion clays produced are shown in Table 5.1.

Preparation of Epoxy – Clay Nanocomposites. The pristine glassy epoxy polymer was formed by mixing the epoxy monomer (EPON 826) with the curing agent (Jeffamine D230) at 50°C for ~30 min, outgassing of the liquid mixture at room temperature and curing in RTV silicone rubber molds at 75°C for 3 hrs and, subsequently, at 125°C for an additional 3 hrs under nitrogen.

For the preparation of the epoxy – clay nanocomposites the clay was added to the epoxy EPON 826 - curing agent D230 mixture at 50°C by stirring for 30 minutes before outgassing and curing at 75°C and 125°C (procedure *P-1*), similar to the pristine polymer formation. Alternatively, the epoxy EPON 826 was initially mixed with the clay at 50°C for a certain period of time and then the curing agent D230 was added (procedure *P-2*). Pre-mixing of the clay with the epoxy monomer was also done in the presence of low-boiling point organic solvents, eg. acetone, ethanol (EtOH) and isopropyl alcohol (IPA). The epoxy-clay-solvent mixture was stirred at 25°C for 30 min, after which the solvent was then evaporated for 1 hr at 25°C and 30 min at 50°C under stirring and for 1 hr at 75°C under vacuum. The amount of solvent used was 25 wt. % of the epoxy weight and it was kept constant throughout the first 30 min of the epoxy – clay reaction.

In the case of the organic clays and mixed-ion inorganic organic clays, the moles of onium ions present in the clay were counted as contributing to curing process, supplementary to the amine-groups of Jeffamine D230, which was the main curing agent for the formation of the glassy epoxy polymers. The amount of onium ions due to the organic modifier of the clays was always less than 4 % (by moles) of the total amine-groups necessary for complete cross-linking of the

epoxy monomers. The clay loading of the nanocomposites prepared was 6 wt. % (based on silicate content, not including the weight contribution of the organic).

Characterization and Testing of Clays and Nanocomposites. X-ray diffraction (XRD) patterns were obtained on a Rigaku rotaflex 200B diffractometer equipped with Cu K α X-ray radiation and a curved crystal graphite monochromator, operating at 45 KV and 100 mA. The diffraction patterns were collected between 1 and 12° at a scanning rate of 1°/min. Samples of the liquid (gel-like) epoxy-clay mixtures or of the uncured epoxy-curing agent-clay mixtures were prepared by applying a thin film on filter paper mounted on glass slide. Cured composite samples were prepared by mounting a rectangular flat specimen into an aluminum holder.

Transmission Electron Microscopy (TEM) images were obtained on a JEOL JEM-100CX II microscope with a CeB₆ filament and an accelerating voltage of 120 kV, a beam diameter of ~5 μ m and an objective aperture of 20 μ m. The TEM samples were prepared by supporting thin sections (80-100 nm) of the nanocomposite samples onto 300 mesh nickel grids.

Dynamic Mechanical Analysis tests were performed on a DMA 2980 Dynamic Mechanic Analyzer (TA instruments) in the three-point bending mode at a frequency of 1 Hz and amplitude of 20 μ m, from 25°C to 140°C at a heating rate of 4°C/min. The pristine epoxy polymer and the nanocomposite specimens were rectangular bars with dimensions 60 mm x 13 mm x 3 mm.

Thermogravimetric analyses (TGA) were performed using a Cahn TG System 121 Analyzer. The powdered clays, the pristine epoxy polymer and the nanocomposite samples tested were heated to 800°C at a heating rate of 5°C/min under N₂ flow.

The composition of the inorganic and the organic clays was determined by Energy Dispersive Spectroscopy (EDS), CHN and TGA analysis.

5.3 Results and Discussion

Synthesis of Mixed-Ion Inorganic/Organic Diamine Smectite Clay Intercalates. The basal spacing of homoionic organic clay depends on the chain length of the organic alkylammonium ions and the charge density of the layered silicate. Both of these factors contribute to the different configurations of the organic modifier inside the clay galleries (as outlined in chapter 1).^{3,40,41} When almost all inorganic cations are ion-exchanged by onium ions (degrees of ion-exchange ≥ 80 %) the homogeneity of the organic modifier content in the galleries depends on the uniform charge distribution on the surface of the nanolayers, which is higher in the synthetic clays compared to the natural clays. Having a very uniform charge distribution allows for homogenous dispersion of the cations, giving rise to a very consistent interclay spacing and invariant swelling behavior from tactoid to tactoid. However, even with synthetic clays the synthesis of a mixed-ion clay could result in inhomogeneous distribution of the organic cations if the ion exchange is not carried out with some care. Pinnavaia

et al.^{β6-38} developed a method of synthesizing high quality mixed-ion homostructured clays by utilizing water/alcohol mixtures for the ion-exchange bath along with prolonged ion-exchange times. In this way phase-segregated structures that consisted of separate inorganic-rich and organic-rich regions (readily notable by XRD) were minimized and a more homogeneous ion exchange within all the galleries could be achieved. In this case, however, the tendency for large organic surfactants to aggregate into micelles and undergo ion exchange in clusters is lessened by the higher solubility of polypropylene oxide – based surfactants in water relative to a pure alkyl amine.

The target of the present study was to synthesize mixed-ion inorganic/organic smectite clays with a very low onium ion content (onium ion to proton (O^+/H^+) ratio $\sim 1:3$), which would still show a homogeneous distribution of the organic modifier between the nanolayers and permit the intercalation of epoxy resin. The use of a relatively long-chain, primary alpha-omega diamine (Jeffamine D2000) allowed the synthesis of true homostructures with a single 001 reflection. When alkylammonium ions with a C12-C18 carbon chain were stoichiometrically ion exchanged for the inorganic cations in montmorillonite clays with a CEC ~ 100 - 120 meq/100 g, they adopted a lateral bilayer (~ 18 Å) or an inclined paraffin-like structure (~ 20 - 23 Å). The mixed-ion homostructured clays, prepared by partial ion exchange with C18A onium ions, had basal spacings of 18.1, 17.4 and 14.2 Å for O^+/H^+ ratios of 65:35, 50:50 and 35:65, respectively.³⁸ However, when the diprotonated diamine D2000 was used for the ion exchange of the inorganic

clays, the basal spacing of the mixed-ion clay with O^+/H^+ ratio 1:3 was 16.9 Å, as it can be seen from the data in Table 5.1.

Table 5.1 Composition and Basal Spacings of the Homoionic and Mixed-ion Inorganic/Organic clays

Inorganic/organic clays	parent inorganic clay	organic modifier ^a		basal spacings	
		Onium ion (%)	diprotomated diamine	d_{001} (Å)	d_{002} (Å)
H-PGW	Na-PGW	-	-	13.4	-
Li-PGW	Na-PGW	-	-	12.4	-
Li-FH	Li-FH	-	-	12.3	-
H/D2000 ₂₅ -PGW	H-PGW	25	D2000	16.9	-
H/D2000 ₃₅ -PGW	H-PGW	35	D2000	17.8	-
Li/D2000 ₃₅ -PGW	Li-PGW	35	D2000	17.6	-
H/D2000 ₅₀ -PGW	H-PGW	50	D2000	43.7	18.8 ^b
D2000-PGW	Na-PGW	80	D2000	45.5	21.8
Li/D2000 ₆₅ -FH	Li-FH	65	D2000	45.3	21.3
D2000-FH	Li-FH	80	D2000	46.0	23.2
H/C18A _{0.65} -PGW	H-PGW	65	C18A	17.5	-

^a The inorganic clays were ion-exchanged with diprotomated diamine D2000 (Jeffamine, Huntsman Chemical); the Na⁺ content of all the ion-exchanged clays was below 5 %

^b The d-spacing of that broad peak (~19 Å) is related to both the second order reflection and to a second phase of the mixed-ion clays as is discussed in the text

Furthermore, from the X-ray patterns of the D2000-exchanged clays in Figure 5.1, it can be seen that there is no indication of an inorganic-rich phase (d-spacing ~12-14 Å) in all the mixed-ion clays.

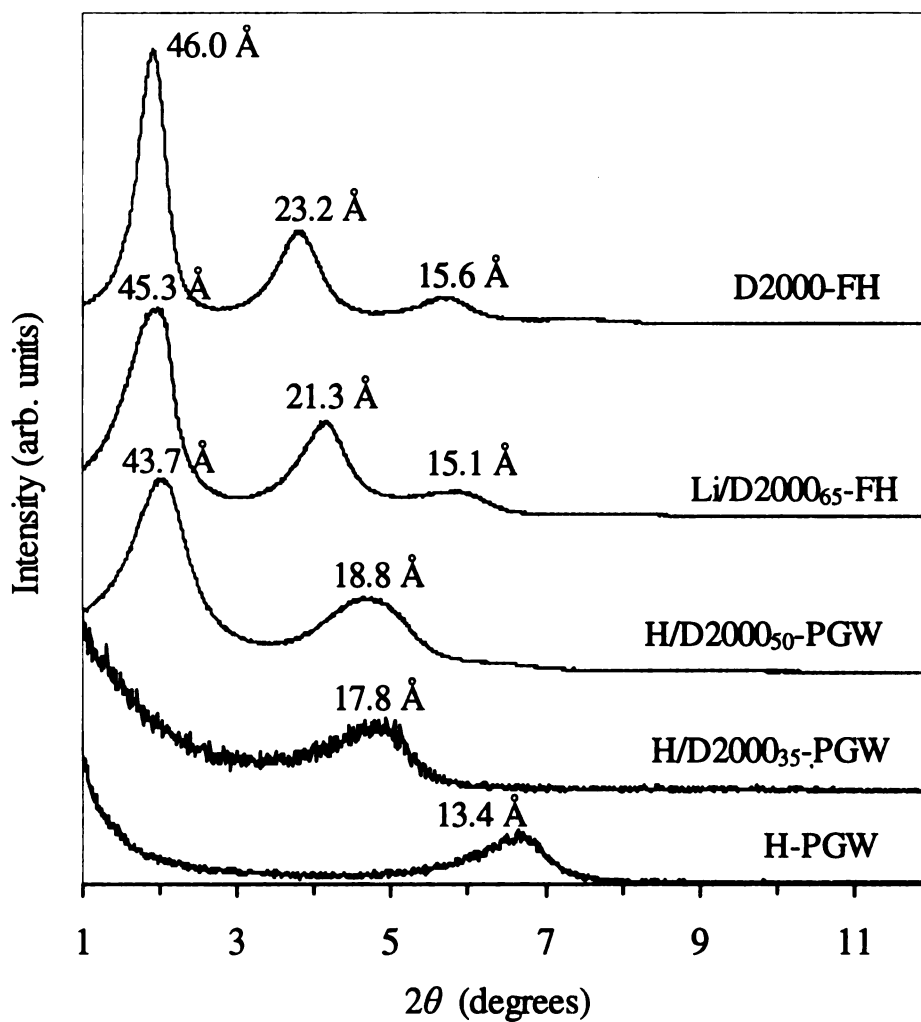


Figure 5.1 X-ray diffraction patterns of the homoionic and mixed-ion inorganic/organic montmorillonite (PGW) and fluorohectorite (FH) clays prepared by ion exchange of the inorganic cations Na^+ , Li^+ or H^+ with onium ions of diprotonated D2000.

The basal spacing for both the homoionic D2000-PGW and D2000-FH organic clays was ~ 46 Å, and multiple orders of reflection could be seen in these XRD patterns, although the higher aspect ratio of the fluorohectorite gives more intense peaks and more distinct higher orders of reflection. The configuration of the long-chain D2000 diamine inside the clay galleries is an inclined paraffin-like structure, as expected for such a large onium modifier. Interestingly, the mixed-ion Li/D2000_{0.65}-FH clay with O⁺/Li⁺ ratio of 65:35 had a very similar d-spacing to the homoionic organic clays, indicating that the end - to - end separation of the diamine modifier is near a maximum value in both instances. The mixed-ion clay H/D2000_{0.5}-PGW with O⁺/H⁺ ratio of 1:1 showed a basal spacing of ~ 44 Å, indicating a more parallel surfactant orientation to the clay surface. The second order reflection was relatively broad and had a d-spacing in the ~ 19 Å range. This region could represent both the 002 reflection and a monolayer diamine arrangement that occurs at roughly the same spacing. More important was the lack of higher angle 12-14 Å 001 distances, which represent unexchanged inorganic portions of the clay sample. At lower degrees of ion exchange, e.g., O⁺/H⁺ ratios of $\sim 3:7$, the d-spacing of the mixed-ion clays was $\sim 17-18$ Å. Even at this low organic content a uniform lateral monolayer structure was observed without the inorganic clay peak. The configuration of D2000-diamine inside the galleries of the mixed-ion clays could be described by mixtures of lateral bilayer and folded-monolayer or inclined-folded layer-to-layer structures, depending on the concentration of the diamine in the galleries. The “folded” or “coiled” structures are unique to polypropylene – based surfactants as such a backbone

permits more random orientation due to the flexible, easy to rotate nature of the carbon – oxygen bond. Lower concentrations (e.g., for onium ions/inorganic cations \leq 35:65) could be represented better with a lateral bilayer structure while at higher loadings of organic modifier (e.g., for onium ions/inorganic cations \geq 65:35) the inclined-paraffin configuration of the diamine molecules would be preferred. For comparison purposes, a mixed-ion H/C18A_{0.65}-PGW was synthesized with O⁺/H⁺ ratio of 65:35; this clay showed a basal spacing of ~17.5 Å. As expected, the smaller onium exchanged in this case adopts a monolayer arrangement even at relatively high loadings. Table 5.1 contains basal spacing and compositional data for all the homoionic and mixed-ion montmorillonite (PGW) and fluorohectorite (FH) clays synthesized in this work.

Epoxy-Clay Nanocomposite Formation from Mixed-Ion Inorganic/Organic Clays. Exfoliation of the clay nanolayers in a polymer matrix first requires the polarity of the interclay region to match that of the polymer precursors, and subsequently that the intragallery polymerization rate is equal to, or better yet greater than, that of the bulk polymer. The chemical modification of the clays with organic modifiers, mainly acidic primary onium ions, provides with the appropriate hydrophobic intragallery environment for initial intercalation of the epoxy resin, and their acidic nature aids in catalytically ring opening the epoxy molecules intercalated into the galleries. The above mechanism can lead to more improved nanocomposites through using diamines, in particular, as the organic modifiers as they eliminate the undesirable effect of the free, dangling

chains invoked on the epoxy by mono-amines that can not be crosslinked into the polymer matrix.^{20,35,39} However, large loadings of the relatively high molecular weight diamine could induce rubberizing effects to the rigid, glassy epoxy polymer matrix and have similar effect to that of the dangling chains of the mono-amines. It would thus be desirable both from the mechanical point of view and for economical considerations to minimize the organic modifiers of the clay additives, yet still achieve high degrees of nanolayer intercalation/exfoliation and improved properties of the epoxy – clay nanocomposites.

The clay nanolayer intercalation and ultimate exfoliation upon mixing the epoxy monomer (EPON 826) with the Li/D2000_{0.65}-FH mixed-ion clay, and after final curing of the nanocomposite is shown in the stacked X-ray patterns of Figure 5.2.

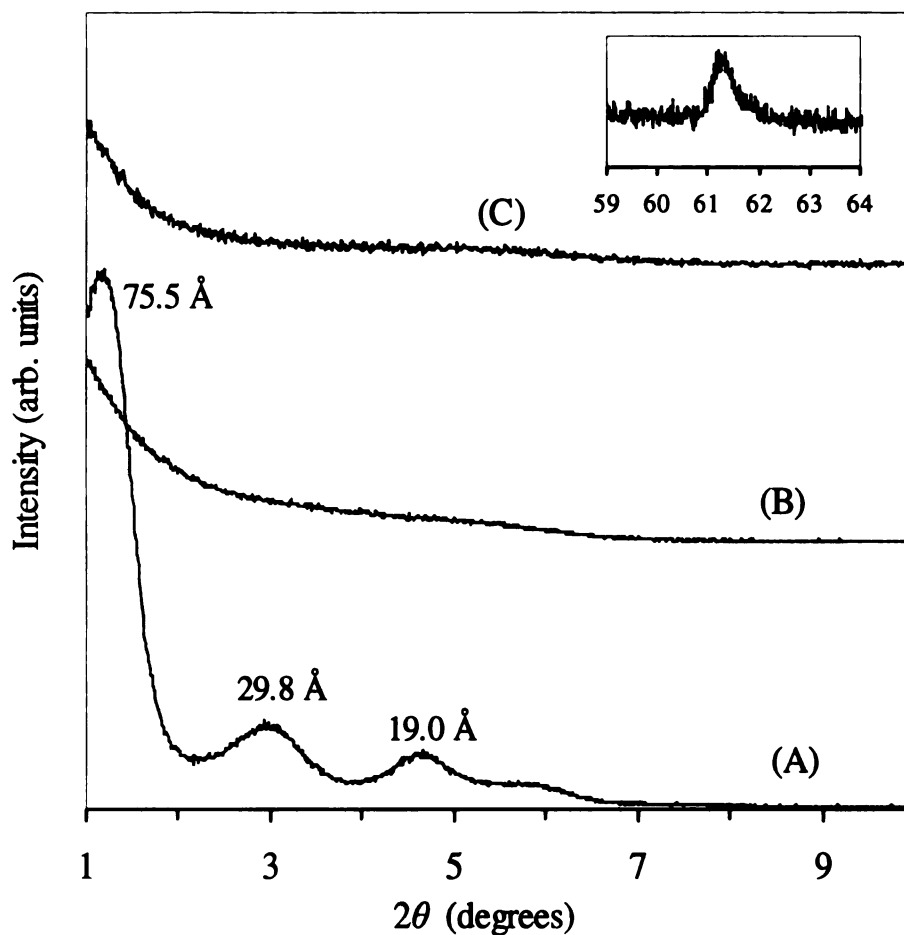


Figure 5.2 X-ray diffraction patterns of mixtures of the mixed-ion clay Li/D2000_{0.65}-FH, the epoxy monomer EPON 826 and the curing agent D230: (A) after intercalation of EPON 826 in Li/D2000_{0.65}-FH at 50°C for 12 hrs, (B) after addition of D230 to the mixture of step A and outgassing at 25°C, and (C) after curing at 75°C, 3 hrs and 125°C, 3hrs (the clay loading was 6 wt. % silicate basis). The inset shows the presence of an in-plane 060 clay reflection in the cured nanocomposite

Pre-mixing of the epoxy monomers with Li/D2000_{0.65}-FH mixed-ion clay (O⁺/Li⁺ ~65:35) at 50°C resulted in a disordered intercalation of the nanolayers with a basal spacing reaching ~75 Å (pattern A). Subsequent addition of the diamine curing agent at the same temperature induced rapid intragallery polymerization and expansion of the nanolayers after a short period of time (pattern B). Upon completion of the curing process at higher temperatures, the nanolayers remained highly separated resulting in the absence of Bragg peaks in the small-angle region (pattern C), similar to case of the homoionic D2000-FH organic clay.³⁹ The mixed-ion clay H/C18A_{0.65}-PGW, which was synthesized by ion-exchanging the protons with C18A-onium ions instead of the diprotonated diamine D2000, resulted in a highly intercalated/exfoliated nanocomposite sample, similar to the Li/D2000_{0.65}-FH mixed-ion clay.

The formation of a high quality thermoset epoxy – clay nanocomposite material with homogenous dispersion of the individual nanolayers throughout the polymer matrix is not only dependent on the catalytic acidity of the organoclay, but on the fabrication conditions as well.³² The sequence of mixing the components of the thermoset epoxy – clay nanocomposite system (clay/diamine curing agent/epoxy monomers), the use of solvents to reduce the viscosity of the system, the temperature and time of curing, and finally the fabrication and molding techniques could have a significant effect on the degree of nanolayer dispersion. Unlike the rubbery epoxy systems, epoxy monomer pre-intercalation inside the clay galleries before addition of the curing agent typically results in higher degrees of nanolayer exfoliation. This is likely more pronounced in the

glassy epoxy polymer synthesis due to the smaller, more nucleophilic D230 curing agent that can prematurely react with the epoxy resin prior to intercalation, as covered in chapter 4. However, in order to avoid gelling of the interclay regions, care should be taken that pre-mixing of the diamine-modified clay with the epoxy monomers does not take place at relatively high temperatures (higher than 50°C) and for a very prolonged period (more than 24 hrs). Heating the epoxy – clay mixture to 50°C is necessary for keeping the viscosity relatively low and boosting the diffusion of the epoxy monomers inside the galleries. An alternative way to reduce the viscosity, and thus increase the diffusion of the epoxy, would be the implication of low-boiling point solvents, such as acetone, ethanol and isopropyl alcohol to the epoxy – clay mixture.

In the case of the nanocomposite samples prepared by mixed-ion clays with lower onium ions to protons ratios (eg. 35:65 and 25:75) a broad, low intensity peak with d-spacing ~17-18 Å was present in the XRD patterns, indicating different degrees of limited nanolayer intercalation, in contrast to the relatively narrow peak with d-spacing ~13.7 Å of the nanocomposite sample formed by the inorganic proton clay (PGW) indicating no intercalation. The qualitative information obtained from observing the rheological and optical properties of the clay – epoxy mixture can be a powerful tool in predicting the nature of the clay in the polymer medium. For instance, the inorganic clay, no matter the sieved particle size, will not invoke as large a viscosity change when added to the resin, and given a short amount of time will settle to the bottom of the resin. An immediate large viscosity increase and unsettling nature of the

~17-18 Å - spaced low organo-content clays preliminarily indicates that these materials will show superior mechanical properties relative to the pristine and inorganic clay-filled epoxy systems.

TEM images of the nanocomposite samples prepared from the mixed-ion Li/D2000_{0.65}-FH fluorohectorite and H/D2000_{0.5}-PGW montmorillonite clays are shown in Figures 5.3a,b and 5.4c,d, respectively. The clay loading in both samples was 6 wt. % (silicate basis).

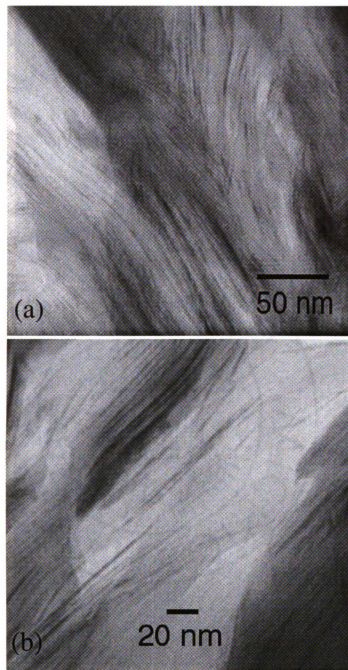


Figure 5.3 TEM images of thin sections of the glassy epoxy nanocomposites prepared from the mixed-ion clays (a,b) Li/D2000_{0.65}-FH. The clay loading of the nanocomposite samples was 6 wt. % silicate basis.

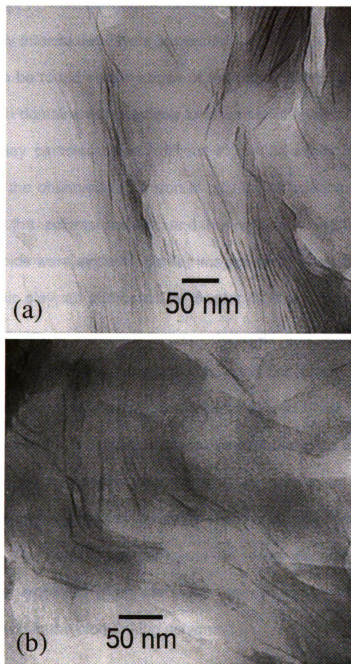


Figure 5.4 TEM images of thin sections of the glassy epoxy nanocomposites prepared from the mixed-ion clays (a,b) H/D2000_{0.5}-PGW. The clay loading of the nanocomposite samples was 6 wt. % silicate basis.

The Li/D2000_{0.65}-FH nanocomposite consisted mainly of clay tactoids with disordered, highly intercalated layers separated by 5–20 nm. Individual, shorter layers could also be found on the edges of the primary dispersed particles and most frequently in domains with relatively low number of layers. The high aspect ratio synthetic clay particles proved difficult to exfoliate fully into the polymer matrix, although the observed expansion of clay layers adequately exposes the clay surface to the polymer matrix, and no regions of tightly bound, non-intercalated tactoids were evident. Similar images were noted for the homoionic D2000-FH organic clay, as addressed in chapter 4. The importance of equally exfoliated clay layers in both homoionic organoclay and partially exchanged mixed-ion clay cannot be understated, as this is the first example of a reduced-organic system that competes with a pure organic layered silicate.

A more disordered intercalated or partially exfoliated state was found in the H/D2000_{0.5}-PGW nanocomposite, where most of the nanolayers were separated by more than 10 nm space, still generally keeping parallel orientations within larger domains. The more expanded layer – to – layer separation noted in the natural clay is as expected given the much reduced aspect ratio, resulting in easier migration within the crosslinking polymer.

Properties of the Nanocomposites.

Dynamic Mechanical Analysis

(DMA) tests were applied in order to investigate the effect of the homoionic and the mixed-ion clay nanolayer reinforcement on the mechanical properties of the glassy epoxy polymer. The DMA technique provides two different moduli, an

elastic modulus (E') which is called storage modulus and is related to the ability of the material to return or store energy when an oscillatory force is applied to the polymer specimen and an imaginary (loss) modulus (E'') which relates to the ability of the material to lose energy. The ratio E''/E' is called tan delta ($\tan\delta$) and typically reaches a maximum at the glass transition (T_g) of the polymer. A more in-depth explanation of the DMA theory and mechanics is provided in chapter 4. The DMA tests of this study were conducted in a three-point bending (flexural) mode while other modes, like the torsional mode, are also commonly used.³² The curves in figure 5.5a and 5.5b show the dependency of the storage modulus and the $\tan\delta$ (maximum value at the glass transition temperature) for representative nanocomposite samples prepared by homoionic and mixed-ion clays, at a clay loading of 6 wt.% (silicate basis).

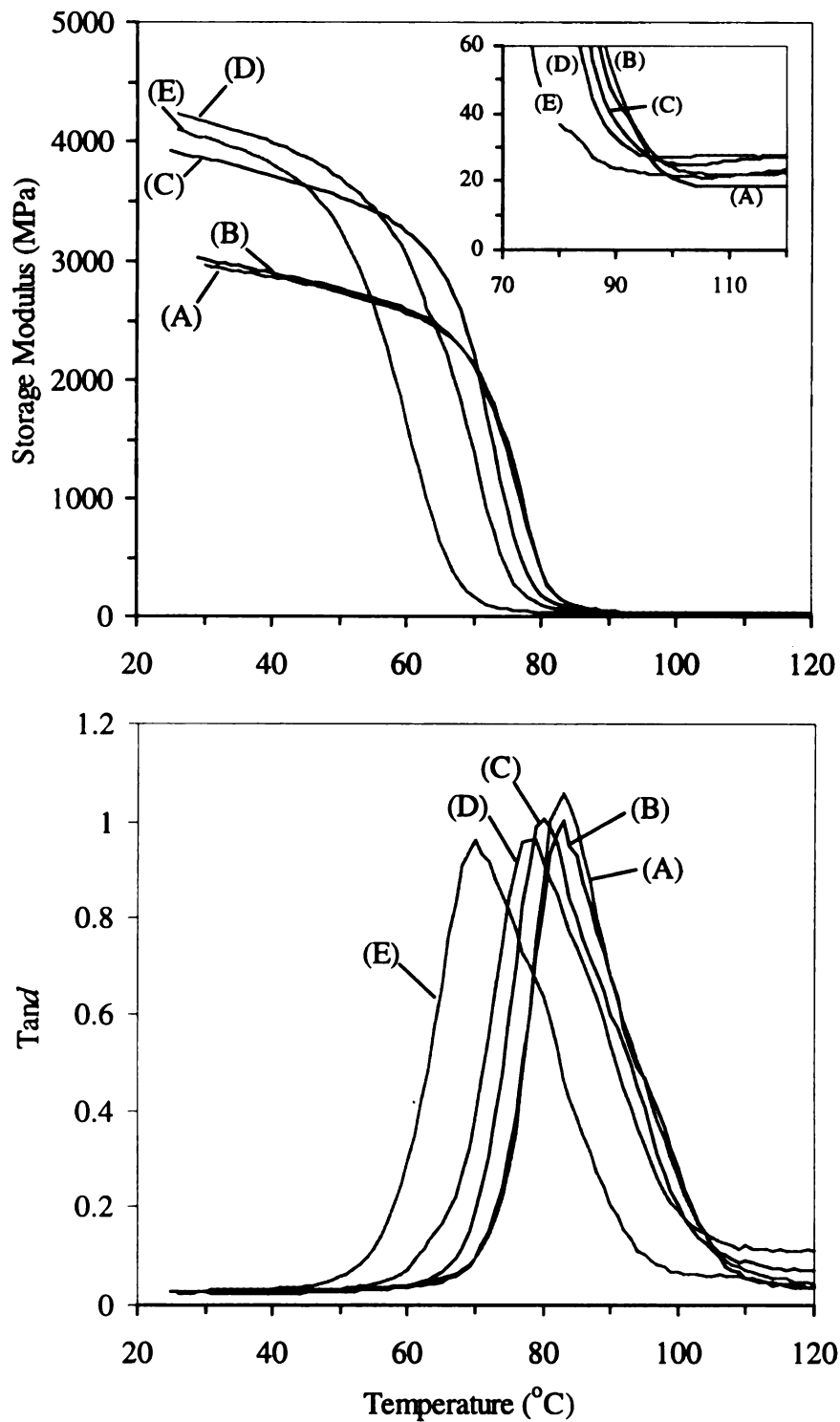


Figure 5.5 Dynamic Mechanical Analysis measurements: (a) Storage Modulus vs. temperature and (b) $\tan\delta$ vs. temperature, for (A) Pristine-A epoxy polymer and for the nanocomposite samples prepared from (B) H-PGW, (C) H/D2000_{0.25}-

PGW, (D) Li/D2000_{0.65}-FH, (E) D2000-PGW. The clay loading of the nanocomposite samples was 6 wt. % silicate basis .

The data in Table 2 refers to the storage modulus values of the pristine polymer and the nanocomposite samples at 40°C (glassy region, below T_g) and at 120°C (rubbery region, above T_g), and to the T_g values of the samples.

Table 5.2 Dynamic Mechanical Analysis and Thermal Analysis data of the pristine epoxy polymer and the clay-polymer nanocomposite samples ^a

Samples	storage modulus (E')		T_g ($\tan\delta$) ($^{\circ}\text{C}$), \pm 2	thermal stability (TGA data) ^d ($^{\circ}\text{C}$)
	at 40 $^{\circ}\text{C}$ (GPa), \pm 10%	At 110 $^{\circ}\text{C}$ (MPa), \pm 10%		
Pristine epoxy-A	2.9	18.4	82.6	373
Pristine epoxy-B ^b	3.0	20.1	75.5	361
H-PGW	2.9	22.1	82.8	354
Li-PGW	2.7	19.9	82.3	356
Li-FH	3.1	25.2	85.2	351
H/D2000 ₂₅ -PGW	3.7	26.0	80.2	342
H/D2000 ₃₅ -PGW	3.8	26.8	79.0	339
H/D2000 ₃₅ – P2 ^c	3.6	38.3	85.1	342
Li/D2000 ₃₅ -PGW	3.5	24.1	81.7	342
H/D2000 ₅₀ -PGW	3.3	22.7	78.0	339
H/D2000 ₅₀ -PGW – P2	3.2	28.0	82.6	341
H/D2000 ₅₀ -PGW – <i>P2/acetone</i>	3.6	35.2	83.1	339
H/D2000 ₅₀ -PGW – <i>P2/EtOH</i>	3.4	32.4	83.1	330
H/D2000 ₅₀ -PGW – <i>P2/IPA</i>	3.6	31.6	80.4	347
D2000-PGW	3.8	21.5	69.8	336
D2000-PGW – P2	3.6	24.0	75.1	339
Li/D2000 ₆₅ -FH	4.0	27.6	78.0	328
D2000-FH	3.9	30.5	73.7	323
H/C18A _{0.65} -PGW-P2	3.5	34.2	84.4	340

^a The nanocomposite samples were named from the inorganic/organic clay used; the clay loading of the samples was 6 wt.% silicate basis

^b Substitution of 4 % mole D2000 (organic modifier of clays) for D230 (curing agent) in the pristine epoxy polymer

^c *P2* refers to the nanocomposite samples prepared by pre-mixing of epoxy monomers with the clays; all the rest of the samples in Table 2 were prepared by direct addition of the clays in the epoxy – curing agent mixture (*P1*)

^d Temperature at which the weight loss in TGA was 1.5 %

The storage modulus and the T_g of the nanocomposite sample formed by the inorganic H-PGW montmorillonite clay were similar to those of the pristine epoxy polymer. The inability of the inorganic clay to swell with epoxy resin created two distinct regions in the epoxy material, with the majority of the clay settling to the bottom of the specimen by the time crosslinking was completed. Despite poor mixing with the epoxy, an interesting finding was that there was no damage by oxidation or premature thermal decomposition as would be expected due to the presence of protons on the clay. While those protons trapped in the interior, unwetted clay galleries should not contribute to the acid-catalyzed thermal decomposition, the exterior protons ordinarily would be expected to affect the thermal decomposition as is noted in the TGA of proton – containing organoclays. The important difference in the inorganic clay – epoxy case is that a large amount of neutral amine (Jeffamine curing agent) is added to the mixture,

and these basic molecules can sequester the free surface protons, and eliminate their detrimental affect on the premature thermal degradation of the epoxy network. This is a significant find in that if methods are developed to pre-exfoliate inorganic clay layers through disruption of the preferred face – to – face stacking, then inexpensive proton clays could be employed as the reinforcement phase.

The nanocomposite sample formed by the homoionic D2000-PGW organic clay showed a ~25 % increase in storage modulus in both the glassy and rubbery region, while a 35% and 65 % increase, respectively, was found for the D2000-FH organic clay, indicating the improved reinforcing properties of the high-aspect ratio fluorohectorite nanolayers compared to the montmorillonite nanolayers. Direct comparisons of the D230 – Epon 826 pristine epoxy (no normalizing addition of D2000 present) to the nanocomposites indicates that there is a sacrifice in the glass transition temperature in the final hybrid systems. This is not an accurate comparison, however, as the small amount of D2000 present on the organoclay in the nanocomposites contributes to the crosslinking of the epoxy, and a more direct comparison of the normalized pristine epoxy (including the same ~4 % mole D2000 content) reveals nearly no change in T_g .

Not surprisingly, a similar or even higher increase in storage modulus without any significant changes in T_g could be achieved with the mixed-ion clays, even for the nanocomposite sample prepared from a mixed-ion clay with a O^+/H^+ ratio of 1:3 (fig. 5.2 and table 5.2). This is due to the reduction of high molecular weight D2000 content in the final nanocomposite, while still permitting

intercalation of epoxy and partial exfoliation of the reduced-organic clays. Specifically, the nanocomposite sample formed from the H/D2000_{0.25}-PGW clay showed a 30% and 40% increase of storage modulus in the glassy and rubbery region respectively, the sample prepared from H/D2000_{0.50}-PGW exhibited a 25% and 70% increase, the sample formed from H/ODA_{0.65}-PGW showed 20% and 85% increase, and the sample formed from Li/D2000_{0.65}-FH showed 40% and 50% increase. The T_g for all these samples ranged from ~78 – 84°C compared to 83°C of the pristine glassy epoxy polymer. The increase in storage modulus is in the same range found in previous studies with homoionic organic clays,^{25,32,34} but it should be mentioned that the absolute modulus values of the pristine epoxy polymer of this work (e.g. ~3 GPa below T_g and ~18 MPa above T_g) are higher than those previously reported.

As alluded to earlier, thermogravimetric analyses of the mixed-ion clays showed that when the protons were present in the sample, the decomposition of the organic modifier, diamine D2000, occurred at lower temperatures compared to an homoionic organic clay or to a mixed-ion clay in which the inorganic cation was Li^+ instead of H^+ (curves A and B in Fig. 5.6). However, the above proton – catalyzed decomposition was not transferred to the glassy epoxy – clay nanocomposite samples, as the thermal stability of the samples formed by the H⁺/D2000 mixed-ion clays was uninfluenced despite the presence of protons as noted in the TGA curves shown in figure 5.6 and the data in table 5.2.

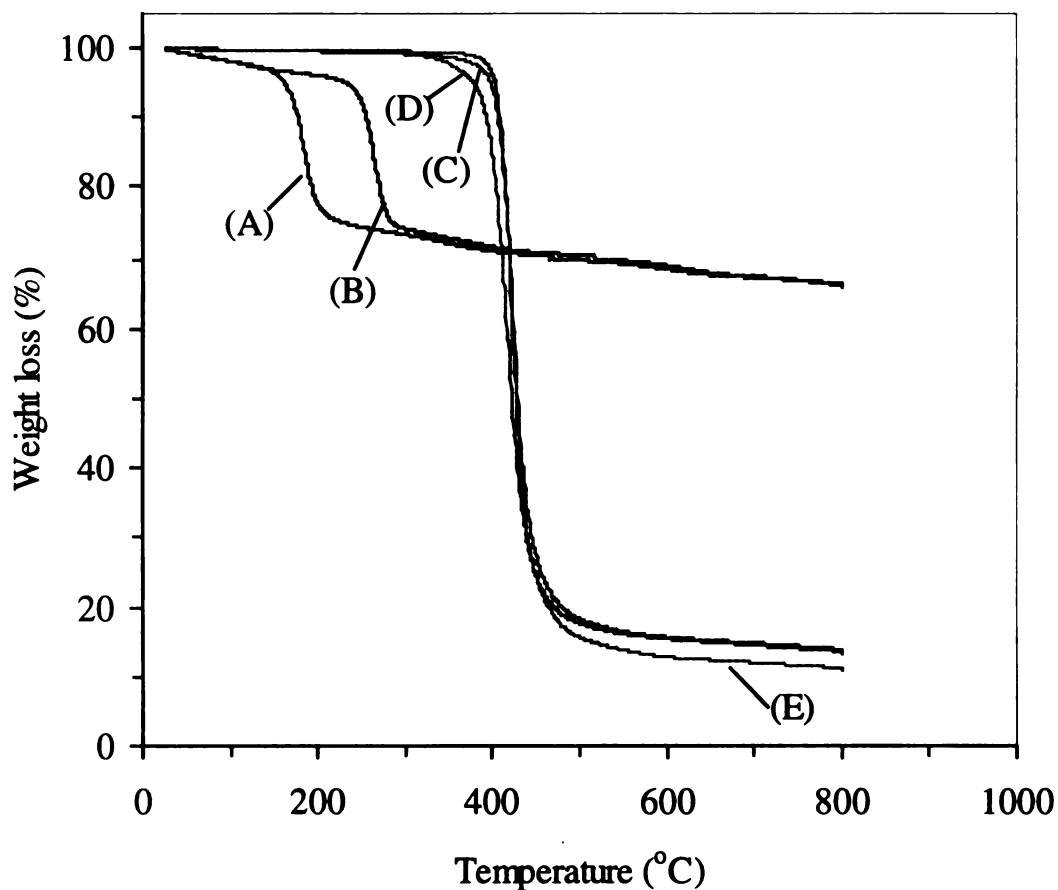


Figure 5.6 TGA curves of the mixed-ion clays (A) H/D2000_{0.35}-PGW and (B) Li/D2000_{0.35}-PGW, the nanocomposites prepared from (C) H/D2000_{0.25}-PGW and (D) D2000-PGW clays, and of the Pristine-A epoxy polymer (E). The clay loading of the nanocomposite samples was 6 wt. % silicate basis.

The high thermal stability of the nanocomposites prepared from both the homoionic and the mixed-ion diamine-modified clays suggested that the surface onium ions of the diamine were incorporated into the polymer network, resulting in nanocomposites with improved interfacial and physical properties. This is apparent as the onset of organic degradation was higher in the nanocomposites containing protonated amine – modified clay relative to the protonated amine clay itself.

5.4 Conclusions

The thermoset glassy epoxy – clay nanocomposites prepared from reduced organic content, mixed-ion smectite clays in this work have been shown to be successful in synthesizing exfoliated systems. Most significantly, the ability of the inorganic – containing homostructured clay to swell with epoxy resin, just as is the case with homoionic organoclay, represents the first example of a more cost effective, non-fully organic clay suitable for nanocomposite synthesis. Additionally, the presence of protonated diamines, while lessened in content, have sufficient acidic catalytic nature to bias the intragallery polymerization and ultimately force apart the clay layers. Impressive mechanical improvements of the nanocomposites were noted, as with the homoionic diamine – modified clays covered in chapter 4, however, by reducing the content of large molecular weight modifiers, the reduction in glass transition temperature and the overall rubberizing affect of the D2000 curing agents was greatly diminished. The mixed-ion smectite clays, in which the organic modifier was reduced by nearly

70%, could be used in various thermoset or thermoplastic polymer matrices for a more economical and effective means of fabricating polymer – clay nanocomposites.

5.5 References

- (1) Vaia, R. A.; Giannelis, E. P. *MRS Bull.* **2001**, *26*, 394-401.
- (2) Pinnavaia, T. J., Beall, G.W., eds. *Polymer - Clay Nanocomposites*; John Wiley & Sons Ltd, New York, 2000.
- (3) LeBaron, P. C.; Wang, Z.; Pinnavaia, T. J. *Appl. Clay Sci.* **1999**, *15*, 11-29.
- (4) Lagaly, G. *Appl. Clay Sci.* **1999**, *15*, 1-9.
- (5) Krishnamoorti, R.; Vaia, R. A.; Giannelis, E. P. *Chem. Mat.* **1996**, *8*, 1728-1734.
- (6) Giannelis, E. P. *Adv. Mater.* **1996**, *8*, 29-&.
- (7) Okada, A.; Usuki, A. *Mater. Sci. Eng. C-Biomimetic Mater. Sens. Syst.* **1995**, *3*, 109-115.
- (8) Chin, I. J.; Thum-Albrecht, T.; Kim, H. C.; Russell, T. P.; Wang, J. *Polymer* **2001**, *42*, 5947-5952.
- (9) Hsiue, G. H.; Liu, Y. L.; Liao, H. H. *J. Polym. Sci. Pol. Chem.* **2001**, *39*, 986-996.

- (10) Kommann, X.; Lindberg, H.; Berglund, L. A. *Polymer* **2001**, *42*, 4493-4499.
- (11) Ahuja, S. K.; McGriff, R. B. *Abstr. Pap. Am. Chem. Soc.* **2000**, *220*, 61-COLL.
- (12) Lu, J. K.; Ke, Y. C.; Qi, Z. N.; Yi, X. S. *J. Polym. Sci. Pt. B-Polym. Phys.* **2001**, *39*, 115-120.
- (13) Curliss, D. B. *Abstr. Pap. Am. Chem. Soc.* **2000**, *219*, 43-POLY.
- (14) Gam, K. T.; Sue, H. J. *Abstr. Pap. Am. Chem. Soc.* **2000**, *219*, 223-PMSE.
- (15) Kang, J. H.; Lyu, S. G.; Sur, G. S. *Polym.-Korea* **2000**, *24*, 571-577.
- (16) Pinnavaia, T. J. *Science* **1983**, *220*, 365-371.
- (17) Usuki, A.; Kawasumi, M.; Kojima, Y.; Okada, A.; Kurauchi, T.; Kamigaito, O. *J. Mater. Res.* **1993**, *8*, 1174-1178.
- (18) Usuki, A.; Kojima, Y.; Kawasumi, M.; Okada, A.; Fukushima, Y.; Kurauchi, T.; Kamigaito, O. *J. Mater. Res.* **1993**, *8*, 1179-1184.
- (19) Kojima, Y.; Usuki, A.; Kawasumi, M.; Okada, A.; Fukushima, Y.; Kurauchi, T.; Kamigaito, O. *J. Mater. Res.* **1993**, *8*, 1185-1189.
- (20) Lan, T.; Kaviratna, P. D.; Pinnavaia, T. J. *Chem. Mat.* **1995**, *7*, 2144-2150.
- (21) Usuki, A.; Kato, M.; Okada, A.; Kurauchi, T. *J. Appl. Polym. Sci.* **1997**, *63*, 137-139.
- (22) Vaia, R. A.; Jandt, K. D.; Kramer, E. J.; Giannelis, E. P. *Chem. Mat.* **1996**, *8*, 2628-2635.

- (23) Burnside, S. D.; Giannelis, E. P. *Chem. Mat.* **1995**, *7*, 1597-1600.
- (24) Lan, T.; Kaviratna, P. D.; Pinnavaia, T. J. *Chem. Mat.* **1994**, *6*, 573-575.
- (25) Messersmith, P. B.; Giannelis, E. P. *Chem. Mat.* **1994**, *6*, 1719-1725.
- (26) Lan, T.; Pinnavaia, T. J. *Chem. Mat.* **1994**, *6*, 2216-2219.
- (27) Wang, M. S.; Pinnavaia, T. J. *Chem. Mat.* **1994**, *6*, 468-474.
- (28) Kojima, Y.; Fukumori, K.; Usuki, A.; Okada, A.; Kurauchi, T. *J. Mater. Sci. Lett.* **1993**, *12*, 889-890.
- (29) Yano, K.; Usuki, A.; Okada, A.; Kurauchi, T.; Kamigaito, O. *J. Polym. Sci. Pol. Chem.* **1993**, *31*, 2493-2498.
- (30) Fu, X.; Qutubuddin, S. *Polymer* **2001**, *42*, 807-813.
- (31) Zerda, A. S.; Lesser, A. J. *J. Polym. Sci. Pt. B-Polym. Phys.* **2001**, *39*, 1137-1146.
- (32) Brown, J. M.; Curliss, D.; Vaia, R. A. *Chem. Mat.* **2000**, *12*, 3376-3384.
- (33) Ke, Y. C.; Lu, J. K.; Yi, X. S.; Zhao, J.; Qi, Z. N. *J. Appl. Polym. Sci.* **2000**, *78*, 808-815.
- (34) Massam, J.; Pinnavaia, T. J. *Material Research Society Symposium Proceedings* **1998**, *520*, 223-232.
- (35) Wang, Z.; Pinnavaia, T. J. *Chem. Mat.* **1998**, *10*, 1820-1826.
- (36) Pinnavaia, T. J.; Shi, H.-z.; Lan, T. In *U.S.*; (Board of Trustees Operating Michigan State University, USA). Us, 1999, p 24 pp.

- (37) Pinnavaia, T. J.; Shi, H.-Z.; Lan, T. In *PCT Int. Appl.*; (Michigan State University, USA). Wo, 2000, p 102 pp.
- (38) Pinnavaia, T. J.; Wang, Z. In *U.S.*; (Board of Trustees Operating Michigan State University, USA). Us, 2001, p 25 pp.
- (39) Triantafillidis, C. S.; Sislo, M. R.; LeBaron, P. C.; Pinnavaia, T. J. *Abstracts of Papers, 222nd ACS National Meeting, Chicago, IL, United States, August 26-30, 2001* 2001, IEC-109.
- (40) Lagaly, G. *Solid State Ion.* 1986, 22, 43-51.
- (41) Hackett, E.; Manias, E.; Giannelis, E. P. *J. Chem. Phys.* 1998, 108, 7410-7415.